

**An Autopsical Examination of 40 Year Old
Pre-Tensioned Concrete Channel Girders**

by

Brandon James Mills

A Thesis submitted to the Faculty of Graduate Studies of

The University of Manitoba

in partial fulfilment of the requirements of the degree of

Master of Science

Department of Civil Engineering

University of Manitoba

Winnipeg, Manitoba, Canada

Copyright © 2009 Brandon James Mills

THE UNIVERSITY OF MANITOBA
FACULTY OF GRADUATE STUDIES

COPYRIGHT PERMISSION

**An Autopsical Examination of 40 Year Old
Pre-Tensioned Concrete Channel Girders**

By

Brandon James Mills

A Thesis/Practicum submitted to the Faculty of Graduate Studies of The University of
Manitoba in partial fulfillment of the requirement of the degree
Of

Master of Science

Brandon James Mills©2009

Permission has been granted to the University of Manitoba Libraries to lend a copy of this thesis/practicum, to Library and Archives Canada (LAC) to lend a copy of this thesis/practicum, and to LAC's agent (UMI/ProQuest) to microfilm, sell copies and to publish an abstract of this thesis/practicum.

This reproduction or copy of this thesis has been made available by authority of the copyright owner solely for the purpose of private study and research, and may only be reproduced and copied as permitted by copyright laws or with express written authorization from the copyright owner.

ACKNOWLEDGEMENTS

I would like to thank Aftab Mufti, P.Eng., PhD, for giving me the opportunity to fulfill my goal of achieving a masters' degree and to do so with such an interesting project. I would also like to thank Aftab Mufti, P.Eng., PhD, Mike Lau P.Eng., PhD., and Asnee Pochanart P.Eng., PhD. for their technical guidance and support.

Thank you to the laboratory staff of Chad Klowak, Grant Whiteside and Evangenline Murison for their support in the structures laboratory. I would also like to thank Hugues Vogel for his support in the laboratory and being there to answer my many questions.

Thank you to the administrative staff at ISIS, and to ISIS Canada for their funding of the project.

Thank you to Lafarge Canada Inc. for their help levelling my core samples for concrete strength testing and to The National Testing Laboratories Ltd. for their expedient analysis of the air-void samples.

Finally, I would like to thank my family for their support and encouragement throughout this endeavour.

ABSTRACT

This thesis report examines six decommissioned pre-tensioned concrete channel girders which were part of the Canadian National Railway overpass on the Trans-Canada Highway No. 1 (CN Overpass on TCH Site No. 0709-00) east of Portage La Prairie constructed in 1965. The six girders are representative of the various levels of deterioration observed on the in-service bridge.

In the summer of 2006, UMA Engineering Ltd. (now AECOM) was contacted by Manitoba Highways and Infrastructure to inspect the Trans-Canada Highway rail overpass. Several of the girders in the center span were said to be in poor condition. The webs had been subject to water leakage through the shear keys and concrete cover loss ranging from 25 mm to 100 mm from the bottom of the webs was observed.

The primary objective of this research was to determine the remaining capacity of the 40 year old girders in flexure and shear when subjected to monotonic loading. Non-destructive testing was also carried out including material sample testing (concrete strength, air-void content and chloride ion content). Additionally, the girders were load rated using both the Canadian Highway Bridge Design Code: Bridge Evaluation and the American Association of State Highway Officials: Load and Resistance Factor Rating methods.

Given the analysis of the data of the six girders that were comprehensively examined, their experimentally observed capacities surpassed the theoretical capacity on the order of

27 and 47 percent for bending and shear respectively. The concrete strength testing demonstrated an increase of 36 percent to that of the design value. The material tests revealed the cause of the deterioration of the girder webs was due to cyclic freeze-thaw affects.

Using the experimentally observed moment and shear capacities allowed the CHBDC load rating method to achieve a favorable rating. However, the AASHTO LRFR method did not achieve a passing rating for all girders.

As a result of this research work it was recommended that research of pre-stressed girders be conducted to reduce the level of conservatism of flexure and shear capacities calculated within the Canadian and American design codes, that within Manitoba bridges of this nature should be load tested to increase the accuracy of the load rating analysis, and that post service bridge components be experimentally examined to narrow the gap between theory and qualitative analysis, and quantitative performance characteristics to increase the level of understanding and knowledge of bridge component reactions to expected service inputs.

TABLE OF CONTENTS

ACKNOWLEDGEMENTS	i
ABSTRACT	ii
LIST OF FIGURES	vi
LIST OF TABLES	x
1. INTRODUCTION.....	1
1.1 Overview.....	1
1.2 Background	1
1.3 Objectives	3
1.4 Scope of Work	3
2. LITERATURE REVIEW	7
2.1 Pre-tensioned Concrete Structural Members	7
2.2 Bridge Damage and Deterioration	9
2.2.1 Truck Loading and Effects.....	9
2.2.2 Environmental Damage	11
2.3 Non-destructive Testing.....	17
2.3.1 Concrete Strength and Compressive Testing.....	17
2.3.2 Chloride Ion Content Testing.....	19
2.3.3 Determination of Air Void Properties in Hardened Concrete	21
2.4 Bridge Evaluation and Load and Resistance Factor Rating.....	23
2.4.1 Canadian Highway Bridge Design Code Bridge Evaluation.....	23
2.4.2 AASHTO Load and Resistance Factor Rating	28
3. SPECIMEN REPORT.....	34
3.1 Girder Properties.....	34
3.2 Theoretical Calculations	38
3.2.1 Theoretical Pre-stressing Force Losses.....	38
3.2.2 Theoretical Flexural Moment Capacity	39
3.2.3 Theoretical Shear Capacity	39
3.2 Specimen Condition.....	40
3.3 Lateral Post-tensioning Strand and Grout Condition.....	53

4.	EXPERIMENTAL PROGRAM.....	54
4.1	General Experimental Setup	54
4.2	Flexural Testing Setup	56
4.2.1	Instrumentation	56
4.2.2	Testing Procedure	59
4.3	Shear Testing Setup	60
4.3.1	Instrumentation	60
4.3.2	Testing Procedure	64
4.4	Compressive Strength Cylinder Testing	64
4.5	Chloride Ion Content Determination	65
4.6	Air Void Ratio and Spacing Factor Determination.....	66
5.	EXPERIMENTAL RESULTS.....	67
5.1	Flexure Testing Results.....	67
5.2	Shear Testing Results.....	77
5.4	Concrete Strength Testing Results.....	89
5.5	Chloride Ion Content Testing Results.....	93
5.6	Air Void Ratio and Spacing Factor Testing Results.....	94
6.	LOAD RATING RESULTS.....	96
6.1	CHBDC Bridge Evaluation.....	97
6.1.1	Influence Analysis of Evaluation Loading Levels.....	97
6.1.2	Assumptions and Load Factors	99
6.1.3	Theoretical Bridge Evaluation Results	100
6.1.4	Experimental Bridge Evaluation Results	102
6.2	AASHTO Load and Resistance Factor Rating	105
6.2.1	Influence Analysis of Loading Levels	105
6.2.2	Assumptions and Load Factors	106
6.2.3	Theoretical Load Rating Results.....	107
6.2.4	Experimental Load Rating Results	110
7.	CONCLUSIONS & RECOMMENDATIONS.....	114
	REFERENCES.....	117
	APPENDIX.....	119

LIST OF FIGURES

Figure 1-1: Underside of the north span of the Portage La Prairie CN overpass.	5
Figure 1-2: Underside of the center span of the Portage La Prairie CN overpass.	5
Figure 1-3: Portage La Prairie CN overpass elevation and cross section view.	6
Figure 2-1: Corrosion of steel reinforcement in concrete at various cover depths over time [12].	14
Figure 2-2: Probability of steel failure versus chloride ion concentration of concrete [13].	14
Figure 2-3: The microstructure of concrete paste [14].	15
Figure 2-4: Surface of a finely lapped slice of concrete containing 5.6 percent total air voids [14].	22
Figure 3-1: Schematic of elevation and cross sectional profiles.	36
Figure 3-2: Stirrup and pre-stressing detail.	37
Figure 3-3: Transverse cracking through the diaphragm of girder one.	42
Figure 3-4: Longitudinal cracking on web at the post-tensioning ducts of girder one.	43
Figure 3-5: Longitudinal cracking on the bottom of east web of girder two.	44
Figure 3-6: Longitudinal cracking on the side of east web at the bottom of girder two.	44
Figure 3-7: Water leaching stains on the web of girder two.	45
Figure 3-8: A long view of the east web including lost concrete and strand corrosion of girder three.	46
Figure 3-9: Strand corrosion near the mid-span on the east side of girder three.	46
Figure 3-10: Surface scaling and a ruptured strand on the east side of girder three.	47
Figure 3-11: Transverse cracking through the diaphragm of girder three.	47
Figure 3-12: Longitudinal cracking on web at post-tensioning ducts of girder three.	48
Figure 3-13: Cracking and water leakage stains on the web at the post-tensioning ducts of girder four.	49
Figure 3-14: Cracking and water leaching stains at the post-tensioning duct on the west web of girder five.	50
Figure 3-15: Strand corrosion, lost concrete and surface scaling on the east web of girder five.	50
Figure 3-16: Significant concrete loss on the east web near support of girder five.	51

Figure 3-17: Web cracking and delamination, corrosion staining and surface scaling of girder five.....	51
Figure 3-18: Surface scaling on the west web of girder six.....	52
Figure 3-19: Exposed and corroded strands on the web of girder six.	53
Figure 4-1: Loading frame detail.	55
Figure 4-2: Flexural testing instrumentation setup.	58
Figure 4-3: The loading frame of the flexural test setup.	59
Figure 4-4: Strain gauge rosette on the web of girder at the point of loading.	61
Figure 4-5: Shear electronic instrumentation setup including strain and pi gauge rosettes.	62
Figure 4-6: Shear testing instrumentation setup.	63
Figure 5-1: Load versus displacement for flexural test one.....	69
Figure 5-2: Deflection over the length of the girder for various loads during flexural test one.	69
Figure 5-3: Flexural testing at the maximum deflection of girder one.	70
Figure 5-4: Flexural cracks at the mid-span region on the west side of girder one.	70
Figure 5-5: Load versus displacement for flexural test two.	72
Figure 5-6: Deflection over the length of the girder for various loads during flexural test two.	72
Figure 5-7: Long view of failure at the mid-span on the east side of girder two.....	73
Figure 5-8: Close up of the failure zone at the mid-span on the east side of girder two.	73
Figure 5-9: Load resistance versus displacement for flexural test three.....	75
Figure 5-10: Deflection over the length of the girder for various loads during flexural test three.	75
Figure 5-11: Comparison of pi gauge and strain gauge results for flexural test three.	76
Figure 5-12: Failure near the mid-span on the east side of girder three.	76
Figure 5-13: Load resistance versus displacement for shear testing of girder four.	80
Figure 5-14: Deflection over the length of the girder for various loads during shear test one.....	80
Figure 5-15: Failure near the quarter span on the west side of girder four.....	81
Figure 5-16: Failure near the quarter span on the east side of girder four.....	81
Figure 5-17: Load resistance versus displacement for the shear testing of girder five.....	83

Figure 5-18: Deflection over the length of the girder for various loads during shear test two.....	83
Figure 5-19: Failure near the quarter span on the west side of girder five.	84
Figure 5-20: Failure at the support on the west side of girder five.	84
Figure 5-21: Failure between the support and quarter span on the east side of girder five.	85
Figure 5-22: Diagonal cracking at the quarter span on the east side of girder five.	85
Figure 5-23: Load resistance versus displacement for shear test three.....	87
Figure 5-24: Deflection over the length of the girder for various loads during shear test three.....	87
Figure 5-25: Failure near the quarter span on the west side of girder six.....	88
Figure 5-26: Failure zone on the east side of girder six.....	88
Figure 6-1: Moment at various location for E1, E2, and E3 evaluation loading.	98
Figure 6-2: Shear at various locations for E1, E2, and E3 evaluation loading.	98
Figure 6-3: CHBDC rating factors at various locations along the length of girders one, two, and four.	100
Figure 6-4: CHBDC rating factors at various locations along the length of girder three.	101
Figure 6-5: CHBDC rating factors at various locations along the length of girder five.....	101
Figure 6-6: CHBDC rating factors at various locations along the length of girder six.	102
Figure 6-7: Moment at various locations for the HS-20 and HSS-30 truck loading.	105
Figure 6-8: Shear at various location for the HS-20 and HSS-30 truck loading.	106
Figure 6-9: AASHTO rating factors at various locations along the length of girders one and four.....	108
Figure 6-10: AASHTO rating factors at various locations along the length of girder two.....	108
Figure 6-11: AASHTO rating factors at various locations along the length of girder three.....	109
Figure 6-12: AASHTO rating factors at various locations along the length of girder five.	109
Figure 6-13: AASHTO rating factors at various locations along the length of girder six.....	110
Figure A-1: CHBDC evaluation level one, CL1-W truck and lane load [22].	119
Figure A-2: CHBDC evaluation level two, CL2-W truck and lane load [22].	120

Figure A-3: CHBDC evaluation level three, CL3-W truck and lane load [22].	121
Figure A-4: AASHTO LRFD design live load [24].	122
Figure A-5: AASHTO HS-20, HSS-25 and HSS-30 design truck and lane loading.	123
Figure A-6: AASHTO legal loads [24].	124
Figure A-7: AASHTO permit truck example [24].	125

LIST OF TABLES

Table 3-1: Girder sectional properties.	35
Table 3-2: Strand strength, pre-stress losses and final pre-stressing force.	38
Table 3-3: Theoretical calculations of nominal flexural capacity.	39
Table 3-4: Theoretical calculations of nominal shear capacity.	40
Table 3-5: Condition catalogue of each girder.	41
Table 5-1: Flexural testing results.....	67
Table 5-2: Comparison of experimental versus theoretical nominal flexural capacity.....	68
Table 5-3: Shear testing results.....	77
Table 5-4: Comparison of experimental versus theoretical nominal shear capacity.	78
Table 5-5: Experimental results from the compression strength tests.	89
Table 5-6: Concrete strength correction parameters.	90
Table 5-7: Increases in nominal flexural capacities due to the increase of concrete strength.	92
Table 5-8: Increases in nominal shear capacities due to the increase of concrete strength.	92
Table 5-9: Chloride ion content testing results.	93
Table 5-10: Hardened concrete air void property testing results.....	95
Table 6-1: Comparison of theoretical and experimental rating factors for girder one at the mid-span.....	103
Table 6-2: Comparison of theoretical and experimental rating factors for girder two at the mid-span.	103
Table 6-3: Comparison of theoretical and experimental rating factors for girder three at the mid-span.	103
Table 6-4: Comparison of theoretical and experimental rating factors for girder four near the quarter span.	103
Table 6-5: Comparison of theoretical and experimental rating factors for girder five near the quarter span.	104
Table 6-6: Comparison of theoretical and experimental rating factors for girder six near the quarter span.....	104
Table 6-7: Comparison of theoretical and experimental rating factors for girder one at the mid-span.....	111
Table 6-8: Comparison of theoretical and experimental rating factors for girder two at the mid-span.	111

Table 6-9: Comparison of theoretical and experimental rating factors for girder three at the mid-span.	111
Table 6-10: Comparison of theoretical and experimental rating factors for girder four at the quarter span.	111
Table 6-11: Comparison of theoretical and experimental rating factors for girder four at the quarter span.	112
Table 6-12: Comparison of theoretical and experimental rating factors for girder six at the quarter span.	112

1. INTRODUCTION

1.1 Overview

This thesis report contains seven sections. In this section the reader is introduced to the background history behind the project, is given the project objectives, and the scope of the research work. In the second section, a review of literature that pertains to the subject matter of the project is discussed. Definitions and fundamentals of concrete deterioration, material testing and bridge load rating methods are examined. A thorough specimen report is contained in section three. Here, a detailed description of the condition of each of the specimens as well as the girder properties is performed. The experimental test program is explained in section four. This includes the instrumentation and load configuration details, and test parameters. Section five summarizes the test results and compares them against the theoretically obtained values. Section six contains the load rating of the test specimens and compares the results using the theoretical values versus the experimentally observed values. Finally, section seven gives conclusions and recommendations.

1.2 Background

The six pre-tensioned concrete channel girders which were tested and discussed within this report were part of the Canadian National Railway overpass on the Trans-Canada Highway No. 1 (CN Over-pass on TCH Site No. 0709-00) east of Portage La Prairie and were constructed in 1965. The bridge structure was a four lane bi-directional (two lanes per direction of traffic) design. The three span overpass consisted of 16, 19810 mm long, 864 mm deep, 1219 mm wide girders per span. The girders were transversely post-

tensioned, simply supported on elastomeric bearing pads and topped with a 50 mm asphalt wearing surface on a hot-poured waterproofing membrane. The overpass was designed to AASHTO H-20 design truck and lane loading.

In 1989, rehabilitative works were required and carried out. These works included the installation of new expansion and fixed joints, approach and bridge guard rails, precast concrete median barriers, deck drains, asphalt overlay on top of the hot-poured waterproofing membrane, and minor abutment concrete modifications.

In the summer of 2006, UMA Engineering Ltd. was contacted by Manitoba Infrastructure and Transportation to inspect the Trans-Canada Highway rail line overpass. Many of the girders in the center span were said to be in poor condition. The webs had been subject to water leakage through the shear keys which caused the concrete to spall off; the loss of concrete ranged from 25 mm to 100 mm from the bottom of the webs. Longitudinal cracks were observed near the bottom of the webs as well. At the regions of significant web spalling, steel strands of the bottom layer were aggressively corroded or missing all together. Transverse cracks were seen on many of the interior diaphragm at mid height. Reflective cracking on the wearing surface along the shear keys was also observed as was a difference of elevation among the girders. It was concluded that the girders were no longer able to affectively distribute wheel loads to neighboring girders. A loading rating using the AASHTO load resistance factor rating (LRFR) method demonstrated that the bridge was not fit for service as the analysis did not yield a passing load and resistance factor rating for the HSS-25 or the HSS-30 design truck and lane loads.

Due to these aforementioned deficiencies, UMA Engineering Ltd. concluded that the existing girders would have to be replaced, and the structure as a whole was no longer adequate for heavy truck loading. It was recommended that the bridge would require significant rehabilitation and that it would be more economically viable to reconstruct the overpass. As a result, Manitoba Infrastructure and Transportation decommissioned the bridge which was later demolished and rebuilt.

1.3 Objectives

The primary objective of this research was to determine the remaining capacity of the 40 year old pre-tensioned girders in flexure and shear when subjected to monotonic loading. In addition, four different non-destructive tests were carried out including material sample testing and natural frequency determination. The material tests were completed to provide the in situ properties of the concrete such as strength, probability of steel corrosion, and susceptibility of the concrete to frost damage.

The capacities of each girder obtained from laboratory testing were compared against the standard theoretical analysis calculations. These theoretical and experimental capacities were further analyzed within the current North American load rating methods. Finally, the importance of this research will be discussed.

1.4 Scope of Work

The requirements of this project the University of Manitoba was asked to fulfill were:

- To test the capacity for flexural resistance of three of the six girders.

-
- To test the shear resistance of the remaining three girders.
 - To test 12 core samples, two from each girder for their compression strength.
 - To test 12 core samples, two from each girder for water-soluble chloride ion content and penetration.
 - To test 12 core samples, two from each girder to determine the air-void properties of the concrete.
 - To perform a load rating of each girder using the Canadian Highway Bridge Design Code (CHBDC Chapter 14).

Additional objectives that were carried out included:

- A bridge rating evaluation using the American Association of State Highway Transportation Officials Load and Resistance Factor Rating (AASHTO LRFR).
- A catalogue of the condition of each girder prior to testing.

It was felt that the completion of these tasks would be sufficient to determine the condition of the test specimens and provide valuable insight into the condition and behavior of in-service pre-stressed concrete channel girders.

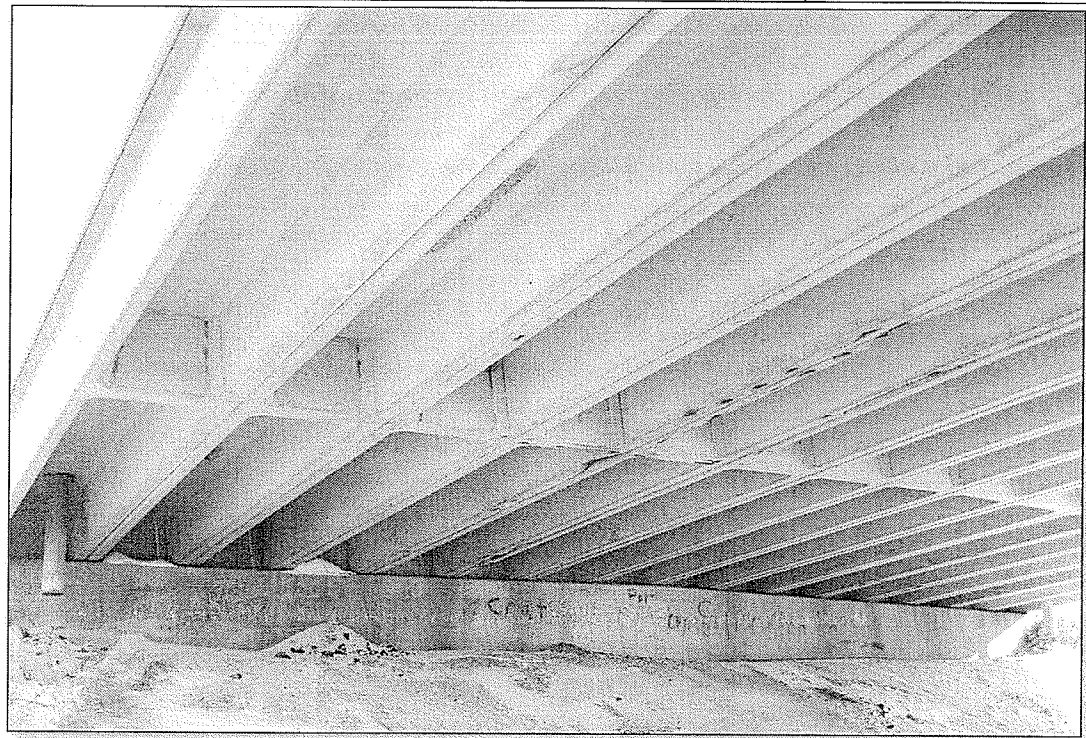


Figure 1-1: Underside of the north span of the Portage La Prairie CN overpass.

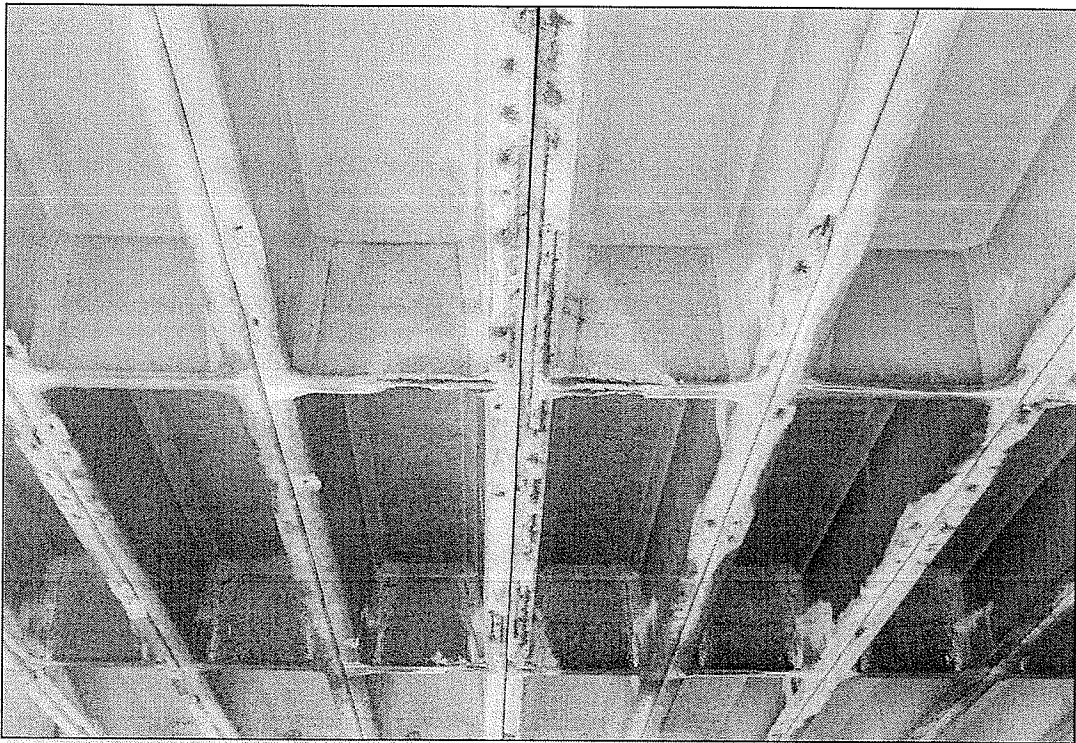


Figure 1-2: Underside of the center span of the Portage La Prairie CN overpass.

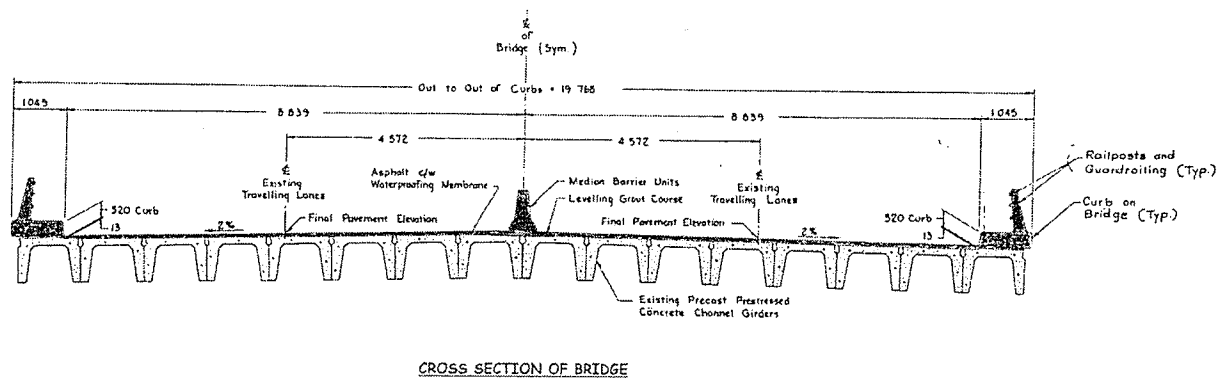
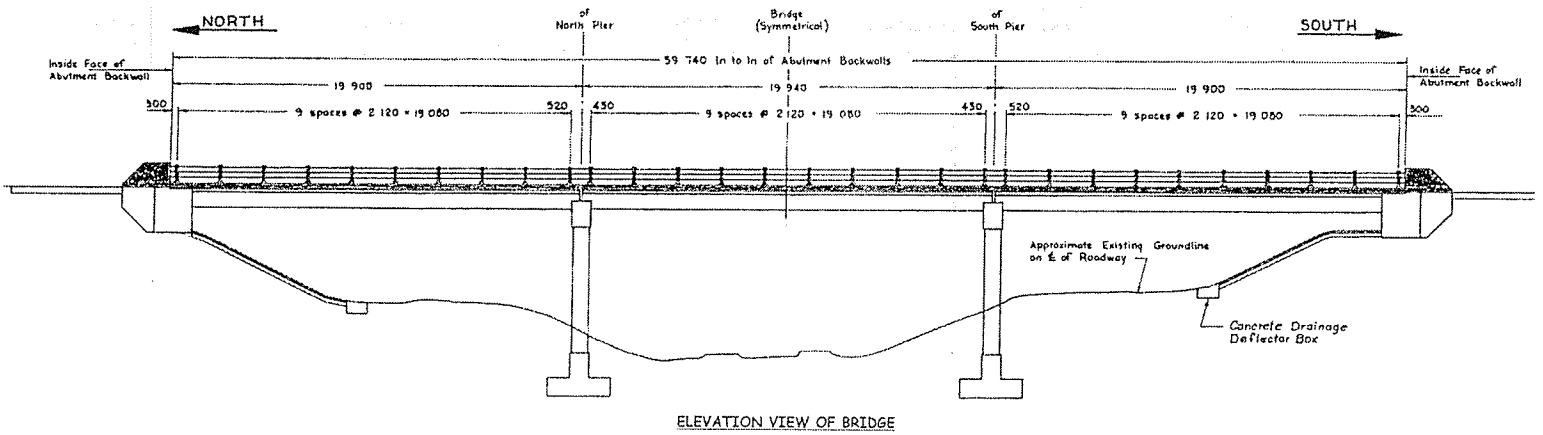


Figure 1-3: Portage La Prairie CN overpass elevation and cross section view.

2. LITERATURE REVIEW

2.1 Pre-tensioned Concrete Structural Members

The use of pre-stressed concrete for bridge applications has gained popularity over the last fifty to sixty years as they have allowed engineers to span greater lengths. Pre-stressed concrete bridges also have the advantage of economy over the life span of the structure. Both initial and operational costs are usually lower than other structural designs. Precast pre-stressed components are also easier to erect than cast-in-place components decreasing building time.

Pre-stressing is a method of concrete reinforcement where wire strands (typically seven wire low-relaxation) are tensioned with the aid of a stressing jack within a steel formwork where concrete is poured and then left to cure. The ultimate tensile strength of typical seven wire low-relaxation strands is 1725 to 1860 MPa. The strands are tensioned to 70 to 80 percent of this stress [1]. After twelve to sixteen hours of curing, the strands are cut and the force within the strands from tensioning is transferred to the concrete causing an eccentric compressive axial force within the member. The immediate effect is an elastic shortening of the member resulting in a small loss of pre-stressing force. The overall effect however, greatly increases the load carrying capacity.

To achieve this, the strands are positioned as far from the center of gravity as possible in the bottom of the member. This eccentric tension force counteracts the self-weight and superimposed dead loads resulting in an initial positive camber. To achieve favorable profile of strands closer to the girders' center of gravity, tendons may be singly and

doubly draped. In either case the eccentric axial force also serves to reduce stresses in the extreme tensile fiber of the member eliminating cracking during loading. At the same time it is undesirable to over tension the strands causing concrete crushing or compressive cracking. The stress in the extreme fiber (top or bottom) is given by the general equation [2]:

$$\sigma = \frac{P}{A} \pm \frac{Pe}{S} \pm \frac{M}{S} \quad (Eq. 1)$$

Where:

- σ = Stress
- A = Total cross-sectional area of the concrete
- e = Eccentricity of strands from the center of gravity of the member
- M = Moment cause by loading and self-weight
- P = Pre-stressing force
- S = Section Modulus

In order for a structure to meet service limit state, loads must not push the stress in the bottom tensile fiber beyond the allowable percentage of rupture strength of the concrete of the top compressive fiber beyond the allowable compressive stress at any point along the member at any time during its design life. This includes during the manufacturing and erection process where the members' orientation, location of support and condition of transportation vehicle may be different than in service [3].

There are several factors which decrease the force of the tensioned strands over time. These include creep and shrinkage of the concrete as well as relaxation of the strand. Under sustained compressive stresses, concrete has a tendency to incur gradual increases in strain; this is known as concrete creep [4]. Shrinkage on the other hand occurs when the concrete loses moisture and reduces in volume. Although this effect is visually imperceptible it does play a role in decreasing strand force. Strand relaxation is the reduction of stress in the strand while the strain is held constant. The factors of creep, shrinkage, and relaxation are interdependent and occur non-linearly adding to the complexity of the member and making it more difficult to accurately predict the member behavior at service limit state.

2.2 Bridge Damage and Deterioration

The major factors that contribute to the deterioration of bridge structures are the load spectra (weight, axle configuration and repeated loading) imposed on them as well as environmental factors [5]. The following two subsections will cover these topics and explain their role in the reduction of the life span of bridge infrastructure.

2.2.1 Truck Loading and Effects

The vast majority of Canada's bridge infrastructure was constructed between 1950 and 1965. Since then the standard truck and trailer (five to six axle truck) gross vehicular weight (GVW) has increased nearly 40 percent [6]. This can have negative implications in terms of increased moment and shear loads, fatigue loading, and dynamic vibration.

Increasing gross vehicular weight has an effect on flexural and shear live loads experienced by bridge infrastructure. This is detrimental to the health of bridges by pushing forces in the extreme member fibers beyond serviceability limit state causing cracking. This leads to the increased infiltration of moisture into the concrete via cracks. The significance of this will be examined in the next subsection. Additionally, a concrete bridge component which is repeatedly loaded beyond its service capacity has a greater propensity to give way to fatigue damage and failure.

Fatigue is exacerbated by increased axle loads and truck volumes. Fatigue strength is a property of structural members defined as the maximum percentage of the static load capacity that can be sustained over a given number of cycles [7]. Fatigue is the repeated loading of a structure which over time cause permanent and increasing internal damage provided the load repetition and their amplitudes are great enough. It should be noted that undamaged pre-stressed bridge components rarely succumb to fatigue as traffic loading induces stresses within the tolerable design range [8].

Advancements in material knowledge and technology over the last few decades have allowed engineers to design more slender longitudinal members. This, combined with heavier truck loads has increased the dynamic vibration of longitudinal bridge members. Increased vibration can become an issue of unnecessary repeated loading and fatigue. The current methods of design incorporating serviceability limit state (deflection to span ratio) do not adequately address the problem of vibration [9]. According to the Ontario Highway Bridge Design Code and Commentary 1983, "It is now well established that the

dynamic load allowance in a bridge is dependent on its first natural frequency” [9]. In other words, increases in frequencies of significant amplitude will create more repeated loading before the vibration has been damped. To mitigate this, a dynamic load allowance factor must be employed.

2.2.2 Environmental Damage

Presence of Chloride Ions in Concrete

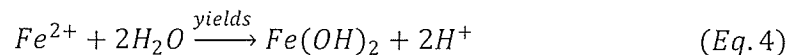
Chloride ions are a major contributor to the deterioration of reinforced and pre-stressed concrete structures. Chloride ions are found in de-icing salts and seawater. Structures located in climates where de-icing salts are required to remove ice from roadway surfaces such as Manitoba show vulnerability to corrosion at localized regions of the structure. These regions include expansion joints, anchorage zones, and spacing between beams. The effect of traffic and environmental factors can lead to joint failures allowing salts to penetrate through to the girders below. Largely, the ability of concrete to resist corrosion of the reinforcement within depends greatly on the concretes’ permeability [10]. Permeability is influenced, in service, mostly by freeze-thaw damage [10]. This effect will be discussed in the next subsection.

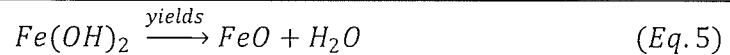
There are three types of corrosion of pre-stressing steel: uniform corrosion, pitting corrosion and stress corrosion. Uniform corrosion affects the surface of the steel and occurs when steel is unprotected and exposed to the environment. Pitting corrosion results from dissimilar materials and environments which cause stress concentrations.

Cracking corrosion of the steel generally originates at the point of a corrosion pit and leads to the rupture of wires due to high localization stresses.

Generally, the corrosion of steel in concrete is a function of the alkalinity in the environment surrounding the steel. In a higher pH environment, the tendency of steel to corrode is very low. Yet, steel corrosion can still occur in an alkali environment when in the presence of chloride ions. This mechanism of corrosion is an electrical-chemical reaction where chloride ions serve as a catalyst and allows the formation anodic and cathodic regions in the steel. This electro-chemical reaction does not require two dissimilar metals but just dissimilar chemical composition in the steel.

Iron in the presence of water and oxygen reverts to its most stable state, iron oxide, losing two electrons in the process. The region of the steel which has converted to iron oxide is positively charged. The unchanged steel becomes positively charged by comparison. To continue this anodic reaction, the negative charge needs to be neutralized. This requires the conversion of water and oxygen into hydroxide ions. A precipitate is formed from the hydroxyl and iron ions. If exposed to oxygen, the precipitate forms ferric hydroxide. Further exposure to oxygen and water forms ferric oxide which is also known as rust. This process is shown with the following chemical equations:





To reduce or prevent this effect, a suitable reinforcement should be used such as fiber reinforced polymer bars or stainless steel and a good quality concrete with adequate cover. The permeability of concrete cover increases exponentially with the water/cement ratio [11]. Therefore to reduce chloride penetration it is beneficial to use concrete with a lower water/cement ratio. Vibration of the concrete mix during pouring is also advantageous not only for workability and compactability but also for the impermeability and resistance to frost damage. The thickness of concrete cover over the reinforcement lengthens the path of penetration and decreases the rate by which the chloride and oxygen can migrate into the concrete. The relationship between cover of concrete and deterioration of steel is a function of time [11]. Figure 2-1 illustrates the predicted deterioration with respect to various cover depths over 11, 14, and 16 years. From the figure, the data presented suggests that a concrete cover of at least 50 mm be designed to reduce steel and consequently concrete deterioration of the structure over its service life.

In Figure 2-2, the probability of steel corrosion initiation is displayed as a function of percent chloride concentration per weight cement. A chloride ion concentration of one percent or less does not have a significant impact on steel corrosion. However, a chloride ion concentration of 1.5 percent or greater is likely to cause corrosion.

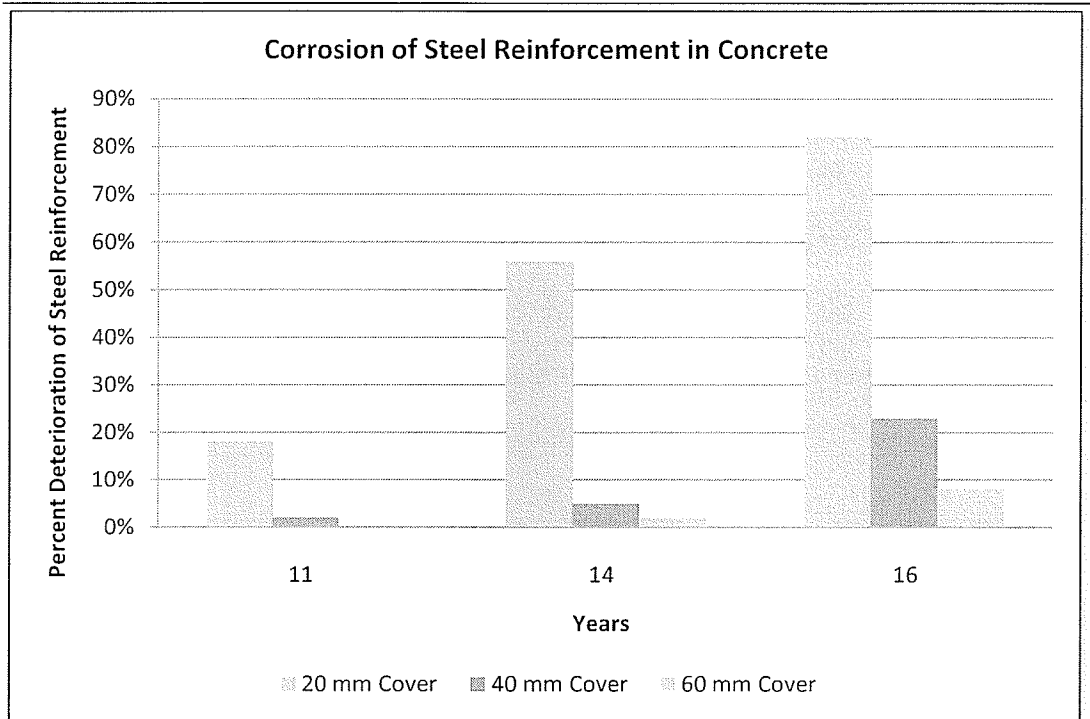


Figure 2-1: Corrosion of steel reinforcement in concrete at various cover depths over time [12].

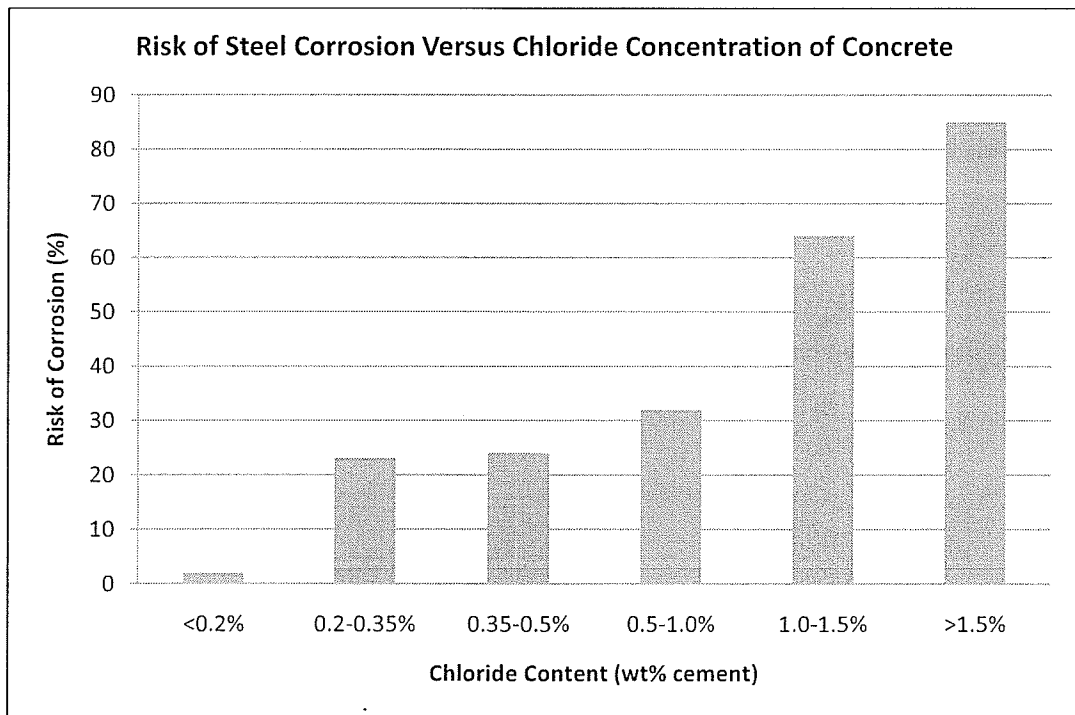


Figure 2-2: Probability of steel failure versus chloride ion concentration of concrete [13].

Air Void Content and Freeze-Thaw Damage

All concretes contain a small amount of air as a result of the mixing operations. These air voids can range in diameter from 0.01 mm to 10 mm in size [14]. Typically, large diameter voids (entrapped air) are irregular in shape whereas smaller ones (entrained air) tend to be spherical. An average sized air void is about 0.10 mm the entrained air generally comprises 1 to 3 percent of the total concrete volume [14].

To understand the role air voids play it is necessary to be familiar of the microstructure of concrete paste. The concrete paste encompasses roughly 25 to 30 percent of the total concrete mix [14]. The paste is made up of paste gels, interstitial pores between the paste gels where moisture is incapable of freezing and capillaries where moisture is capable of partial freezing. The interstitial pore diameters range in size from 5×10^{-7} to 25×10^{-7} mm while capillaries are an order of magnitude larger, typically ranging from 10×10^{-6} to 50×10^{-6} mm [14]. Figure 2-3 depicts the physical location and the size of the various micro-structural components within the concrete matrix.

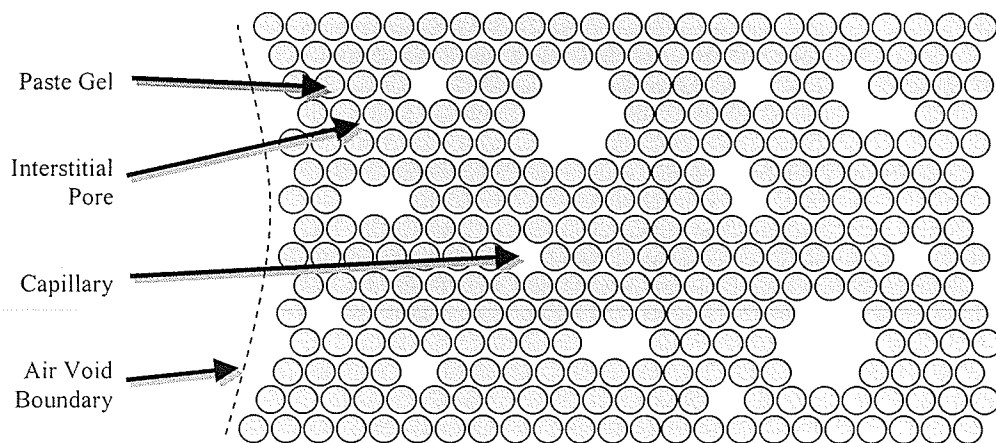


Figure 2-3: The microstructure of concrete paste [14].

Air voids are necessary to release interstitial moisture pressures within the paste. Water is released from the interstitial pores to the capillaries which are sufficiently small enough to prevent normal crystal growth. Water and ice within the capillaries has a higher free energy than in the air voids and therefore has higher interstitial pressures. Crystal growth occurs normally within the air voids and the pressures caused by freezing of moisture are significantly less. Each air void acts to protect a zone of cement paste around it from damage. Therefore it is highly beneficial to have a sufficient number of well distributed air void within the concrete mix to reduce the damage. This is shown in research completed by T. Cho in 2007, which compared entrained air-pore percentages of 0.8% and 8.4% and found that at lower air entrained percentages, there was a 70% increase in freezing strain [15]. Stresses caused by ice formation can crush the paste resulting in surface scaling and internal cracking.

Surface scaling occurs from the loosening of aggregate due to paste disintegration and results in a reduction of concrete strength. The concrete has a specific resistance to freezing and subsequent thawing; however after 200 to 300 cycles, scaling become evident [15]. Experimental studies have shown however, that after hundreds of freeze-thaw cycles, scaling of concrete only reduced the concrete mass by five percent [15]. The more serious damage is thought to occur internally. Internal cracking caused by accumulated micro-cracking can result in an increase moisture permeability of the concrete and eventually lead to total deterioration.

2.3 Non-destructive Testing

Non-destructive testing are tests which do not have a negative structural impact on the bridge resistance capacity and is a valuable measure by which an engineer can assess the in situ condition of a bridge which may require repair, maintenance or replacement. The methods covered within this report in are concrete strength testing, air void and spacing testing, and chloride ion concentration and penetration testing. Beyond this, material analysis often used to define the physical properties of the concrete and can present the engineer with a true picture of how a bridge is performing. Sampling from the in-service bridge should only be taken from a location that is not crucial to its structural integrity.

2.3.1 Concrete Strength and Compressive Testing

Compressive strength (f'_c) is one of the most, if not the most important property of concrete. Usually, a compression test is carried out when the compressive strength of a concrete structure is suspected to be less than that of design such as the case of an underperforming bridge. Generally though, concrete increases in strength as it continues to age. This increase in strength is represented by the following equation [16]:

$$f'_{c(t)} = f'_{c(28)} \left(\frac{t}{4 + 0.85t} \right) \quad (\text{Eq. 6})$$

Where: $f'_{c(t)}$ = Compressive strength at time “t” (MPa)

$f'_{c(28)}$ = 28 day compressive strength (MPa)

t = Time (days)

The objective behind this testing is to determine the force required to break a concrete cylinder; knowing the area, this force is converted to a strength value. To perform the test, a concrete core sample which is free of reinforcing steel or other irregularities is placed under a monotonically increasing compressive load until failure. When loading the core, it is important to maintain a slow loading rate. Testing of the cores should be conducted in accordance with CSA or ASTM standards.

The CSA standard A23.2-14C details the necessary steps for obtaining and testing drilled cores for compressive strength. As specified, specimens should have a diameter three times that of the nominal maximum aggregate size and have a length of no more than twice the diameter [17]. Those samples with a length-to-diameter ratio less than two require a correction factor to be applied to the measured compressive capacity. (The correction factor table can be found within the standard.) The standard specifies that the sample be cored perpendicular to a horizontal surface so that it may be tested in the axis of loading. The standard also requires the specimen ends to be capped or ground prior to tests for an even surface to load [17].

The mean concrete strength obtained from experimental testing may require correction to reflect the core diameter, sampling size, and moisture condition of the sample. Core samples less than 100 mm in diameter require adjustment to approximate the equivalent strength of 100 mm diameter cores [18]. The equivalent strength then must be increased by eight percent for cores soaked in water for 40 hours or reduced by five percent for cores that have been air dried for seven days prior to testing [18]. The necessary equation

to make these corrections is contained in Annex A14.1 (*Equivalent Material Strengths from Tests of Samples*) of the CHBDC [18].

$$f'_c = 0.9\bar{f}_c \left[1 - 1.28 \left[\frac{(k_c V)^2}{n} + 0.0015 \right]^{0.5} \right] \quad (Eq. 7)$$

Where: f'_c = Equivalent specified compressive strength (MPa)
 \bar{f}_c = Average core strength (MPa)
 k_c = Coefficient of variation modification factor
 n = Sampling size
 V = Coefficient of variation

The in situ compressive strength can also be necessary for an accurate determination of load resistance factor rating which will be discussed later on.

2.3.2 Chloride Ion Content Testing

As previously discussed, the effect of chloride ions on embedded steel is destructive in nature. The water-soluble chloride ion content in concrete can be determined through testing outlined in CSA standard A23.2-4B. To reiterate, the existence of chloride in concrete acts as a catalyst instigating the corrosion of the steel. Salts can infiltrate the concrete surface through pores and reach the steel within. If no significant cracking can be seen, yet corrosion is predicted, an engineer might request this test to provide necessary insight to the probability of corrosion occurring.

The CSA standard (A23.2-4B) utilizes a chemical analysis for the determination of chloride ions present within a given concrete sample. The equation to find the chloride ion content [19] is:

$$Cl, \% = \frac{3.5453VN}{M} \quad (Eq. 8)$$

Where:

- Cl = Percent of chloride ion content
- M = Mass of sample (g)
- N = Exact normality of 0.05 N AgNO₃ solution
- V = Volume of 0.05 N AgNO₃ solution used (ml)

To conduct this test, a small amount of concrete must first be ground into a fine powder. This can be done for example with the use of a hammer-drill fitted with a pulverizing bit. It is important that the sample must not be contaminated so an untainted means of collection is to be used. Depending on the standard by which the test is to be carried out, the pulverized concrete is required to pass through a specific sieve screen size. For the CSA test, the sample is required to first pass through a 315 µm screen, then be transferred to a mortar and combined with 10 ml of hot water to be further pulverized by pestle to pass a 160 µm sieve. Three grams of the slurry are boiled in water for five minutes and left to stand for 24 hours. At this point, the sample is titrated with a silver nitrate reagent (0.05 N solution) and followed by potentiometric monitoring with the goal of achieving a reading of -60 mV [19]. Once reached, the known volume of reagent used is put into the equation and the percent of chloride ion content within the concrete is found.

2.3.3 Determination of Air Void Properties in Hardened Concrete

Guidelines for this test can be found in the ASTM C 457-98. The air void ratio within hardened concrete is directly related to concrete damage via cyclic freeze thawing. This test is a microscopic examination of air content within the concrete. There are two methods for determining the air void content, the linear-traverse method and the modified point-count method. For these methods, the use of a microscope and computer are required. The image seen through the microscope is transferred to a computer where a grid of evenly spaced horizontal and vertical lines is placed over the image. On the image, the portions of the cement paste and voids appear as contrasting colors. For the linear-traverse method a computer program measures the length across each void and non-void that intersects a portion of the grid. The program then averages the lengths of these intersections and computes the air void ratio of the system. The modified point-count method sums the number of intersection points of air voids and cement paste and uses that information to calculate the air void ratio of the sample. Figure 2-4 displays a finely lapped slice of concrete ready for analysis. The white arrows indicate the location of an air void within the hardened concrete matrix.

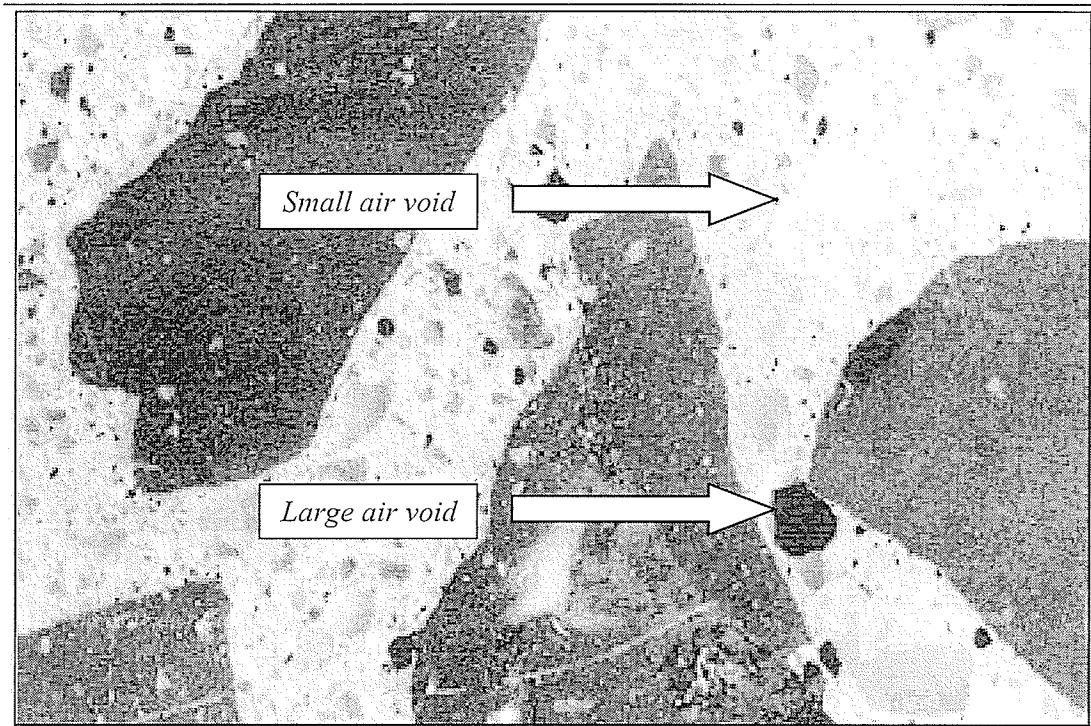


Figure 2-4: Surface of a finely lapped slice of concrete containing 5.6 percent total air voids [14].

This testing also measures other important parameters including the spacing factor, specific surface and void frequency. The spacing factor has the greatest bearing on the durability of the concrete as large spacing may not provide adequate protection of the paste. A desired spacing factor is in the range of 100 to 200 μm with a maximum recommended value of 260 μm [20,21]. The specific surface is the surface area of the voids divided by their volume and should typically range from 24 to 43 mm^{-1} [14]. The void frequency is crucial for the determination of the previous two parameters. The void frequency is the number of voids per unit of traverse length. A satisfactory void frequency should be larger than 315 voids per meter along the traversing length [21].

2.4 Bridge Evaluation and Load and Resistance Factor Rating

Bridge owners perform load ratings for three main reasons. First, although bridges are now designed to last 75 years, bridges will deteriorate to some extent over its life time. This generally leads to a reduction of load carrying capacity. A load rating analysis is required when deterioration occurs to ensure the structure has adequate strength to perform safely. Second, bridges which have been in service for a substantial amount of time were designed using lighter live load weights and axle configurations as well as different design specification. Yet, regardless of the design methods used, bridges are load rated to today's standards to ensure safety. Finally, a load rating would be performed in the case where it is necessary for vehicles carrying loads over the legal weight restriction to cross a bridge. This permit required traffic can reduce the life expectancy of a bridge and can cause permanent structural damage if a load rating is not carried out.

2.4.1 Canadian Highway Bridge Design Code Bridge Evaluation

This section will describe the CHBDC bridge evaluation as it pertains to pre-stressed concrete structures. As outlined in the CHBDC Section 14, the purpose of load rating is to evaluate an existing bridge and determine its ability to carry a specified load safety [22]. This ability to carry load is defined as the un-factored nominal resistance of an element or joint within the bridge. There are three levels of bridge evaluation. Level one is the evaluation of a bridge in its ability to carry a three-unit vehicle such as a rocky mountain double or turnpike double (in normal traffic). Level two is the evaluation of a bridge in its ability to carry a two-unit vehicle such as a typical tractor-trailer (in normal

traffic). Level three is the evaluation of a bridge in its ability to carry a single unit vehicle, specifically trucks, buses or cars (in normal traffic). Figures A-1 through A-3 in the appendix display the specification detail of these evaluation vehicles. Normal traffic is defined as any traffic other than vehicle operating under some sort of permit whether for weight or size.

When determining capacity, stability and load posting, all bridges shall be evaluated using ultimate limit states [22]. This includes ultimate limit state methods using load and resistance adjustment factors, the mean load method or load testing methods. For cases of masonry abutment, masonry piers, and masonry retaining walls, or in the case of any structure where cracking could be detrimental to its stability, a serviceability limit state is to be used. Fatigue limit state shall be carried out if a particular member is fatigue prone or there is significant evidence of fatigue observed during inspection [22].

It is necessary that an inspection of the bridge be completed in order to assess the condition and integrity of all bridge elements. This is important so that damaged or deteriorated components will be considered properly in the evaluation. Determination of material strengths such as minimum yield strength of reinforcing steel, tensile strength of pre-stressing steel, and compressive strength of concrete is also required for proper evaluation. These can be found from (a) the original construction plans, (b) analysis of tests samples obtain from the bridge (for example, a core sample), (c) by age estimation or (d) by another approved method. These are required for a proper resistance calculation of the structure which should be performed using the CHBDC.

Once the nominal resistance has been calculated the loading, both dead and live, is considered. Dead loads include the weight of the bridge member itself and all other permanent components such as utilities, barrier walls, and surfacing and fall into three classes. Class one (D1) includes the load of factory made components and cast-in-place concrete excluding decks. Class two (D2) includes the load of the deck as well as non-structural components. Class three (D3) includes the bituminous surfacing at an assumed thickness of 90 mm. Live loading, as stated above, is categorized into three-unit vehicles, two-unit vehicle and single unit vehicles.

Permit loads are divided into the following classes: Annual or project (PA), bulk haul (PB), controlled (PC), and single trip (PS). Taken from the code these are defined as: Annual or project (PA) vehicles are authorized by permit on an annual basis or for the duration of a specific project, bulk haul (PB) vehicles are authorized by permit to haul bulk divisible loads where axle loads are not to be exceeded but gross vehicle loads may, controlled (PC) vehicles are authorized by permit to carry an indivisible load under supervision. There are no special loading specifications as all other traffic is excluded during the movement of this load over a bridge. Single trip (PS) vehicles are authorized by permit for a single trip without supervision [22].

The CSA-S6-06 makes special provision for dynamic loading and multiple lane loadings as well. If the chosen truck model includes lane loading then no dynamic load allowance need be applied. If the truck only loading model is used then one must apply a dynamic load in accordance with Clause 3.8.4.5 of the code. In the case where multiple lanes are

loaded it is necessary to apply a portion of that load to the members of the lane you are examining. The extent to which the loading is to be applied laterally is defined in Table 14.3 of the code.

To find dead and live load factors it is first necessary to determine a target reliability index value (β). The target reliability factor represents the level of safety provided by the bridge elements and depends on the behavior of the bridge which includes system behavior, element behavior, and inspection level [23]. The load factors are statistically derived and represent reliability under extreme scenarios of normal traffic loads in Canada [23].

Once material strength, loading, and all other factors are known, the live load capacity factor can be calculated. This factor is a ratio of resistance less dead loads to live loads where a value greater than one is the desired result. The general equation for live load capacity [22] is:

$$F = \frac{UR_r - \Sigma a_D D - \Sigma a_A A}{a_L LL(1 + I)} \quad (\text{Eq. 9})$$

Where:

- A = Force effects due to addition loads (wind, creep, etc.)
- D = Nominal unfactored dead load
- F = Rating factor
- I = Nominal unfactored dynamic component of live load
- LL = Nominal unfactored static live load

R_r = Factored resistance of structural component

U = Resistance adjustment factor

α_A = Load factor for force effects due to addition loads (wind, creep, etc.)

α_D = Dead load factor

α_L = Live load factor

Alternatively, the mean load method for ultimate limit states can be used. This method is not based on dead and live load factors as is with the general method of load rating. Instead, it uses coefficients of variation and bias coefficients based on statistical parameters to yield the load factor. The CHBDC commentary provides these parameters to be used with this method. This method can be used in conjunction with in situ test data to refine the statistical parameters. Although gathering data through non-destructive load testing can be expensive and generally recommended for special bridge evaluations, it has the ability to dramatically increase the given load rating of a bridge. In one study by the Ministry of Transport of Ontario in 2005 it was found that while the load and resistance factor method and the mean load method using the default code parameters were comparable, using the mean load method in conjunction with live load data yielded a factor rating 57 percent greater than the other two methods [23]. The equation of mean load factor method [22] is:

$$F = \frac{\bar{R} \exp[-\beta(V_R^2 + V_S^2)^{0.5}] - \Sigma \bar{D}}{\bar{L}} \quad (Eq. 10)$$

Where:	\bar{D}	= Mean dead load effect
	F	= Rating factor
	\bar{L}	= Mean static and dynamic live load effect
	\bar{R}	= Mean resistance
	V_R	= Coefficient of variation for resistance
	V_S	= Coefficient of variation for total load
	β	= Target reliability index

Once the rating factor is calculated a course of action can be taken. The bridge may remain in service, require load posting, or require decommissioning. For values of F greater than or equal to 1.0 for evaluation level one the bridge is determined to be able to resist required capacity and no posting is required. A value of F between 1.0 and 0.3 for evaluation level one, triple posting is required. For an F value less than 0.3 for evaluation level 1 and an F value greater than 0.3 for evaluation level 3, single posting is required. For an F value less than 0.3 for evaluation level 3, it is recommended that the bridge be closed.

2.4.2 AASHTO Load and Resistance Factor Rating

In 2001, AASHTO adopted the new Guide Manual for Condition Evaluation and Load and Resistance Factor Rating (LRFR) of Highway Bridges. This manual reflects current technological advances and builds on the structural reliability approach used in load and resistance factor design (LRFD). Although the LRFD focuses on the design of bridges, the LRFR is a parallel companion to load rate bridges in service. The LRFD and LRFR

are consistent with other bridge design codes in Asia, Canada and Europe. The general goals of the LRFD and LRFR are to reduce maintenance and repair, avoid over design and increase the level of safety of American bridges.

The LRFR rating method rates bridges at two levels: inventory and operating. Under the inventory level evaluation the live load factor (γ_L) is 1.75 whereas the operating level evaluation live load factor is 1.35. The inventory level evaluation rates bridge performance based on standard design loads with respect to the bridge condition. It is accepted that a bridge which passes the inventory level evaluation can accommodate this loading for an indefinite period provide no further environmental deterioration occurs. The operating level evaluation rates bridges on the maximum permissive live load the bridge can remain operational and safe. It should be noted that loads that only pass the operating level evaluation can possibly decrease the life of the structure if applied frequently.

Within the inventory and operating evaluations three limit states are used in the load rating. These include strength, service, and fatigue and are incorporated to ensure safety and serviceability of the structure. The strength limit state evaluation requires the capacity of the structure to resist the permanent and live loads. The service limit state requires the stresses and strains to produce no cracking or deformation. The fatigue limit state evaluation is a check for cyclic stress to ensure minimal cracking due to fatigue. The strength limit state is most crucial as it directly relates to the bridges' overall safety while the service and fatigue limit state analysis may be conducted if necessary. With

regards to pre-stressed concrete components, strength I and service I and III limit states are required for the load rating analysis. The strength I limit state evaluation analyzes a basic load combination relating to the normal use of a bridge. The service I limit state evaluation analyzes permit load combinations for normal operation of the bridge and for checking compression in pre-stressed concrete. Service III analyzes load combinations relating to tension in pre-stressed concrete during service.

The principle equations as found in the AASHTO *Guide Manual for Condition Evaluation and Load and Resistance Factor Rating of Highway Bridges* [24] are as follows:

$$RF = \frac{C - (\gamma_{DC})(DC) - (\gamma_{DW})(DW) \pm (\gamma_P)(P)}{(\gamma_L)(LL + IM)} \quad (Eq. 11)$$

$$C = \phi \phi_C \phi_S R \quad (Eq. 12)$$

Where:

- C = Factored member resistance
- DC = Unfactored composite and non-composite dead loads
- DW = Unfactored wearing surface dead loads
- IM = Dynamic component of live load
- LL = Live load effect
- RF = Rating factor
- R = Member resistance
- γ_{DC} = Load factor for force effects due to composite and non-composite dead loads

γ_{DW} = Load factor for force effects due to wearing surface dead loads

γ_P = Load factor for force effects due to other permanent loads

γ_L = Live load factor

φ_c = Condition factor

φ_s = System factor

φ = LRFD resistance factor

Before beginning a bridge evaluation a thorough field investigation is required. This will provide data on the condition of the structure and minimize the possibility of oversights by the evaluator. In addition, the evaluator is required to calculate the nominal member resistance (R_n) of the structure using the AASHTO LRFD Bridge Design Specifications. The present condition must be taken into account within these calculations.

The structure capacity (C) is a product of the nominal member capacity and the three resistance factors ($\varphi_c, \varphi_s, \varphi$). The general resistance factor (φ) which is used in the LRFD accounts for uncertainties of an element in satisfactory condition. The condition factor (φ_c) is applied to factor in uncertainties due to deterioration. This value ranges from 1.00 for satisfactory condition to 0.85 for poor condition. The system factor (φ_s) accounts for the structural system redundancy. Redundancy relates to the ability of a bridge to carry load after deterioration has occurred. A bridge with a more redundant structural system allows the engineer to be less conservative. Once structural resistance has been established, the loading must be considered.

The live loading (*LL*) is spread over three evaluation levels. First is the design load rating using the HL-93 scheme which consists of the HS-20 design truck or tandem axle and a uniformly distributed design lane load; the heavier of which, governs. Where necessary the evaluator may decide to in the evaluation loading to the HS-25, HSS-25, HS-30 or HSS-30 AASHTO design truck. Within Manitoba the HSS-30 is the chosen design load for bridges on the Trans-Canada Highway. The second level evaluation is legal load rating consisting of the type 3 unit (for short bridges), type 3-S2 unit (for medium span bridges) and the type 3-3 unit (for long span bridges). The third level evaluation is permit loading which is carried out for vehicles above the legal weight restrictions. The classification of these is similar to the CHBDC. Figures A-4 through A-7 in the appendix illustrates the specifications of each of the three loading distinctions.

It should be noted that the live loads described in the above paragraph are static loads. It is necessary to consider the dynamic effects of these live loads. Generally, the truck load is multiplied by a value of 1.33 to account for the dynamic effect heavy trucks transfer to the longitudinal bridge components as they travel over them. In cases where the longitudinal members are greater than 12 meters in span length with a favorable approach and deck conditions, the dynamic load allowance (*IM*) may be decreased.

Bridges that pass the inventory level with the design load require no further evaluation. In other words, all bridges that pass the inventory level with the HL-93 design load will have adequate capacity for AASHTO and state legal loads. However, bridges which only pass the operating level may not necessarily be adequate for legal loading and each legal

loading truck will need to be analyzed. In the case of a bridge failing the legal loading evaluation, the bridge may have to be repaired and/or load restricted (posted) or be taken out of service all together. A bridge that fails the permit loading evaluation is not required to be taken out of service. It is merely indicative that the particular permit load evaluated cannot safely traverse the bridge.

3. SPECIMEN REPORT

This section will discuss all the important girder properties including dimensions, reinforcement details, theoretical losses in pre-stressing, theoretical shear and flexural capacities, and catalogue the condition of each girder prior to testing.

3.1 Girder Properties

The test specimens were pre-stressed concrete channel girders cast in 1965 to act as the primary longitudinal load bearing members. The girder dimensions were 19810 mm long by 864 mm deep by 1219 mm wide. The flange depth and bottom web width were 152 mm. The design compressive strength of the concrete after 28 days of curing was 37.92 MPa.

The pre-stressing reinforcement consisted of 20, 13 mm diameter strands stacked in rows of two, 50 mm apart located in the bottom portion of each web with 50 mm of cover on the bottom and exterior sides. In addition, the girder contains 14, 13 mm diameter singly draped strands stacked in one row of one and three rows of two with 50 mm of cover on the top and exterior sides also located in the webs. All strands were seven-wire strands with a tensile strength of 1724 MPa. The initial force in each strand was 112 kN.

The reinforcement included five longitudinal 13 mm diameter bars. Three were located at the top of the flange at the cross section center and 305 mm of either side of center. Two bars were located at the bottom of the flange 140 mm away from center. All bars had a cover of 50 mm. The stirrup configuration consisted of u-shaped 13 mm diameter

stirrups 381 mm on center throughout the girder. The flange negative moment steel consisted of 13 mm diameter u shaped bars at 381 mm on centre and the flange positive moment steel consisted of 13 mm diameter hat bars at 191 mm on center.

The girders also had ducts at the end block and third-span locations which were used to post tension the girders together. Below, the section properties have been tabulated.

Table 3-1: Girder sectional properties.

Property (and units of measure)	Value
Moment of inertia (mm^4)	31.4×10^9
Cross-sectional area (mm^2)	457986
Distance from center of gravity to bottom, Y_{bottom} (mm)	539
Distance from center of gravity to top, Y_{top} (mm)	325
Mass (kg)	24195
Modulus of Elasticity of Concrete, E_c (MPa)	28899
Depth to pre-stressing @ mid-span, d_p (mm)	614
Pre-stress modulus of elasticity, E_p (MPa)	197000
Area of pre-stressing, A_p (mm^2)	3159
Depth to steel reinforcing, d_s (mm)	69
Modulus of elasticity of reinforcing steel, E_s (MPa)	200000
Area of steel, A_s (mm^2)	633

Schematics of the girder dimensions, reinforcement details and the pre-stressing details are displayed in Figure 3-1 and 3-2.

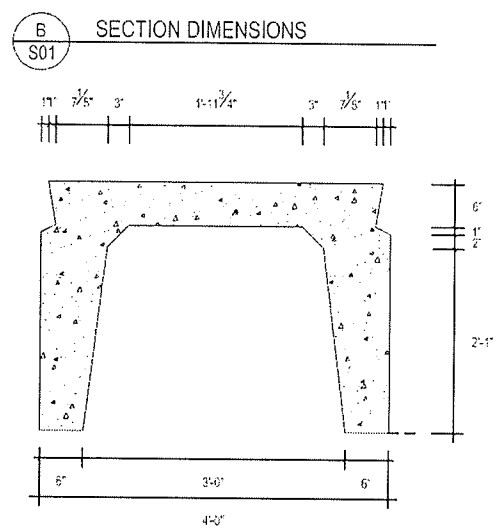
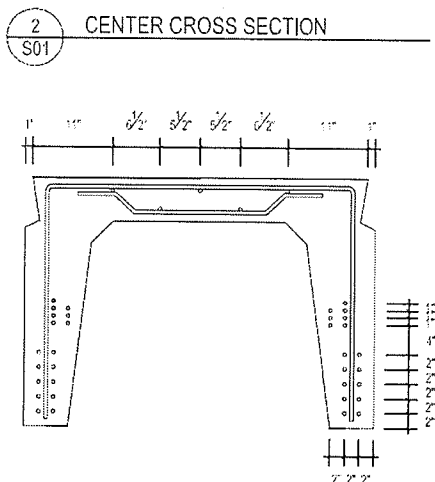
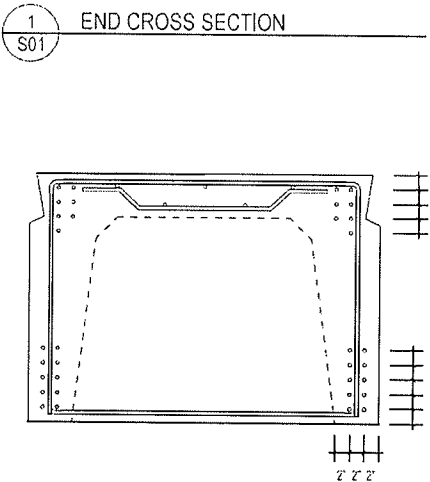
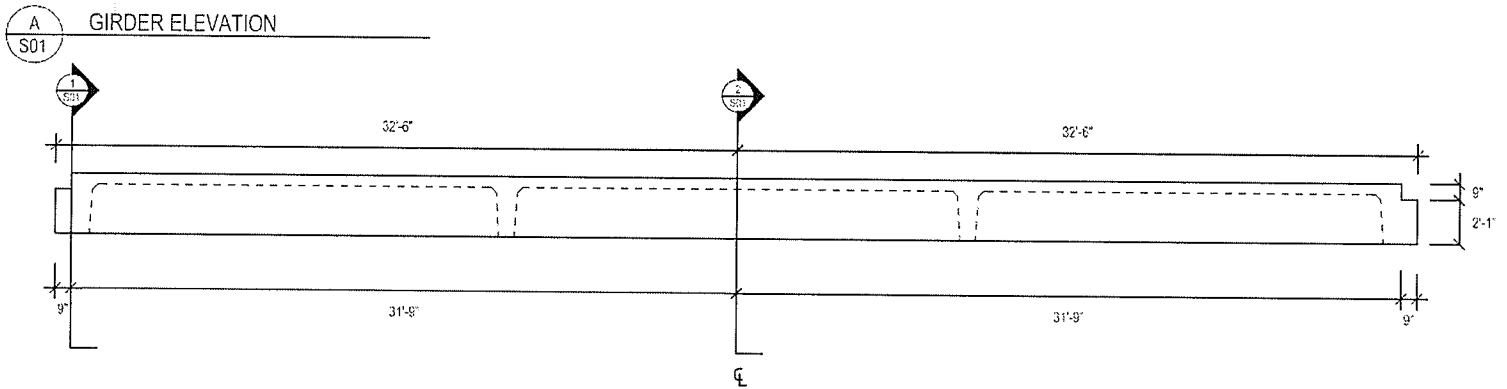
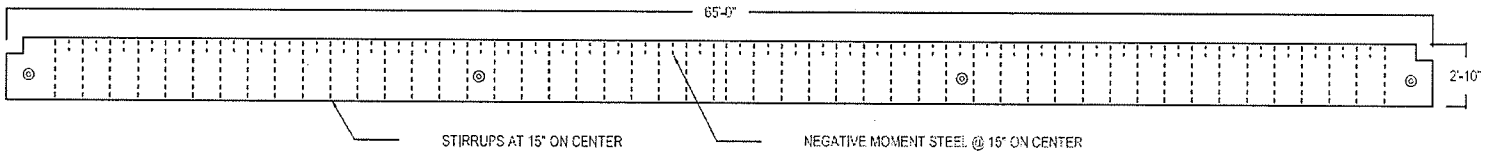


Figure 3-1: Schematic of elevation and cross sectional profiles.

A
S02 ELEVATION VIEW: STIRRUP DETAIL



B
S02 ELEVATION VIEW: PRESTRESSING DETAIL

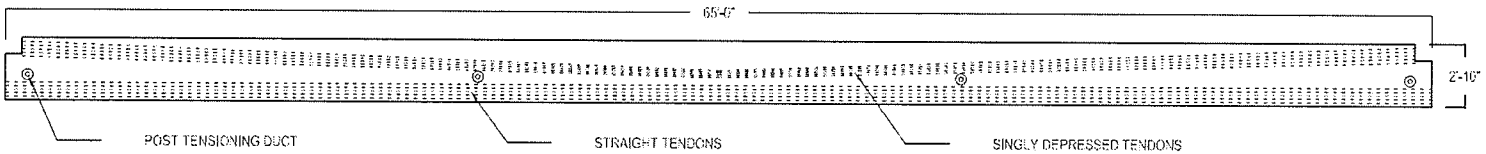


Figure 3-2: Stirrup and pre-stressing detail.

3.2 Theoretical Calculations

This section will cover the theoretical calculations including the initial and long-term pre-stress losses, the flexural moment, and shear force capacity. All theoretical calculations were carried out in accordance with the AASHTO LRFD Bridge Design Specifications.

3.2.1 Theoretical Pre-stressing Force Losses

From the original design drawings, the strand tensile strength was taken as 1724 MPa. The jacking stress was 70 percent of ultimate strength and calculated as 1207 MPa. Anchorage seating losses were ignored as these can be compensated for before casting. The losses before transfer due to elastic shortening equated 111 MPa. Total pre-stress losses, which include, losses before transfer, creep, shrinkage, and relaxation, amounted to 320 MPa thereby yielding a final pre-stress tension of 887 MPa. Based on the pre-stressing area of 3159 mm², the final pre-stress force was calculated to be 2802 kN. These results are summarized in Table 3-2 below.

Table 3-2: Strand strength, pre-stress losses and final pre-stressing force.

Property (and units of measure)	Pre-stress Value
Ultimate Strand Strength, f_{pu} (MPa)	1724
Total Pre-stressed Lost at Transfer, f_{pt} (MPa)	111
Pre-stress Lost After Transfer (MPa)	320
Jacking Stress @ 70% (MPa)	1207
Stress @ Final, f_c (MPa)	887
Force @ Final, P_e (kN)	2802

3.2.2 Theoretical Flexural Moment Capacity

Strain compatibility was followed using AASHTO LRFD Bridge Design Specifications which prescribes an ultimate concrete strain (ϵ_{cu}) of 0.003 to determine the flexural capacity. Two girder condition cases were analyzed; these included an ideal scenario (observed on girders one and two), and a scenario of two strands missing from the bottom layer of reinforcement and 50 mm of concrete loss from the bottom of the webs (observed on girder three). Using the concrete strength listed on the design drawings the nominal flexural capacities were calculated to be 2771 and 2565 kNm, respectively. These results are tabulated below in Table 3-3.

Table 3-3: Theoretical calculations of nominal flexural capacity.

Girder Number	Girder Condition	Design Concrete Strength " f'_c " (MPa)	Theoretical Nominal Flexural Capacity (kNm)
1	Strands and cover intact	37.92	2771
2	Strands and cover intact	37.92	2771
3	50 mm of cover loss, 2 ineffective strands	37.92	2565

3.2.3 Theoretical Shear Capacity

The three different cases of deterioration observed during the condition cataloguing of the three girders tested in shear were each accounted for in the theoretical calculations. These included an ideal scenario (observed on girder four), 50 mm of lost concrete from the bottom of the webs and one ineffective strands (observed on girder six), and 75 mm of lost concrete from the bottom of the webs and two ineffective strands (observed on girder five). Although, the loss of concrete on girder five was up to 100 mm, this was

observed on just one web and so the loss in concrete was averaged between the two webs. It should be noted that the concrete loss was not distributed along the entire length of the deteriorated girders but for this analysis the deterioration was assumed to be uniform. Using the design concrete strength, the nominal shear strength for each of the scenarios was 478, 429, and 451 kN, respectively. Seeking the guidance of academic and industry professionals, a shear loading location of 4.15 meters from the bearing support center was chosen as the zone of critical shear. These results are summarized in Table 3-4.

Table 3-4: Theoretical calculations of nominal capacity.

Girder Number	Girder Condition	Concrete Strength " f'_c " (MPa)	Nominal Shear Capacity (kN)
4	Ideal	37.92	478
5	75 mm of cover loss, 2 ineffective strands	37.92	429
6	50 mm of cover loss, 1 ineffective strand	37.92	451

3.2 Specimen Condition

Each of the six test specimens was carefully examined for elements of deterioration prior to testing. The deterioration observed on each of the girders was of similar type but of differing condition. Each girder was given a relative condition categorization good, fair or poor in comparison to the other girders. A good rating meant there was no horizontal cracking at the regions of pre-stressing. A fair rating meant there was some horizontal cracking at the regions of pre-stressing but no significant concrete cover loss. A poor rating meant web loss had occurred and there was noteworthy strand deterioration. Only girder five had deteriorated to the extent that the second layer of pre-stressing from the

bottom of the webs was exposed. Table 3-5 summarizes the condition of each girder. Figures 3-5 to 3-23 show the various states of deterioration. Where location is described, it is in regards to the orientation of the member within the structures laboratory.

Table 3-5: Condition catalogue of each girder.

Girder	Test	Condition	Characteristics of Deterioration
1	Flexure	Good	<ul style="list-style-type: none"> • Longitudinal cracks located on the webs extending away from the post-tensioning ducts. • Leaching stains visible on webs.
2	Flexure	Fair	<ul style="list-style-type: none"> • Horizontal cracks and rust stains observed on webs on and near the bottom at the mid-span. • Leaching stains visible on webs.
3	Flexure	Poor	<ul style="list-style-type: none"> • Horizontal cracks observed at all ducts. • Surface scaling on east web. • Web loss exposing bottom layers of pre-stressing. • Both pre-stressing strands ruptured on west web. • Water leaching stains visible on webs.
4	Shear	Good	<ul style="list-style-type: none"> • Longitudinal cracks located on the webs extending away from the post-tensioning ducts. • Leaching stains visible on webs.
5	Shear	Poor	<ul style="list-style-type: none"> • Significant web loss (up to 100 mm) on east web. • Leaching stains visible on both webs. • Surface scaling on east web. • Outer strand on east web ineffective.
6	Shear	Poor	<ul style="list-style-type: none"> • Leaching stains visible on webs. • Surface scaling on west web. • Exposed strands on one web with moderate level of corrosion

Girder One

Girder one was characterized as good in relation to the other girders. The only deterioration that was observed during the condition cataloguing were longitudinal cracks 500 to 1000 mm in length located on both webs propagating away from the post-tensioning ducts. These cracks also extended transversely through the diaphragms. These cracks are illustrated in Figures 3-3 and 3-4. Aside from these cracks the girder appeared to be as it was 40 years ago. There was no cover loss or corrosion staining of the concrete which correlate with the relatively low occurrence of water leaching stains seen on the webs. Perhaps most importantly, no vertical flexure cracks or signs of shear distresses were observed throughout the length of the girder.

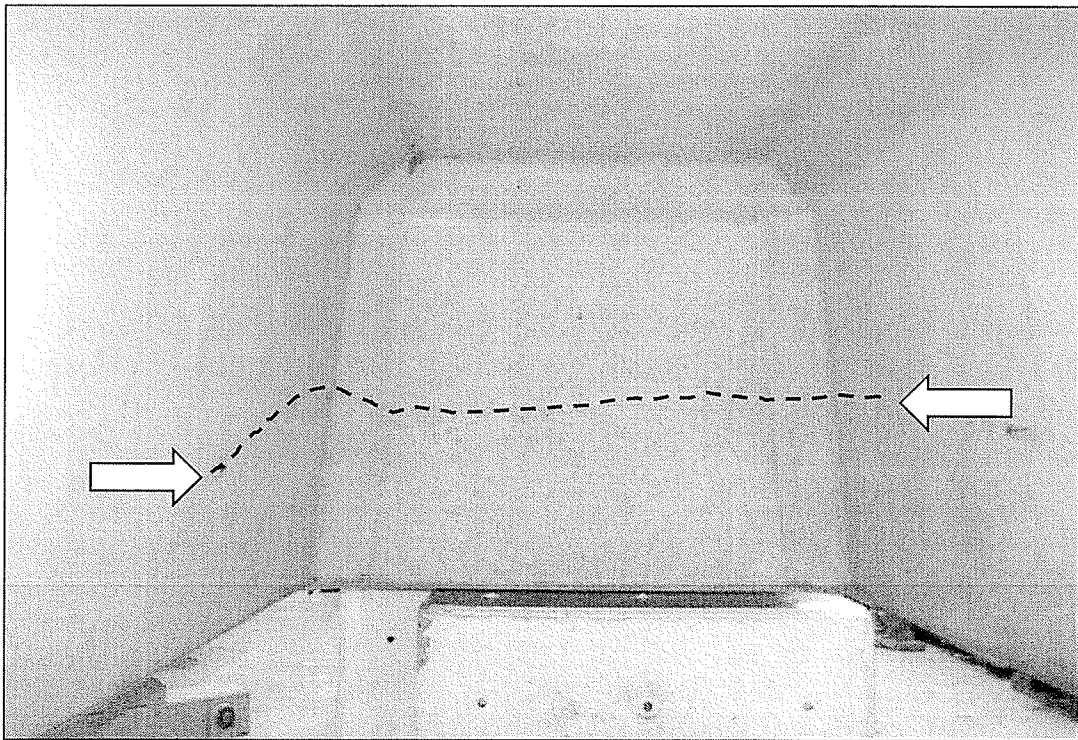


Figure 3-3: Transverse cracking through the diaphragm of girder one.

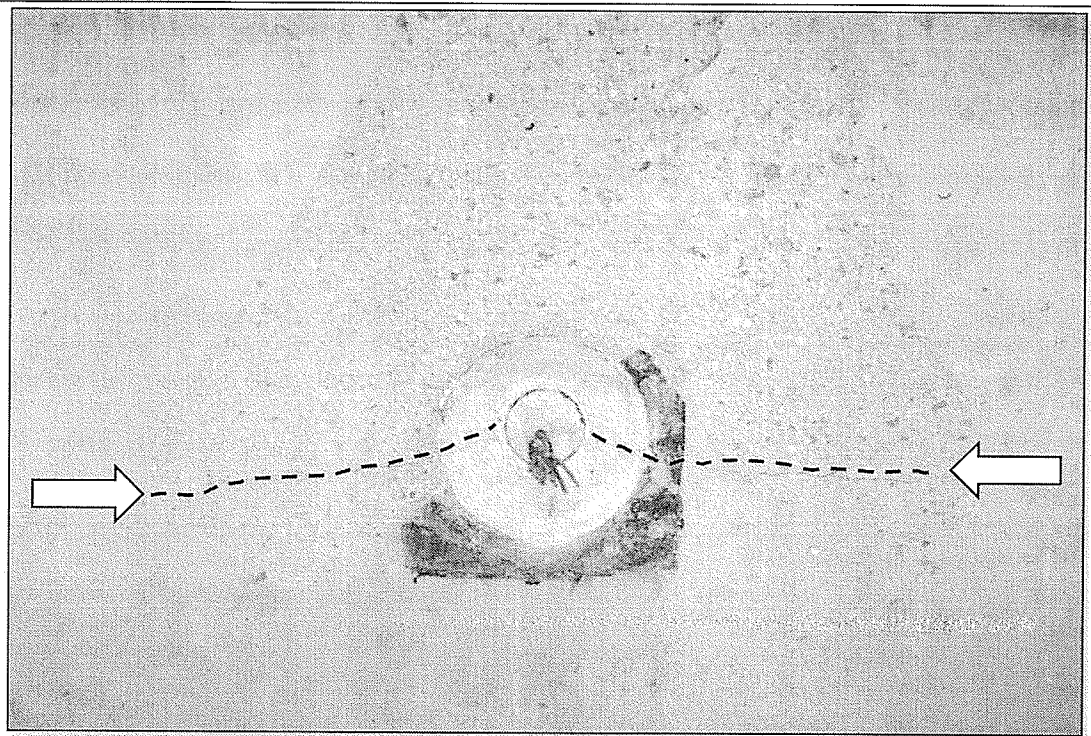


Figure 3-4: Longitudinal cracking on web at the post-tensioning ducts of girder one.

Girder Two

Examination of the second girder revealed much of the same deterioration characteristics with a few additions and was categorized as being in fair condition. No longitudinal cracks around the post-tensioning ducts were observed as there were with girder one. The only signs of deterioration were horizontal cracks and corrosion stains which were noticed on the west side on and near the bottom of the web at the mid-span. These are illustrated in Figures 3-5 and 3-6. Water leaching stains, shown in Figure 3-7, were also observed on the webs indicating that there was water leakage between the girders. There was however, no web loss at all or signs of vertical flexure cracks or shear distress.

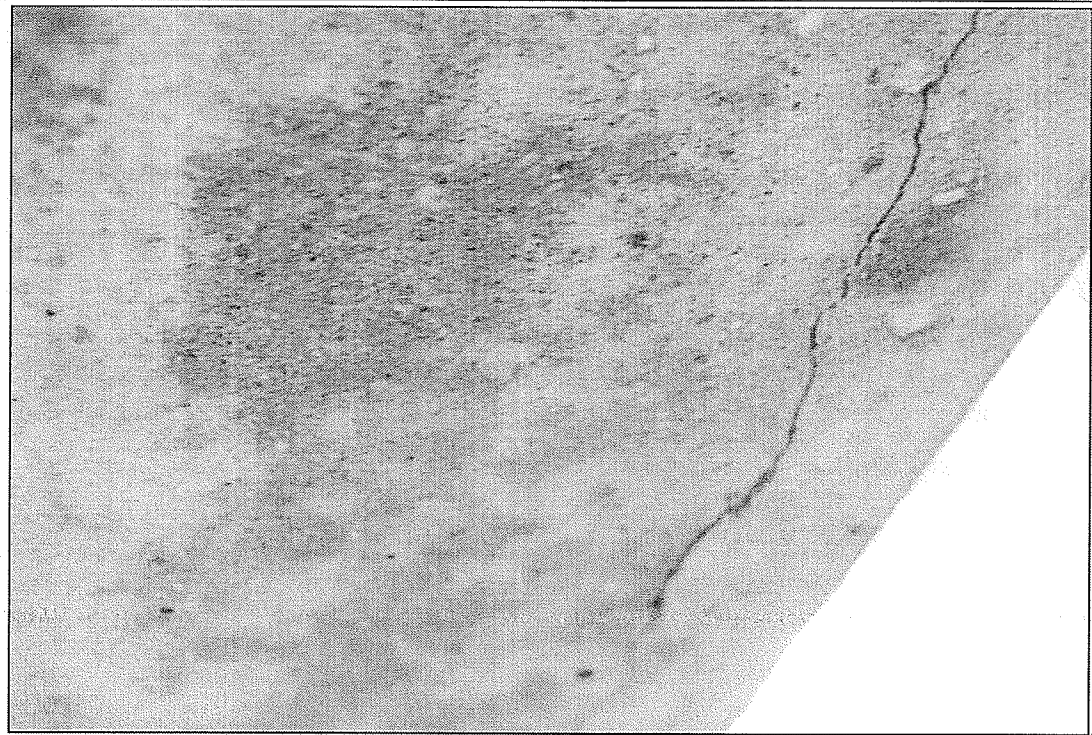


Figure 3-5: Longitudinal cracking on the bottom of east web of girder two.

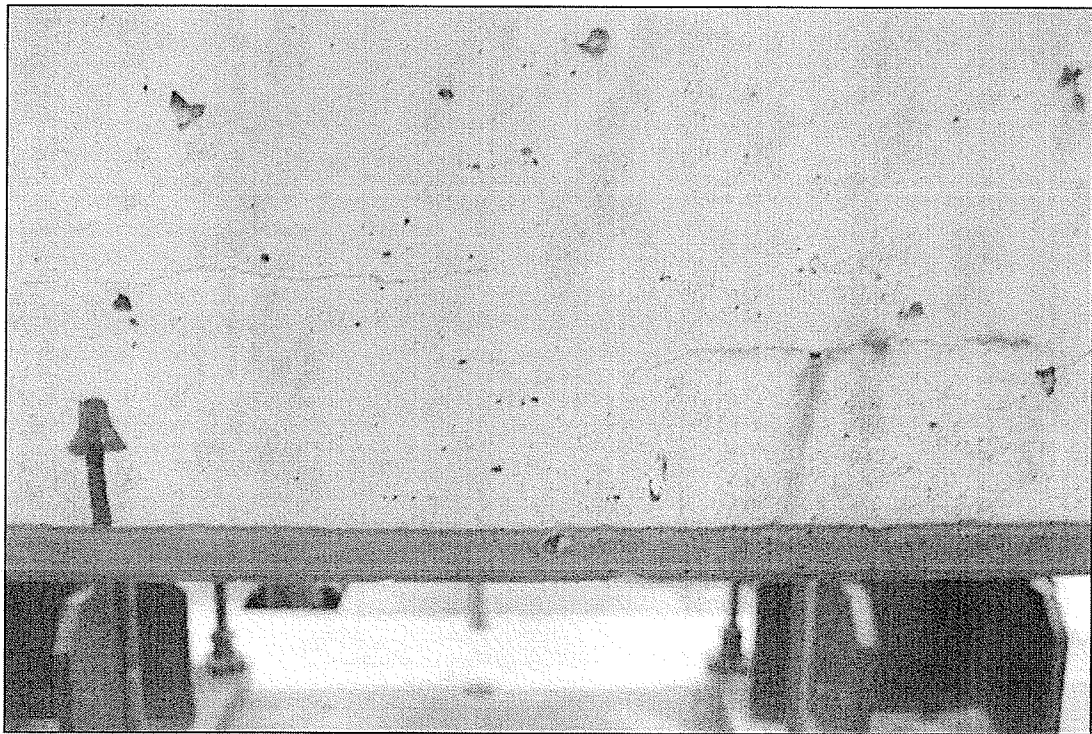


Figure 3-6: Longitudinal cracking on the side of east web at the bottom of girder two.

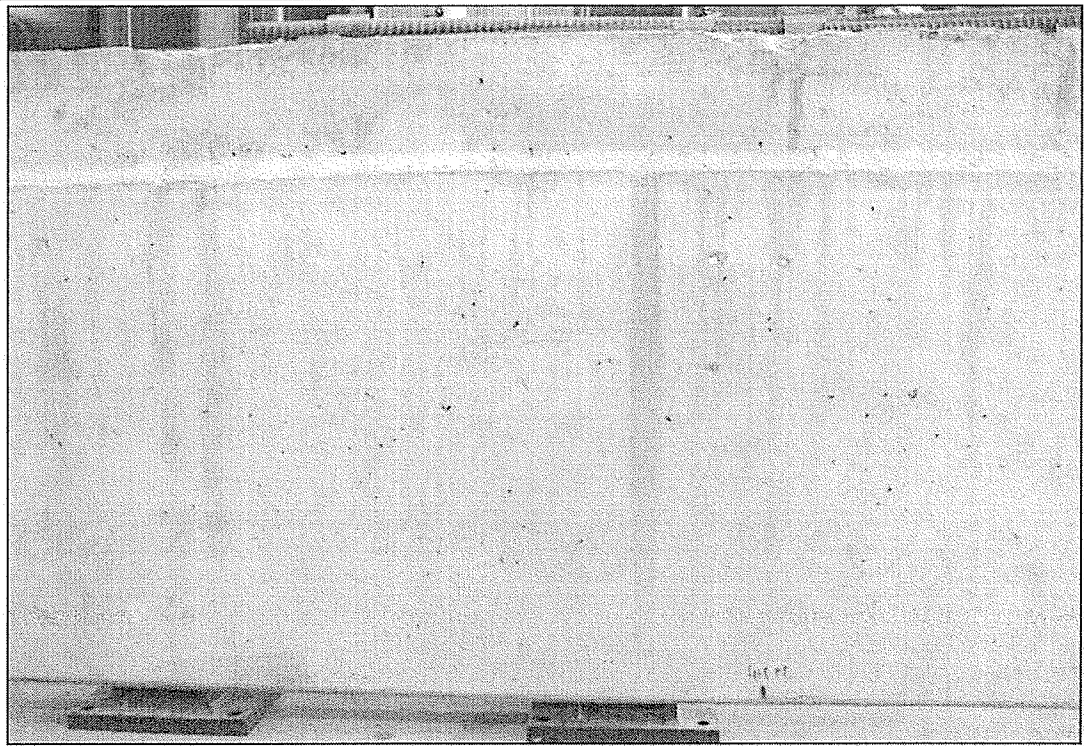


Figure 3-7: Water leaching stains on the web of girder two.

Girder Three

Girder three was in a greater deteriorated state than girders one and two. Horizontal cracks were observed on all ducts which extended transversely through the diaphragms seen in Figures 3-11 and 3-12. Water leaching stains were visible on both webs. The web loss was quite significant and had exposed the bottom layers of pre-stressing on both sides which is depicted in Figure 3-8. Both bottom layer pre-stressing strands had corroded considerably on the east web. This corrosion can be seen in Figures 3-9 and 3-10. Girder three also displayed signs of surface scaling on the east web. As a result of the level of deterioration, girder three was classified as being in poor condition. With that said, no visible vertical flexure cracks or signs of shear distress were observed.

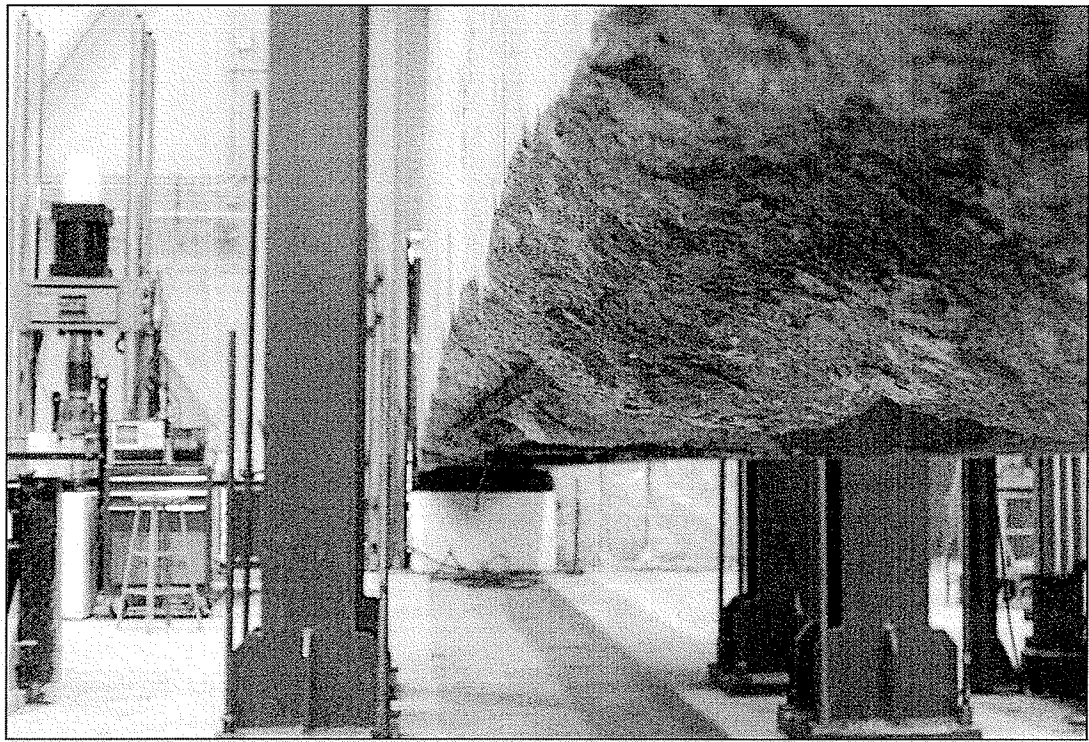


Figure 3-8: A long view of the east web including lost concrete and strand corrosion of girder three.

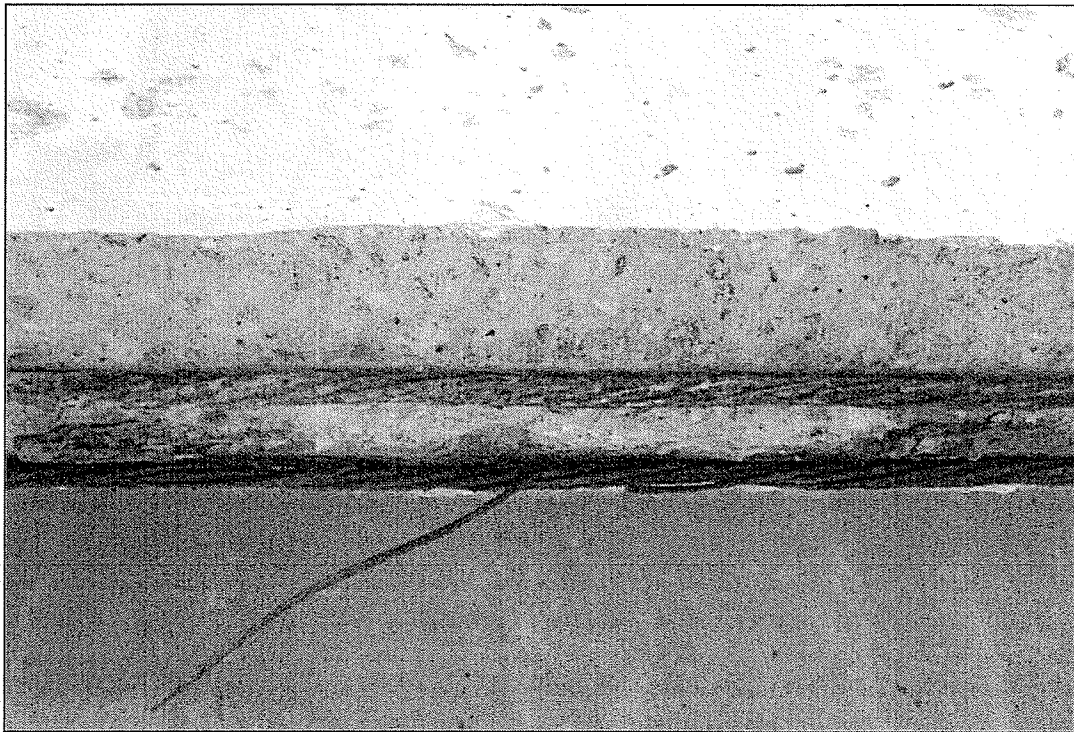


Figure 3-9: Strand corrosion near the mid-span on the east side of girder three.

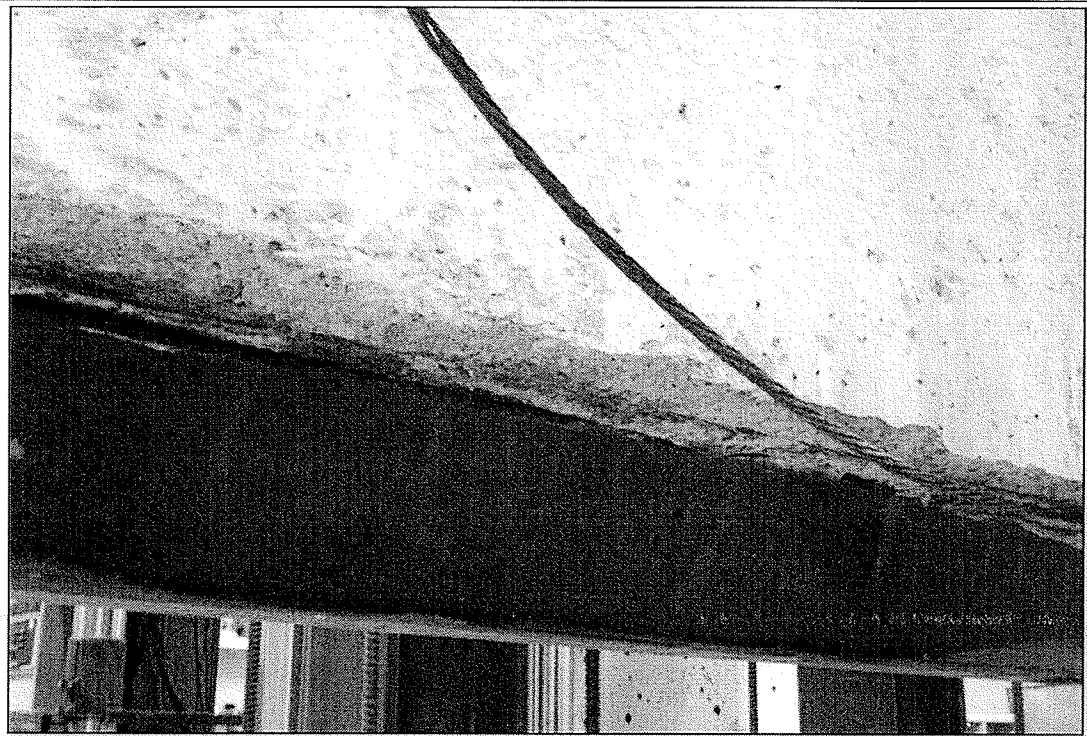


Figure 3-10: Surface scaling and a ruptured strand on the east side of girder three.



Figure 3-11: Transverse cracking through the diaphragm of girder three.

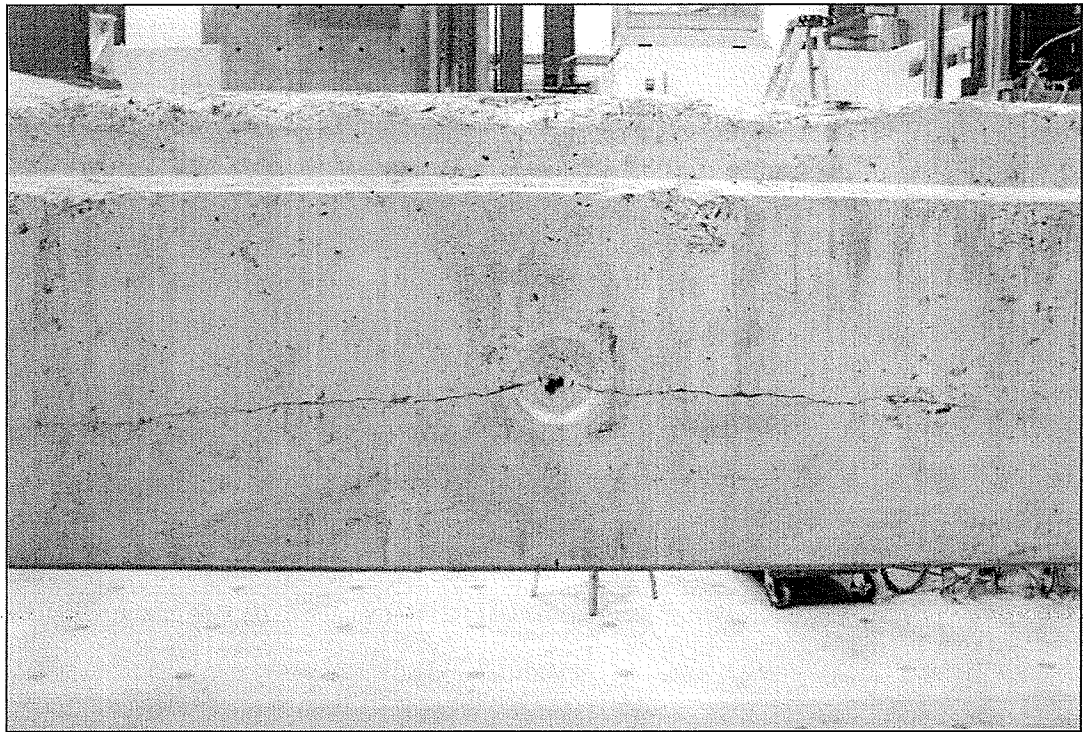


Figure 3-12: Longitudinal cracking on web at post-tensioning ducts of girder three.

Girder Four

The specimen of the first shear test, girder four, was categorized as being in good condition. No concrete cover had spalled from the webs nor were there any delaminations or horizontal cracking observed on the webs at the pre-stressing regions. Water leaching stains were observed on both webs as were longitudinal cracks at the ducts and through the diaphragms. The longitudinal cracking and water leaching stains can be seen in Figure 3-13. As with the previous three girders, no vertical flexure cracks or signs of shear distress were observed.



Figure 3-13: Cracking and water leakage stains on the web at the post-tensioning ducts of girder four.

Girder Five

The fifth girder was in the poorest condition of all the girders tested. Water leaching stains were observed as was surface scaling on the east web. Longitudinal and transverse cracking was seen at the post-tensioning ducts and diaphragms, respectively. This is illustrated in Figure 3-14. Shown in Figures 3-15 and 3-16, the bottom of the webs displayed significant concrete loss and in some locations had lost up to 100 mm on the east web. Figure 3-17 demonstrated concrete cover cracking and steel corrosion staining. There was also considerable strand deterioration at the bottom layer of reinforcement where at least one strand was rendered ineffective. Due to these factors this girder was categorized as being in poor condition. However, no flexural cracks or signs of shear distress were seen.

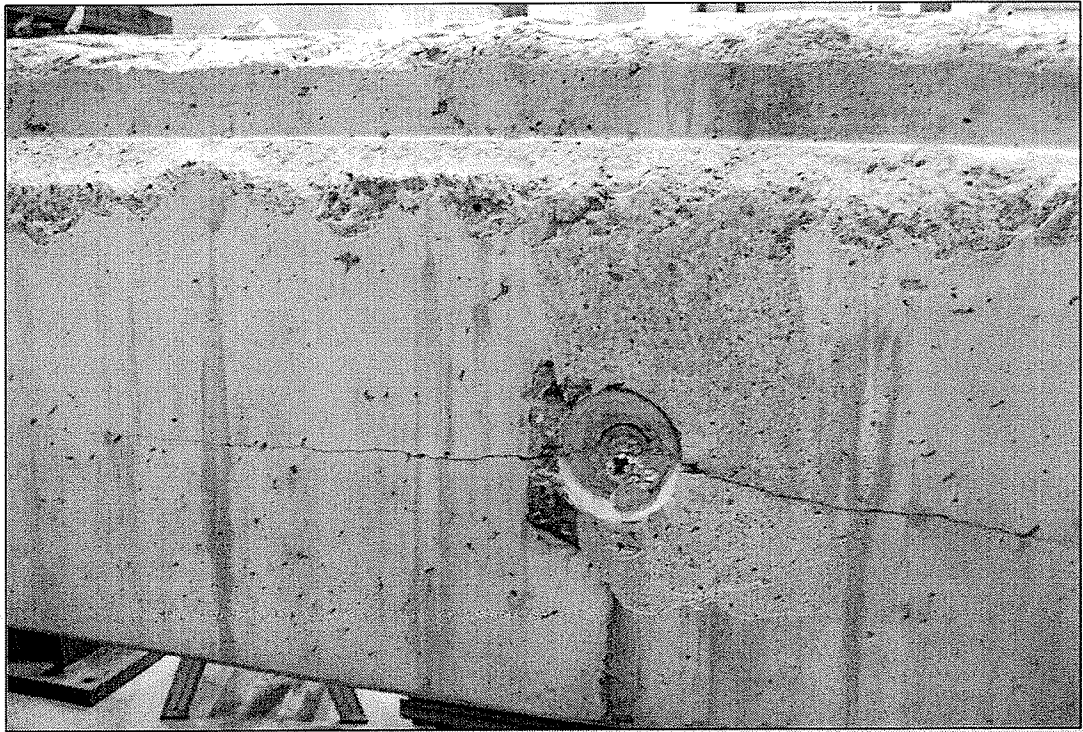


Figure 3-14: Cracking and water leaching stains at the post-tensioning duct on the west web of girder five.

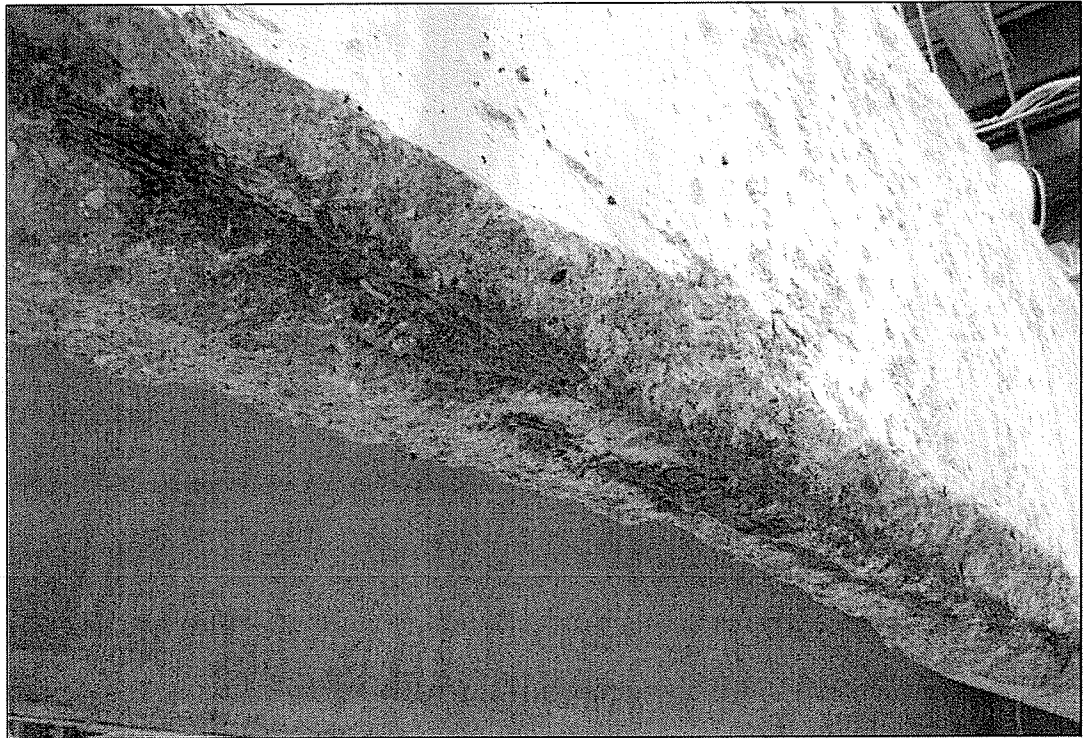


Figure 3-15: Strand corrosion, lost concrete and surface scaling on the east web of girder five.



Figure 3-16: Significant concrete loss on the east web near support of girder five.



Figure 3-17: Web cracking and delamination, corrosion staining and surface scaling of girder five.

Girder Six

Girder six was classified as being in poor condition relative to the other girders. Significant surface scaling was observed on the west web of this girder. This environmental damage can be seen in Figure 3-18. On that same side, the bottom layer of tensioning strands were exposed and corroded. This can be seen in Figure 3-19. Similar to the previous five girders, horizontal cracks that extended away from some of the post-tensioning ducts were observed. At this location, the cracking propagated transversely through the diaphragms as well. On the web opposite to that of the surface scaling, significant water leaching stains were visible. As with the previous five girders no flexural cracks or signs of shear distress were observed.

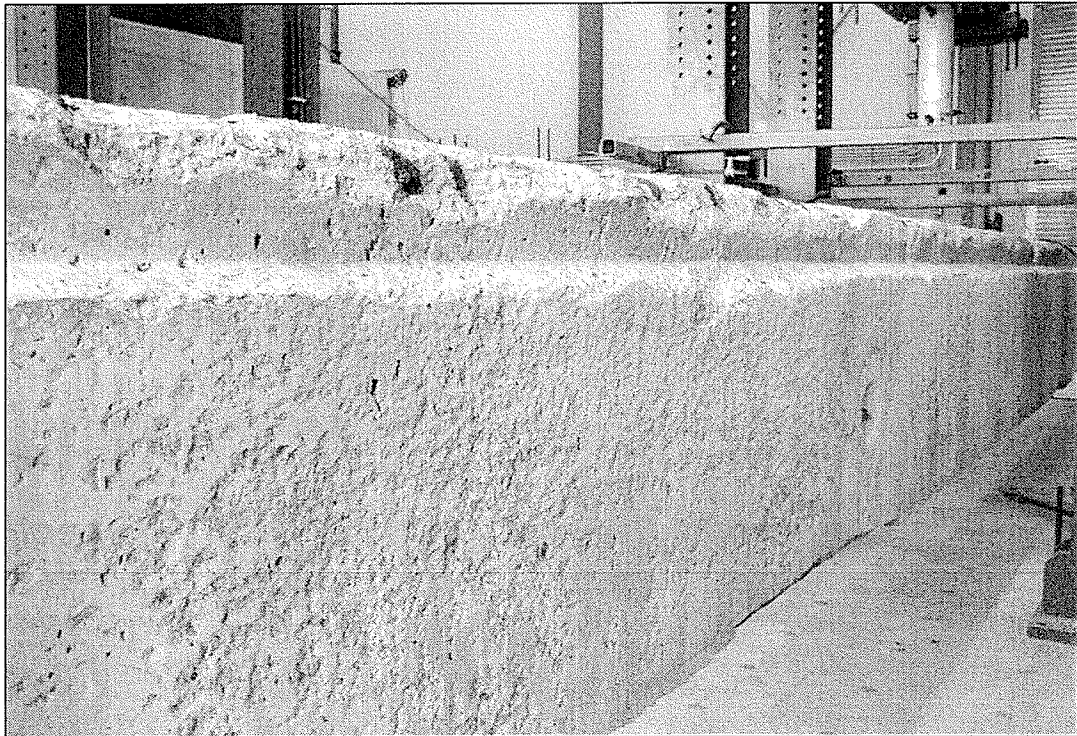


Figure 3-18: Surface scaling on the west web of girder six.



Figure 3-19: Exposed and corroded strands on the web of girder six.

3.3 Lateral Post-tensioning Strand and Grout Condition

Examination of the lateral post-tensioning strand and grout condition from the exterior of the girder revealed cracking within the grout and corrosion of the strands. This corrosion was likely due at least in part to the fact that the girders were stored outside for some time before they were brought into the laboratory for testing. It was also noted that girders five and six both had an ungrouted duct at the end block region. A core sample taken from the post-tensioning duct of girder one showed no strand corrosion but grout which was cracked. The grout cracking is a problem in that post-tensioning stress is decreased reducing the ability of the girders to share load amongst neighboring girders.

4. EXPERIMENTAL PROGRAM

The following section will describe the experimental program. The program is divided into two main sections, girder capacity testing and material testing. The girder capacity testing was broken up into the categories of instrumentation and loading frame details in addition to flexural and shear testing schemes. The core sample testing has been broken up into the categories of compression, chloride ion content, and air-void properties testing.

4.1 General Experimental Setup

The girder was supported at both ends by a bearing support of a width of 300 mm. Due to space limitations in the structures laboratory the center line of the support was placed 457 mm from the end of the girder so that the supports would fully contact the structural floor. The loading mechanism used had a capacity of 890 kN with 450 mm of stroke. Single point loading with a loading block of area 300 mm x 600 mm (roughly equivalent to that of the tire contact area of a heavy truck) was used for all girder tests. The load magnitude was recorded with the use of a load cell which was fixed to the hydraulic jacking device and connected to the data acquisition system.

The loading frame used for all the tests was constructed with two pairs of W310 x 158 steel columns; each connected with two C380 x 50 steel c-channels. A W360 x 110 steel beam spanned across the channels and was held in place by four 100 x 100 mm HSS steel sections. The loading jack was mounted from the midpoint of the spanner beam. Figure 4-1 illustrates the loading frame in full detail.

A
S03

LOAD FRAME DETAIL

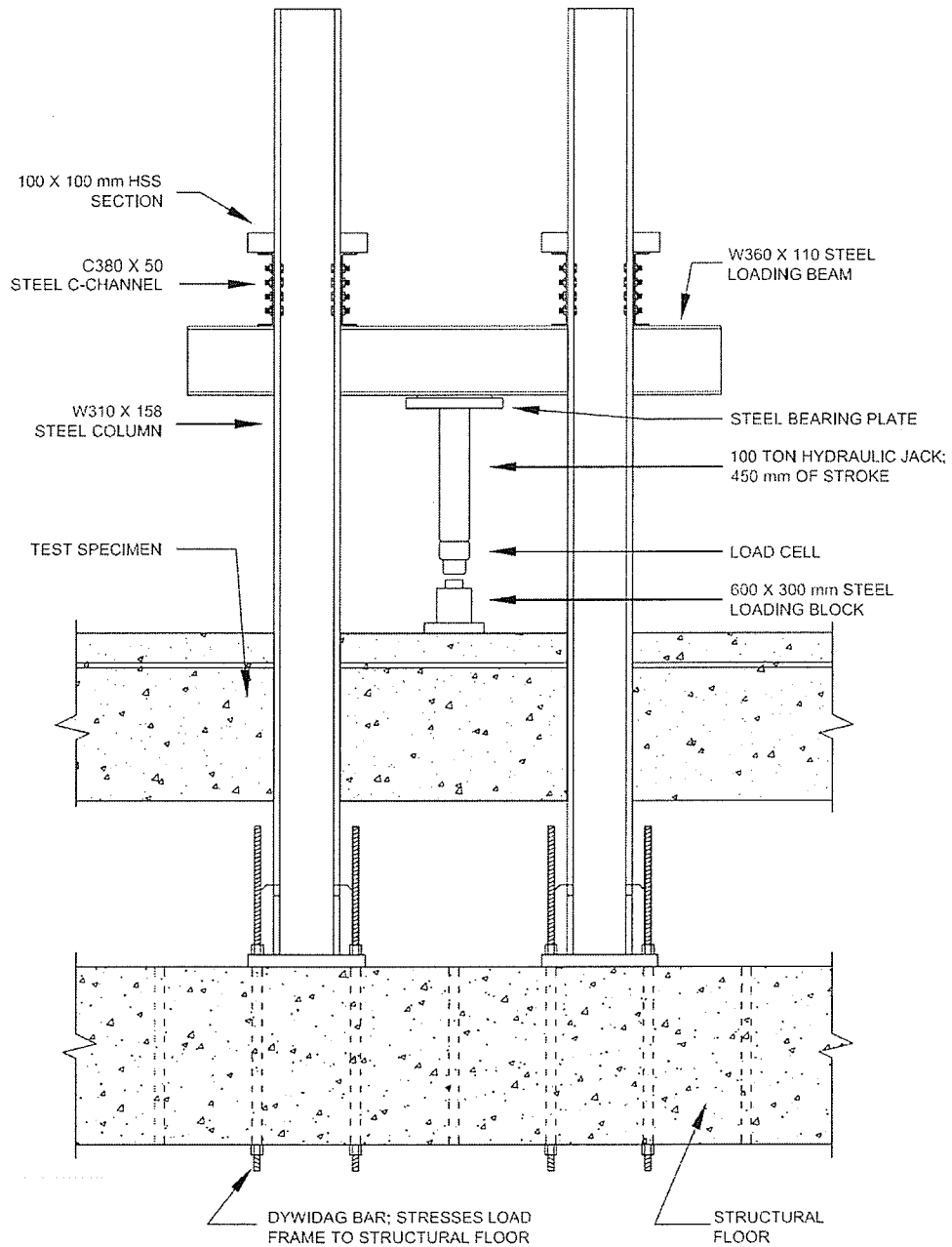


Figure 4-1: Loading frame detail.

4.2 Flexural Testing Setup

4.2.1 Instrumentation

Figure 4-2 displays a plot of the flexural testing instrumentation setup which includes the location of the linear variable displacement transducers (LVDTs), electronic strain gauges and loading area. Figure 4-3 displays a photograph of the loading frame at the girder mid-span for the flexural test setup.

Displacement Measurement

The instrumentation setup included nine LVDTs to measure displacement at various points along the girder. These LVDTs were placed at the supports and at every sixth length (3150 mm) along the girder. One additional LVDT was placed at the point of load to measure flange deflections relative to the webs. The LVDTs were required to measure bearing pad compression, span displacement, any possible torsion, and punching of the flange at the point of load. All nine LVDTs were connected to the data acquisition system during the flexural test and measurements were recorded at a rate of one reading per second.

Strain Measurement

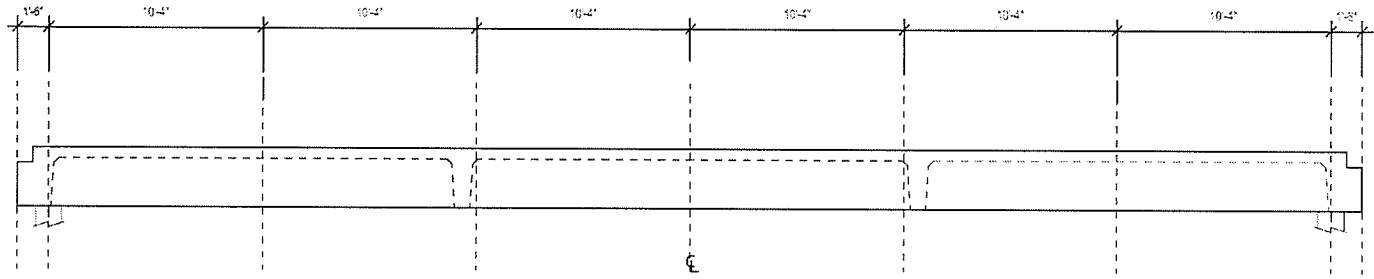
Electronic strain gauges of 60 mm in length were used to measure strains along the length of the girder. Three 60 mm electronic strain gauges (one on top and two on the bottom of each web) were placed at every 3150 mm along the girder as well. All the strain gauges on the top were placed at the transverse center except for those at the center line where two strain gauges were used on each side of the loading plate six inches (150 mm) from

the girder edge. The bottom strain gauges were centered (150 mm from the exterior edge) on the bottom of the both webs. On the third girder, there was significant concrete loss at the center line of the girder which allowed for a 10 mm steel strain gauge to be applied to the exposed strand. A total of 16 strain gauges were wired and connected to the data acquisition system during the flexural test. Strain gauge measurements were recorded at a rate of one reading per second.

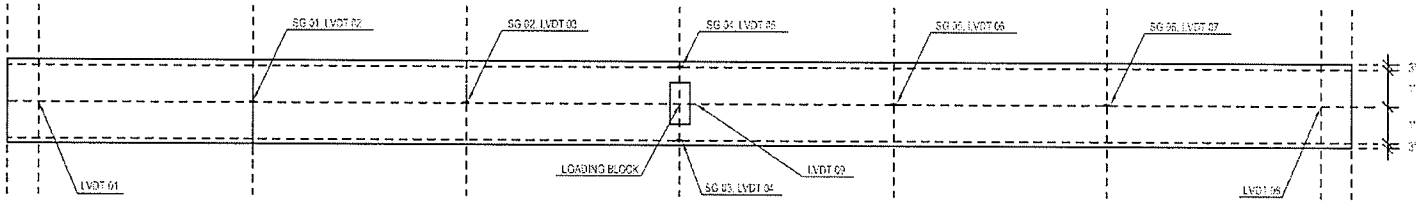
Crack Width and Addition Strain Measurement

Pi gauges were installed to record strains and crack widths. At the center of the span, two 200 mm pi gauges were applied to the exterior side of the webs 50 mm from the bottom. Although not directly fixed to the strands, the pi gauges can adequately record strains in the bottom level of reinforcement after flexural cracking has occurred whereas the electronic concrete strain gauges cannot. Both pi gauges were connected to the data acquisition system during the flexural test and measurements were recorded at one reading per second.

A
S04 STRAIN GAUGE AND LVDT PLACEMENT FOR FLEXURAL TESTING



1
S04 TOP PLAN VIEW



2
S04 BOTTOM PLAN VIEW

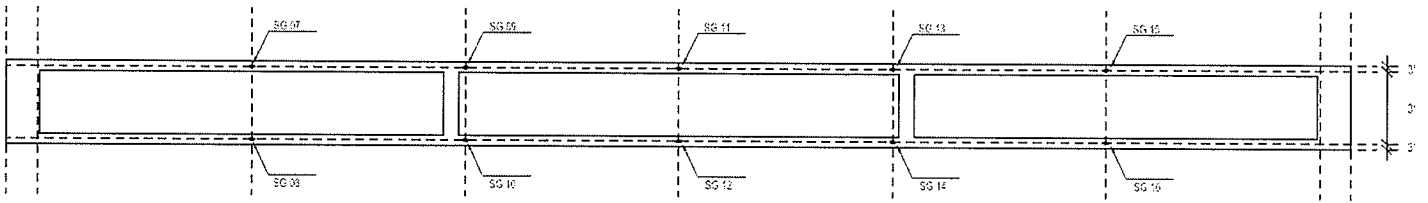


Figure 4-2: Flexural testing instrumentation setup.

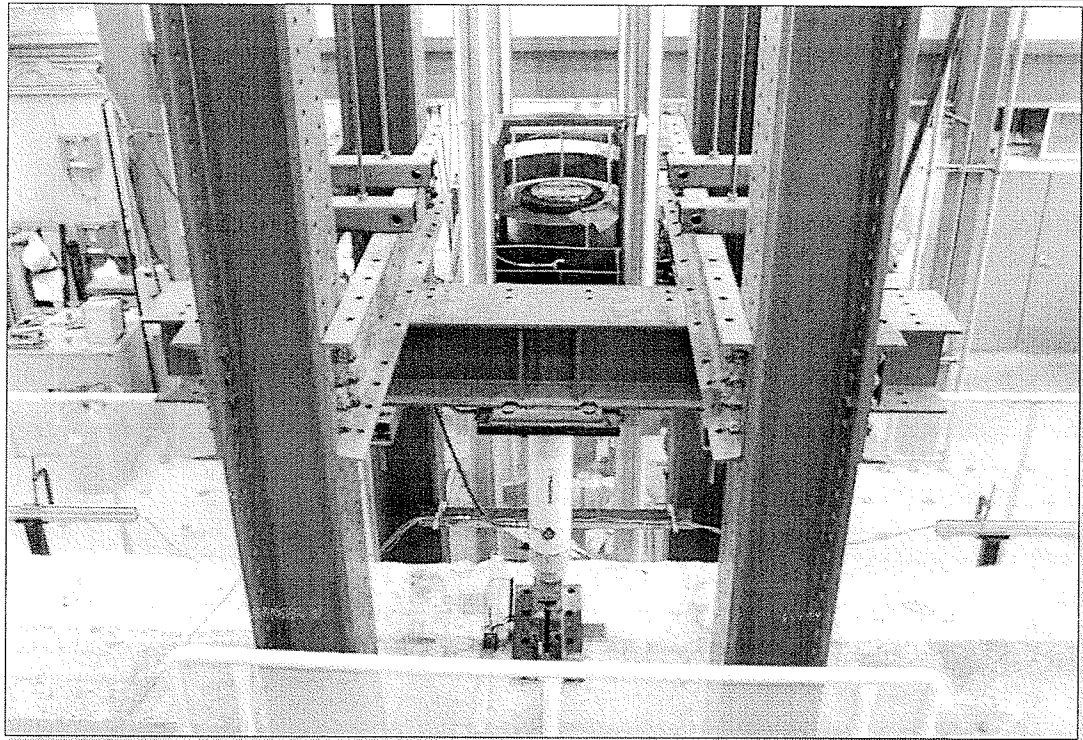


Figure 4-3: The loading frame of the flexural test setup.

4.2.2 Testing Procedure

The loading frame was positioned at the mid-span of the girder. The girders were subjected to monotonic loading in steps of 50 kN to 400 kN. At each step the load was held to allow for inspection of cracks. Once the load had reached 400 kN the LVDTs were reset as they did not have the required stroke to measure deflection without maxing out. After 400 kN, no further inspections were made as it was deemed unsafe to do so. From here the load was increased in steps of 25 kN until failure. After failure had been reached the load was removed and a final inspection was carried out including damage assessment and photography.

4.3 Shear Testing Setup

4.3.1 Instrumentation

Strain Measurement

Three 60 mm electronic strain gauge rosettes were installed on both outer webs directly under the load as shown in Figure 4-4. The rosettes were located at 115, 345, and 575 mm from the bottom of the web displayed in Figure 4-5. Two strain gauges, one on either side of the load were placed on the flange as shown in Figure 4-6. The goal of this procedure was to be able to record principle strains and possibly determine if at the quarter-span the plane cross-section remained plane as the load increased. The 20 electronic strain gauges were wired to the data acquisition system and measurements were recorded at one reading per second.

A rosette of pi gauges was installed at the mid-height locations as shown in Figure 4-5 to confirm the readings given by the electronic strain gauges. In addition, the pi gauges should yield readings to failure where as once a crack occurs through a strain gauge, it no longer functions.

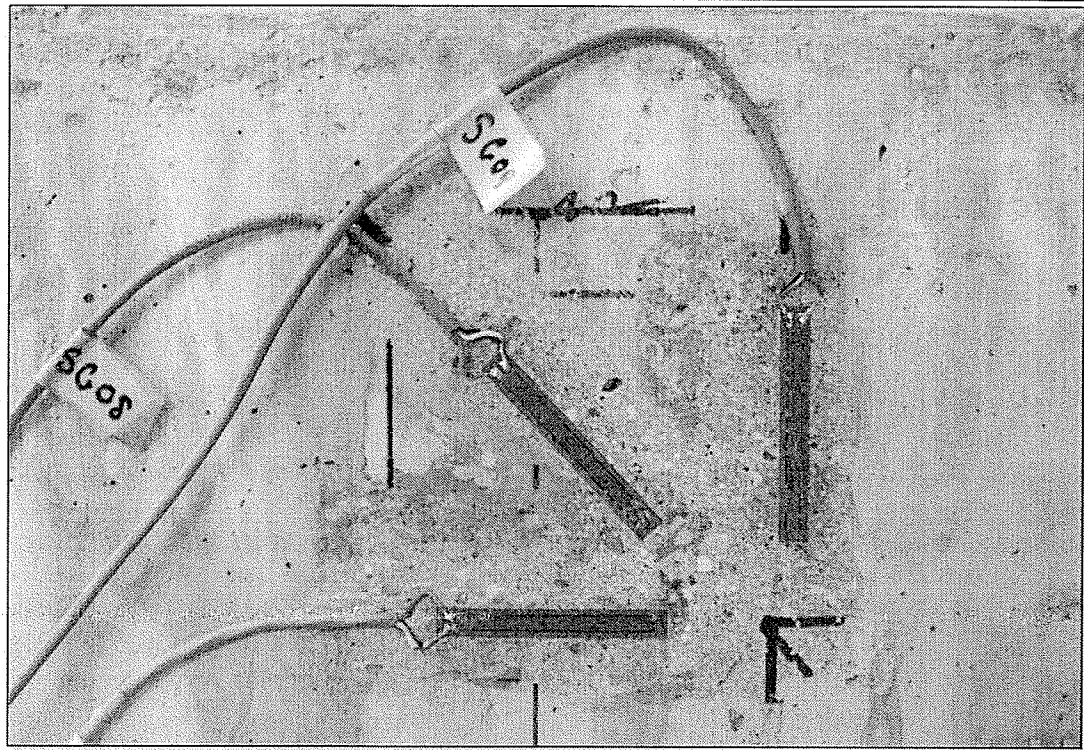


Figure 4-4: Strain gauge rosette on the web of girder at the point of loading.

Displacement Measurement

Five LVDTs were used to measure the displacement along the length of the girder. These were situated at the supports, the mid-span, and one on either side of the point of load. This would allow measurement of bearing pad compaction, span displacement, and any possible torsion. The five LVDTs were wired to the data acquisition system and measurements were recorded at one reading per second.

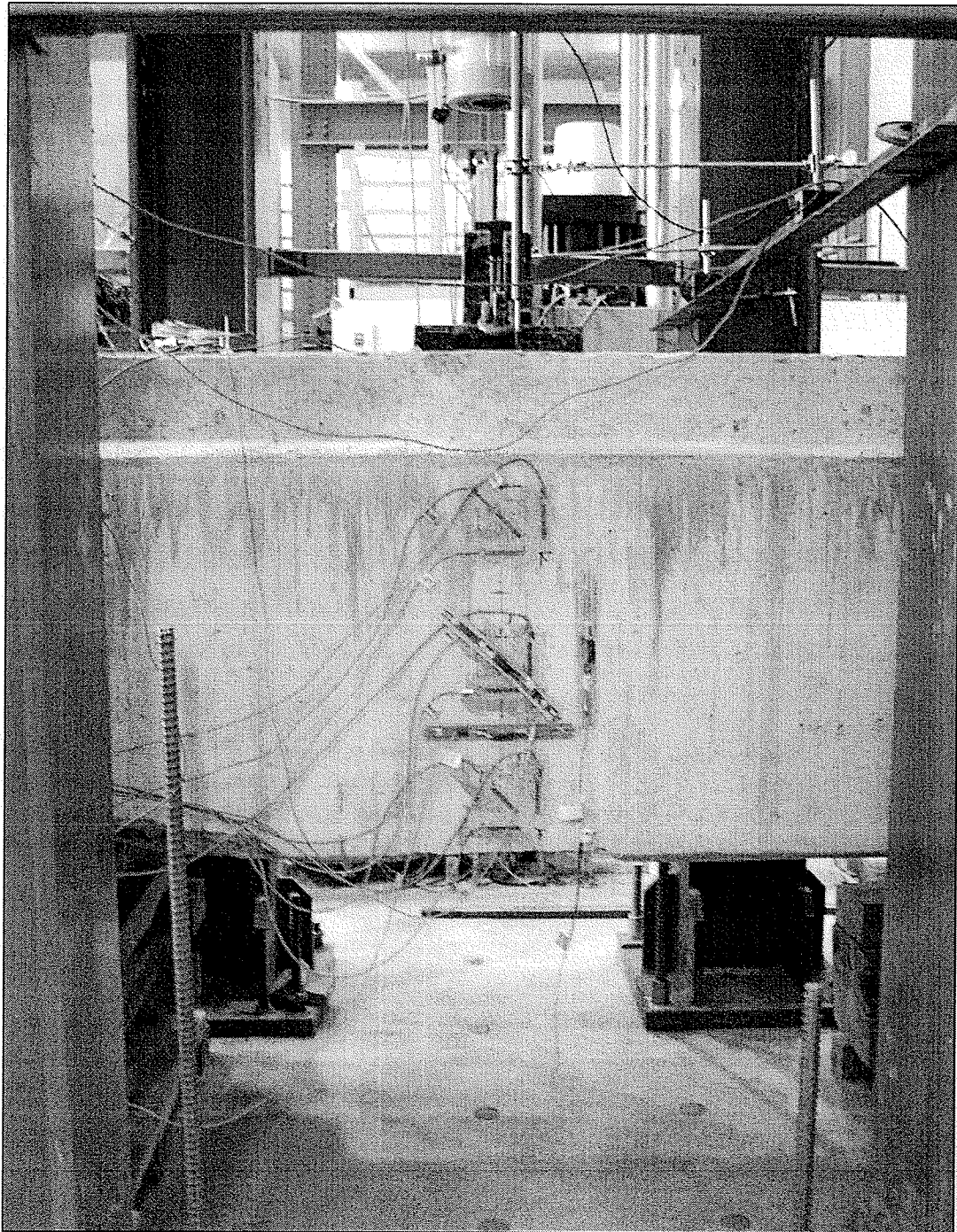
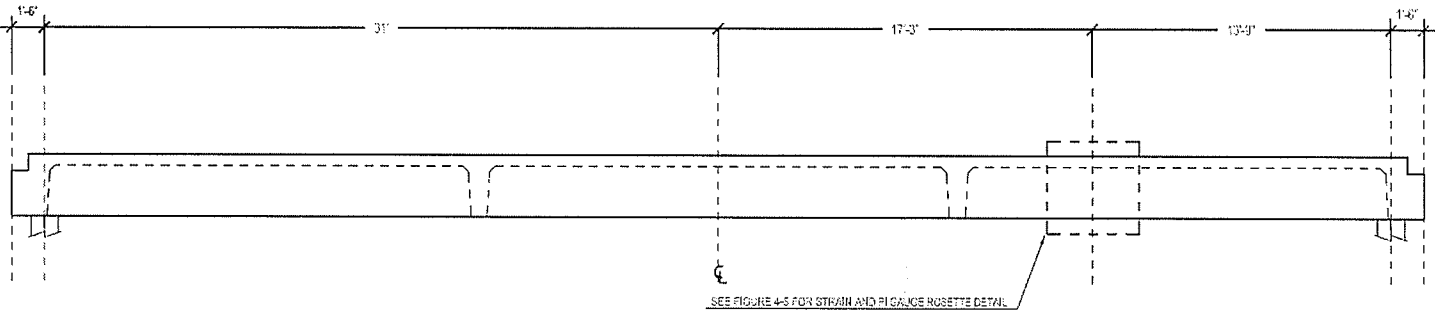


Figure 4-5: Shear electronic instrumentation setup including strain and pi gauge rosettes.

A
S05

STRAIN GAUGE AND LVDT PLACEMENT FOR SHEAR TESTING



B
S05

STRAIN GAUGE AND LVDT PLACEMENT FOR SHEAR TESTING

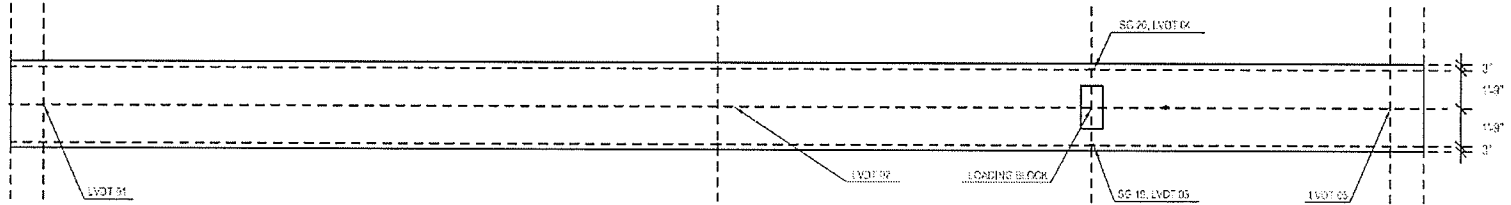


Figure 4-6: Shear testing instrumentation setup.

4.3.2 Testing Procedure

The shear test of girder four had originally been loaded at a distance of 1000 mm from the support face. The girder withstood a load of 750 kN without any observed cracking. It was then decided to interrupt the test to consult with academics and industry professionals as to the most appropriate location to create a shear failure. For a shear crack to propagate a load placed near the quarter-span was required. This notion was confirmed by the professionals we consulted and therefore it was decided to position the load four meters from the face of the bearing support.

Similar to the flexural testing method, the girders were subjected to monotonic loading in steps of 50 kN until 400 kN. At each step the load was held to allow for inspection of cracks. The LVDTs did not need to be reset because the deflection was less for the shear test. After 400 kN, no further inspections were made as it was deemed unsafe. From here the load was increased in increments of 25 kN until failure was reached. After failure had been reached the load was removed and a final inspection was carried out including damage assessment and photography.

4.4 Compressive Strength Cylinder Testing

Two core samples were taken from each girder, one from the flange and one from the web, for the purpose of determining the compressive strength of the concrete. The core samples were of a diameter of 70 mm. The samples were cored within the region of the bearing support and the diaphragm, between the groupings of straight and draped strands of the web and between the negative moment steel and shear reinforcing steel. The cored

samples were taken to Lafarge Canada Inc. to level and square the top and bottom surfaces. The samples were tested uncapped. This was done to ensure that the loading mechanism was a plane to the surface of the ends of the cores. All the concrete cylinders were weighed and measured for height before testing. The samples were loaded monotonically to failure in the small material testing machine at the University of Manitoba McQuade Structures Lab at a rate of 750 N/s. Once each test was complete the failure load and failure mode was recorded. The failure loads were converted to pressures and averaged to yield the mean concrete strength of the girders.

4.5 Chloride Ion Content Determination

To complete a comprehensive study of the chloride ion content with the girders, two core samples were taken from each of the six girders, one from the flange and one from the web. The samples were cored within the same region as those for the strength testing. These cores were marked at one and two inches from the exterior face of the cylinder to provide guidance for drilling which allowed collection of pulverized powder from these regions. Once at least 20 grams of concrete powder had been extracted it was further crushed with a hammer to ensure that all collected material had been pulverized.

The chloride content tests were carried out with the use of the James Instruments Inc. CI-2000 chloride test system. Once the electrode was calibrated with the various acid solutions that came with the kit, an accurately weighed three gram sample from each specimen was dissolved in individual jars containing 20 ml of extraction solution. The chloride ions react electro-chemically with the acid extraction solution. After the powder

was fully dissolved in the extraction solution, the electrode provided was submersed in the solution to measure its voltage potential. This potential was converted to a chloride concentration using the computer module also provided within the kit. The computer automatically applies a temperature correction and the percentage of chloride was displayed directly on the LCD readout. After each test the chloride concentration for each sample was recorded on a data sheet conforming to ASTM standards for this material test.

4.6 Air Void Ratio and Spacing Factor Determination

Two core samples were taken from each of the six girders, one from the flange and one from the web. The samples were cored within the same region as those for the strength and chloride tests. These samples were sent to The National Testing Laboratories Ltd. for analysis. The core samples were tested for air void parameters in accordance with the modified linear point count method outlined in ASTM C457: *Test Method for Microscopical Determination of Parameters of the Air-Void System in Hardened Concrete*.

5. EXPERIMENTAL RESULTS

This section discusses the experimental results. These include the moment, shear, and material testing. Where possible these results are compared against the theoretical expectations.

5.1 Flexure Testing Results

The results of the flexural testing are summarized in Table 5-1. A comparison of experimental versus theoretical flexural capacities is found in Table 5-2. A full synopsis is discussed in the paragraphs below.

Table 5-1: Flexural testing results.

Girder	Maximum Load (kN)	Experimental Flexural Capacity (kNm)	Max Displacement (mm)	Cracking Load (kN)	Max Concrete Strain (microstrains)	Max Tension Strain (microstrains)
1	650	3577	343	238	2852	15379
2	626	3462	317	243	2657	12073
3	575	3224	403	239	3548	16808

The loads recorded for each experiment were converted to a nominal flexural moment using Equation 13. The moment due to the girders' self-weight was calculated and was equal to 505.78 kNm.

$$M_n = \frac{Pl}{4} + 505.78 \text{ kNm} \quad (\text{Eq. 13})$$

For example, the nominal flexural moment for girder one would be:

$$M_n = \frac{(650.09 \text{ kN})(18.90 \text{ m})}{4} + 505.78 \text{ kNm} = 3577.46 \text{ kNm} \quad (\text{Eq. 14})$$

Table 5-2: Comparison of experimental versus theoretical nominal flexural capacity.

Girder	Experimental Nominal Flexural Moment (kNm)	Theoretical Nominal Flexural Capacity (kNm)	Increase Over Theoretical (%)
1	3577	2771	29
2	3462	2771	25
3	3224	2565	26

Girder One

Due to safety concerns the first girder was not taken to failure. However, it was supposed that the girder was loaded very close to its ultimate strength based on comparisons between it and the other girder within this program. This specimen resisted a load of 650 kN at a displacement of 343 mm. This load converted to a total nominal resistance of 3577 kNm which was 29 percent greater than anticipated by theoretical calculations. The cracking load of the girder was 238 kN which was within the expected range of one-third to one-half the ultimate failure load. Once the load had been removed the girder rebounded from a displacement of 343 mm to roughly 40 mm of total displacement. After the test, typical flexural cracks were observed within the central third of the girder. Figures 5-1 and 5-2 display the loading versus displacement plots of the test. Figures 5-3 and 5-4 are photographs taken near ultimate loading of the girder.

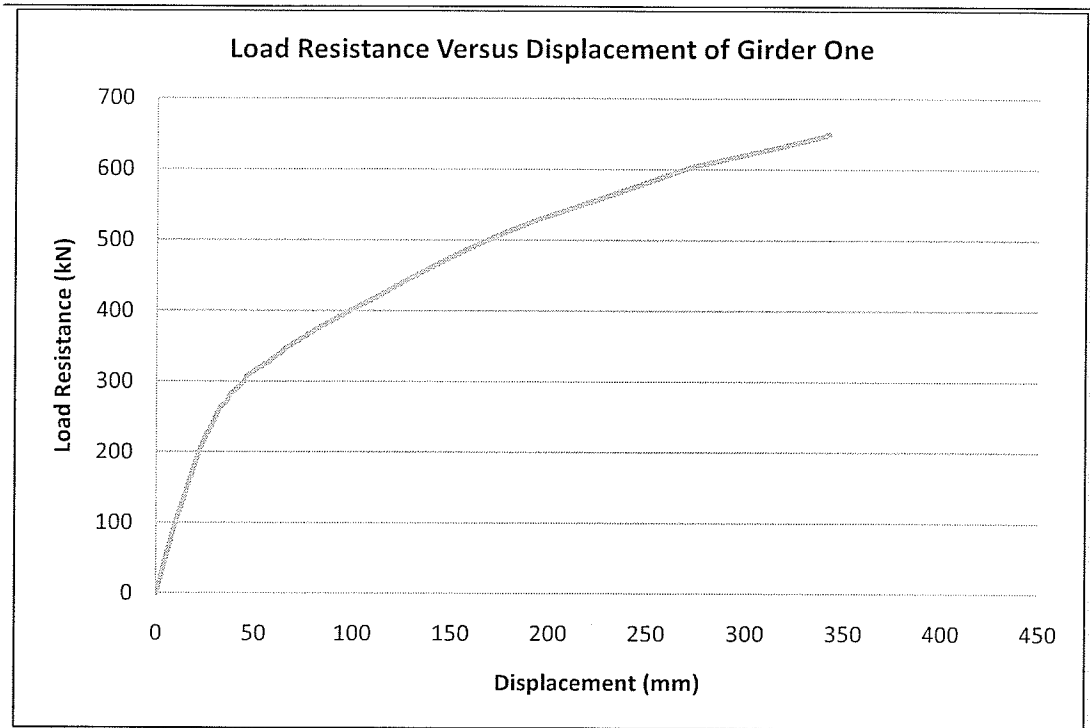


Figure 5-1: Load versus displacement for flexural test one.

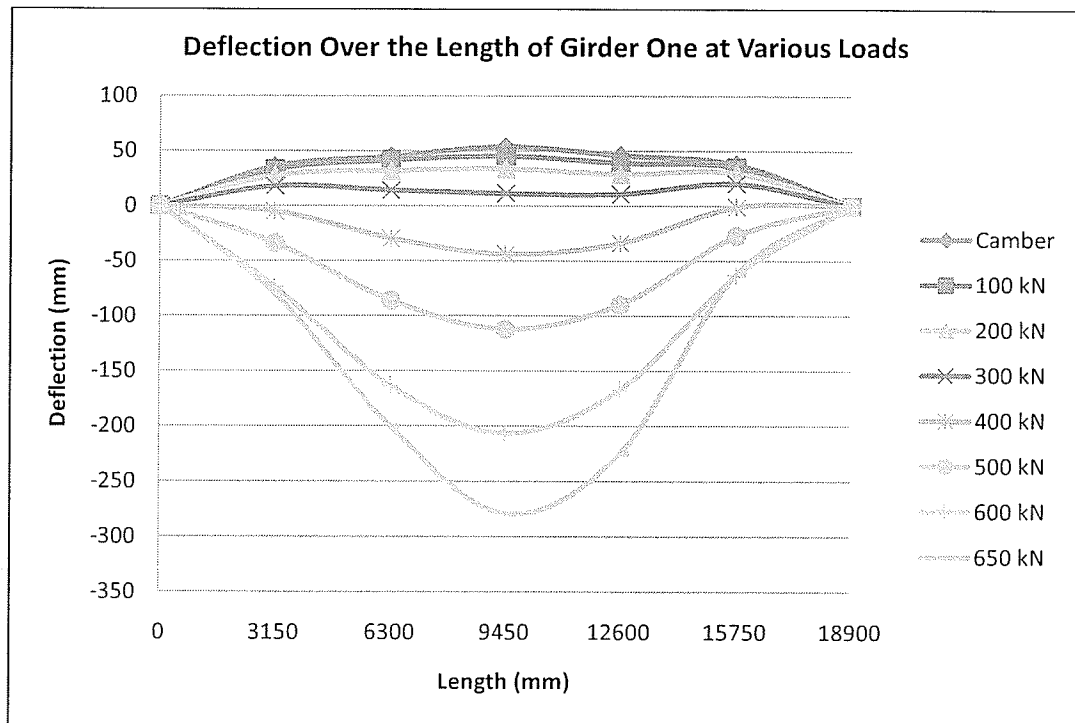


Figure 5-2: Deflection over the length of the girder for various loads during flexural test one.

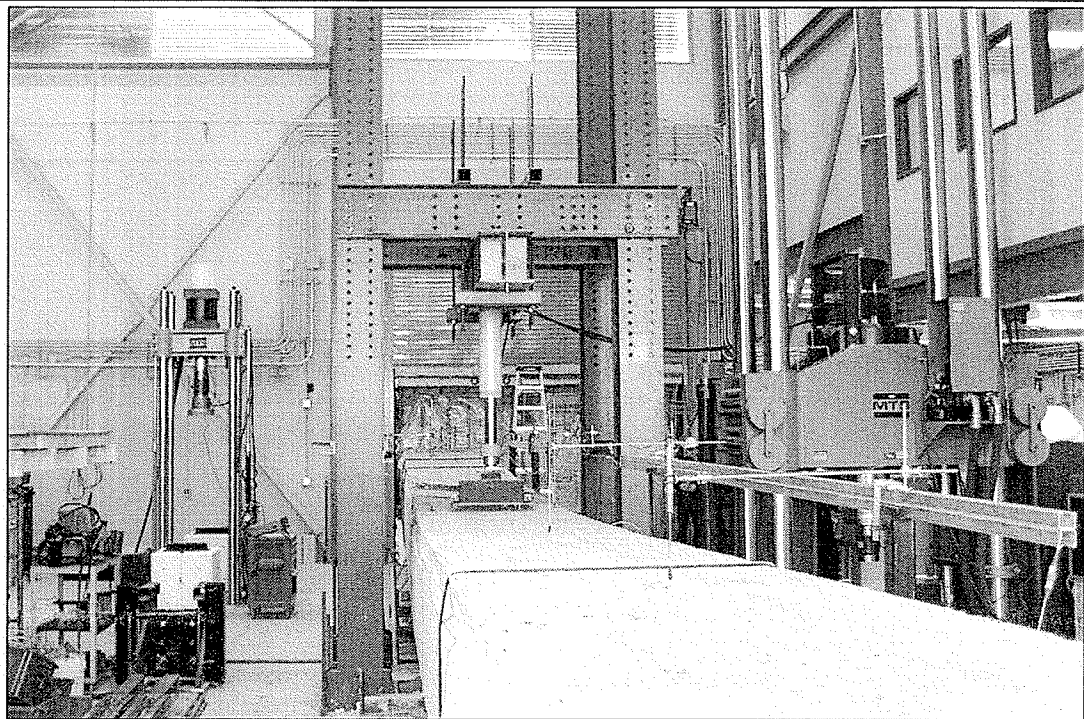


Figure 5-3: Flexural testing at the maximum deflection of girder one.

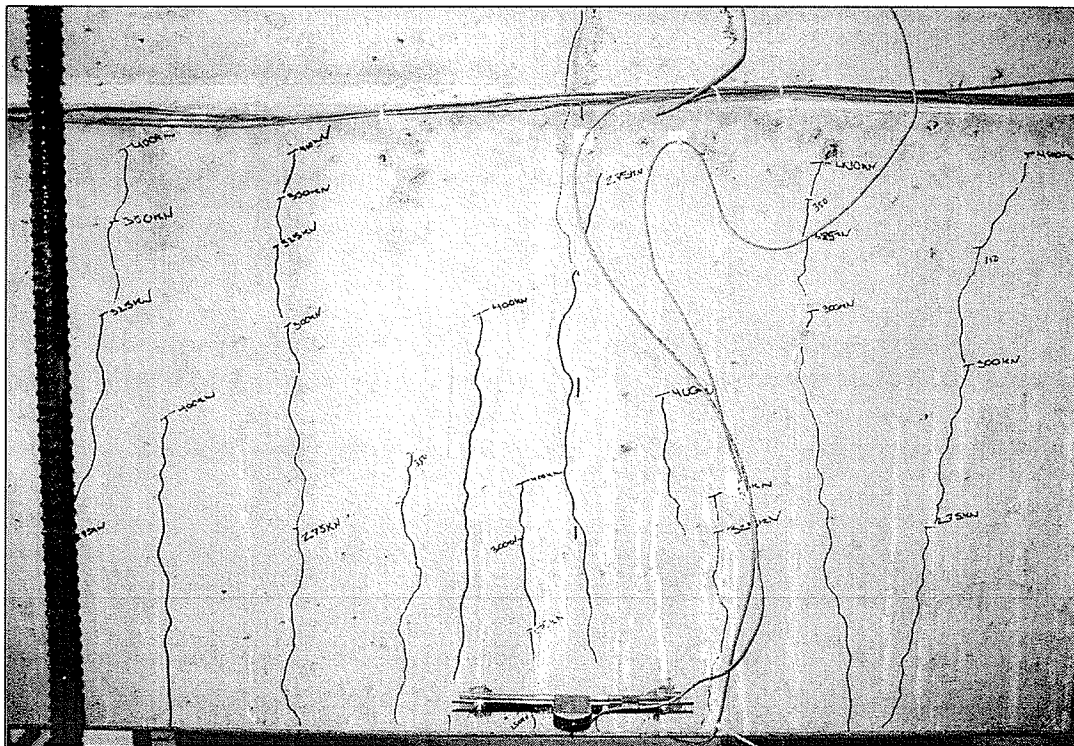


Figure 5-4: Flexural cracks at the mid-span region on the west side of girder one.

Girder Two

Prior to test two, a system of screens was installed in the failure zone to protect the observers and laboratory equipment from potential harm and therefore it was felt that the test could be taken to failure safely. During the test, a problem had occurred which required the test to be stopped and was consequently restarted.

This second test saw the girder monotonically loaded in increments of 50 kN to failure. The formation of cracks were marked every 50 kN to 400 kN. Cracks were not marked beyond 400 kN for safety purposes. Cover loss was observed at loads of 300 kN and greater which was expected due to the cracking at the bottom layer of strand reinforcement seen during the condition cataloguing. The mode of failure was a non-ductile explosion of the compressive zone. The girder reached an ultimate failure load of 626 kN at displacement of 317 mm. At this load, the girders' nominal moment capacity was calculated to be 3462 kNm, 25 percent greater than that calculated theoretically. Figures 5-5 and 5-6 display the loading versus displacement plots of the test. Figures 5-7 and 5-8 are photographs of the girder after failure had occurred.

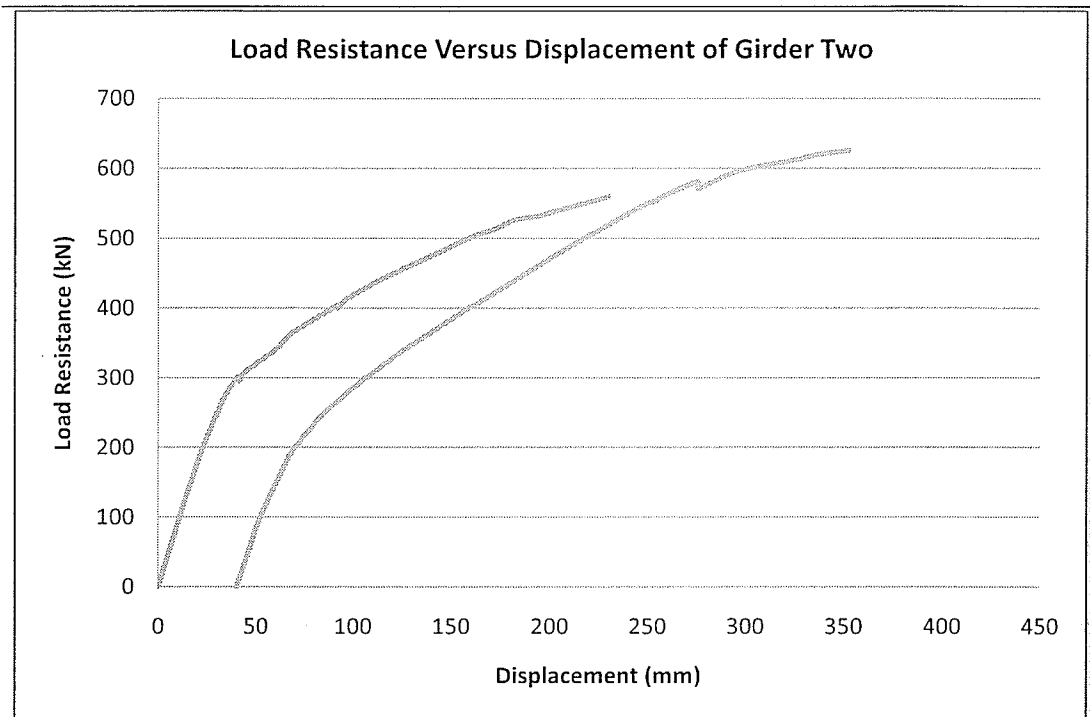


Figure 5-5: Load versus displacement for flexural test two.

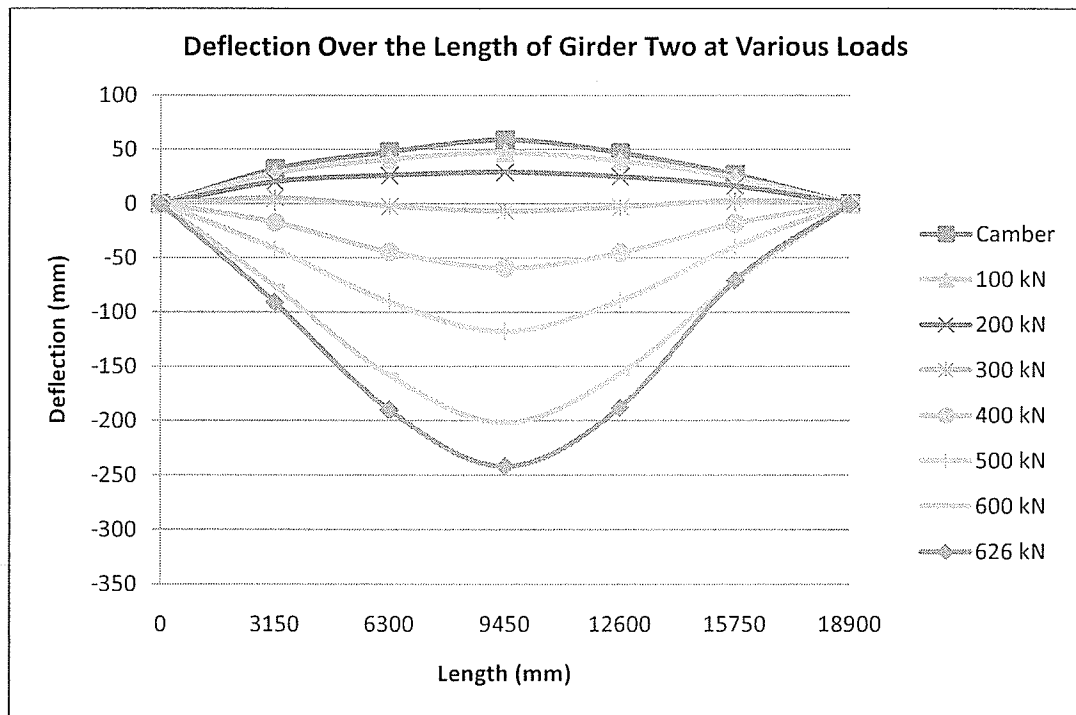


Figure 5-6: Deflection over the length of the girder for various loads during flexural test two.

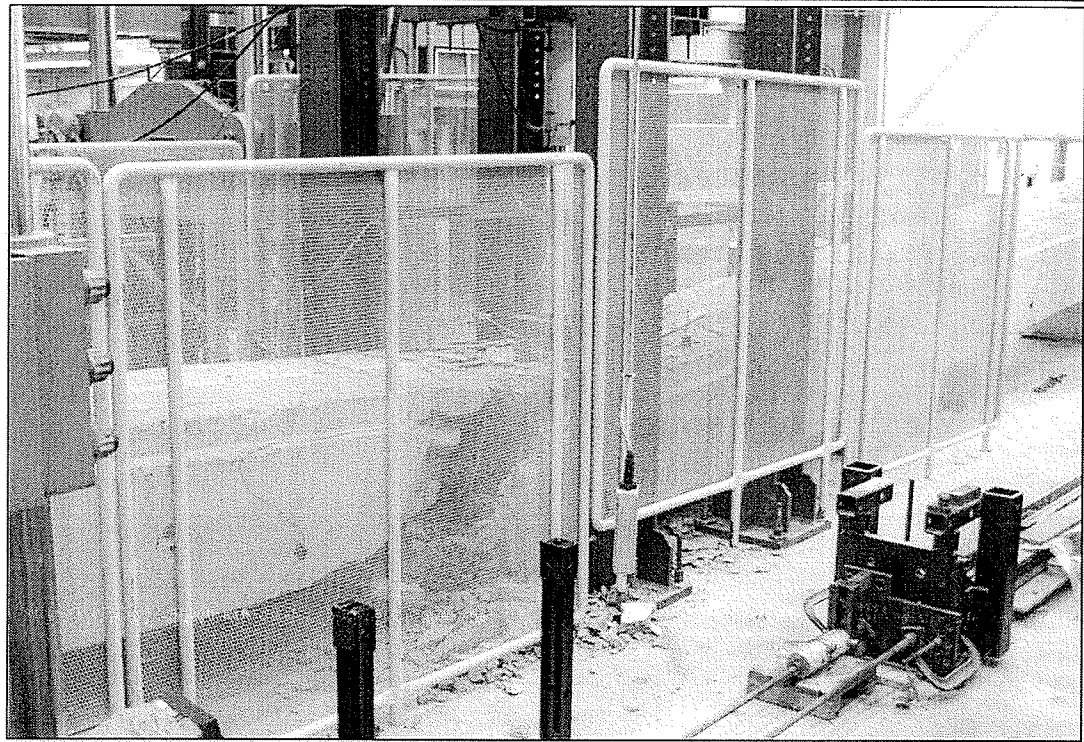


Figure 5-7: Long view of failure at the mid-span on the east side of girder two.

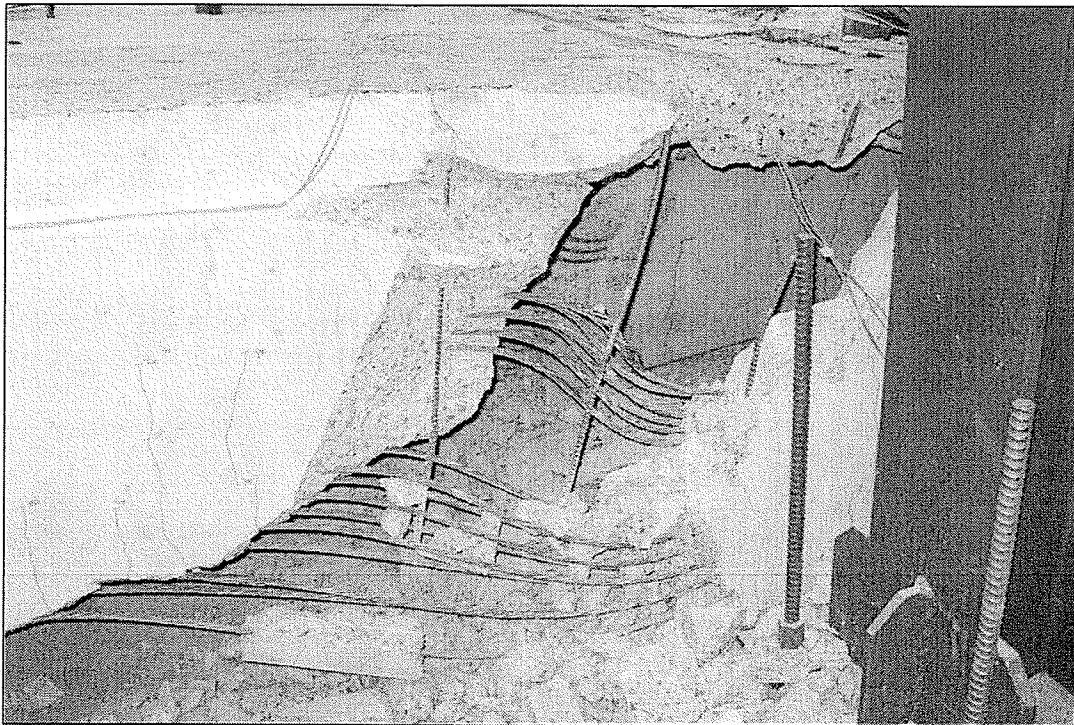


Figure 5-8: Close up of the failure zone at the mid-span on the east side of girder two.

Girder Three

Girder three which was rated as being in relatively poor condition yielded some interesting results. Prior to the test of girder three a steel strain gauge had been installed on one of the exposed strands that was in relatively decent condition. The readings were compared to the readings from the pi gauges affixed to the web at the height of the bottom row of pre-stressing. These results compared favorably and therefore it was concluded that the pi gauge gave an accurate reading of strain in the strand even though they were fixed to the concrete. These results can be seen in Figure 5-11. During the test, two strands of the bottom layer of reinforcement ruptured.

Like the second test, the girder was loaded monotonically to failure. The formation of cracks were marked every 50 kN to a load of 400 kN. Cracks were not marked beyond 400 kN for safety purposes. During the test a considerable amount of web loss due to concrete spalling was also observed. The mode of failure was a non-ductile explosion of the compressive zone. The girder reached an ultimate failure load of 575 kN at a displacement of 403 mm. At this load the girder had a nominal moment resistance of 3224 kNm, which was 26 percent greater than calculated theoretically for a scenario of two ineffective strands and 50 mm of concrete cover loss. Figures 5-9 and 5-10 display the loading versus displacement plots of the test. Figures 5-12 and 5-13 are photographs of the girder after failure was reached.

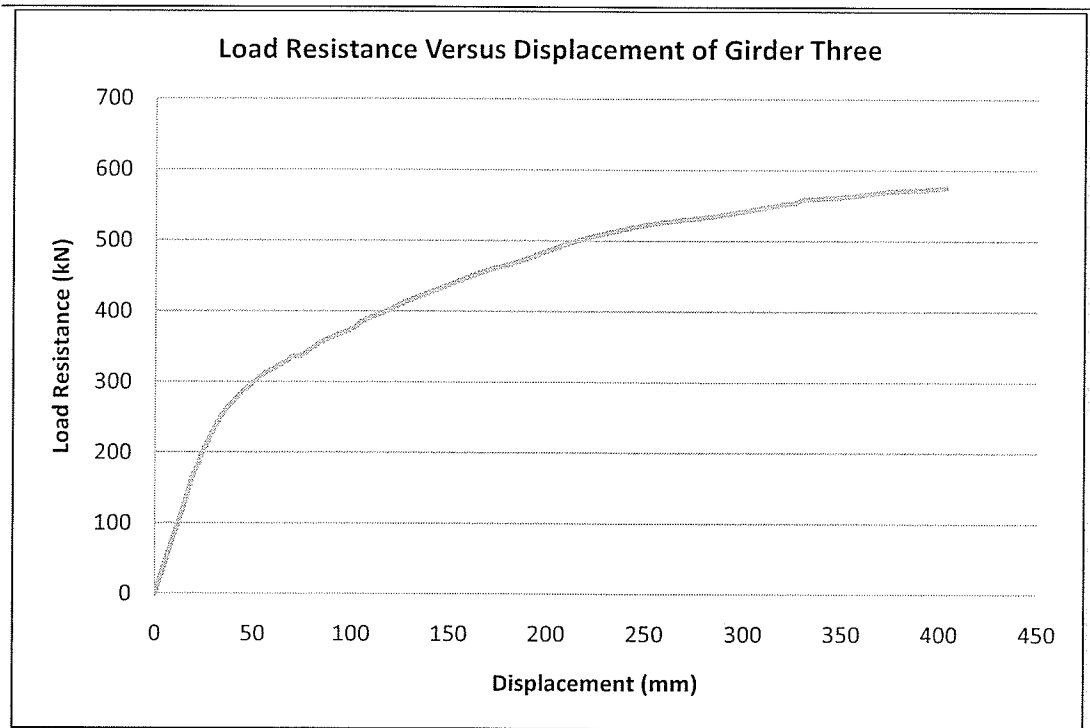


Figure 5-9: Load resistance versus displacement for flexural test three.

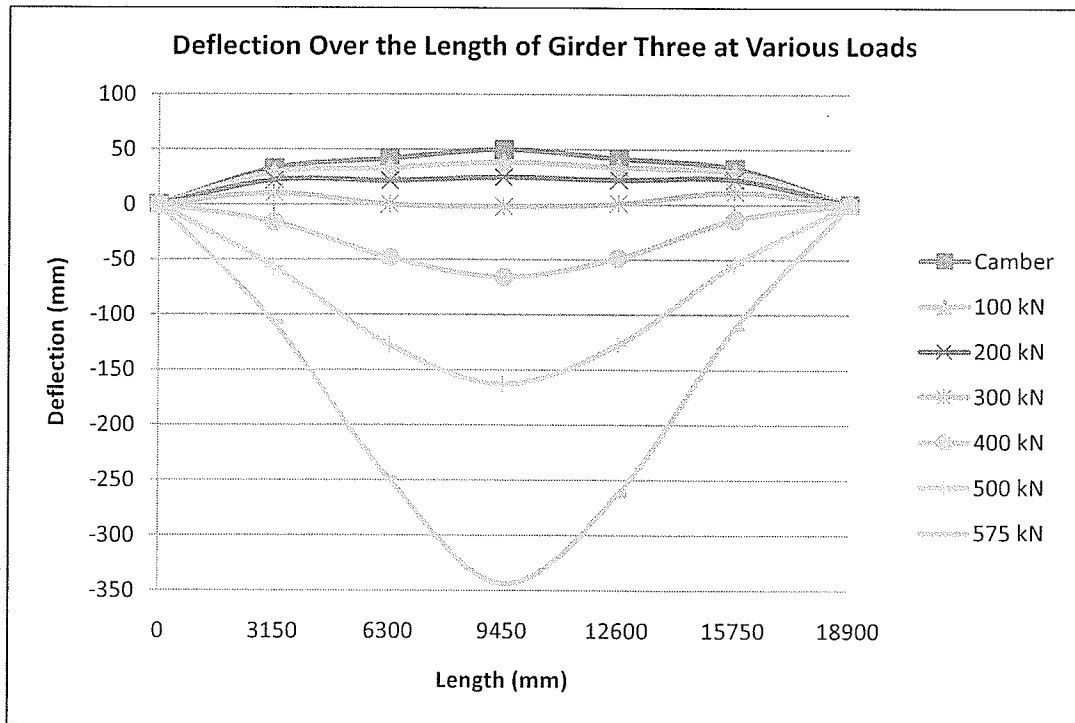


Figure 5-10: Deflection over the length of the girder for various loads during flexural test three.

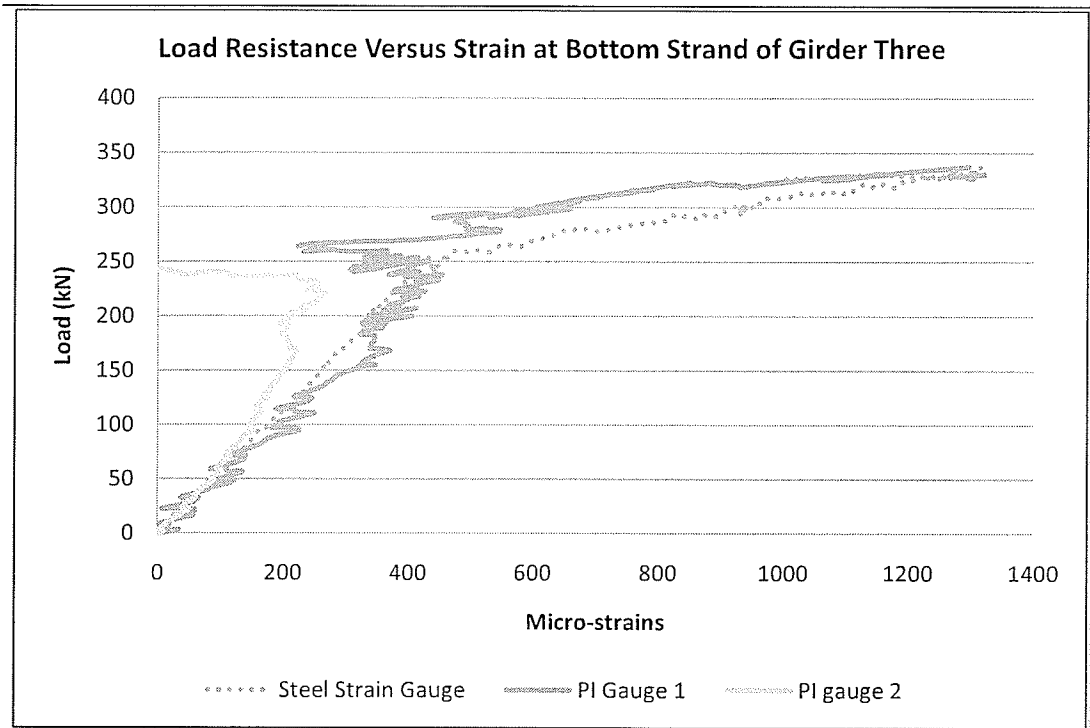


Figure 5-11: Comparison of pi gauge and strain gauge results for flexural test three.

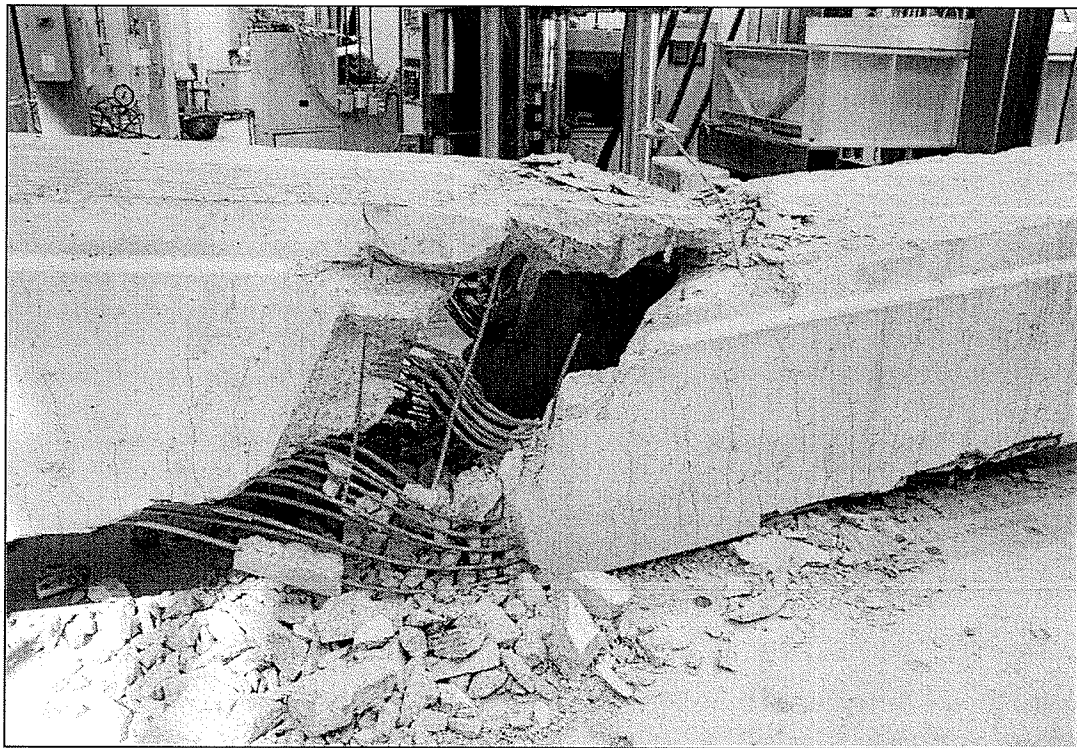


Figure 5-12: Failure near the mid-span on the east side of girder three.

5.2 Shear Testing Results

The results of the shear testing are summarized in Table 5-3. A full synopsis of each test is discussed in the paragraphs below. What is not discussed however, are the results of the strain gauge and pi gauge rosette data. An extensive analysis of the data was conducted and it was found that no discernable or intelligible conclusions could be made. Only one grouping of results acted as predicted but because there was no additional results that acted in a similar fashion, these results were not reported here. It is not certain why the data results did not display any expected patterns. The data acquisition system was checked to verify that each data port was functioning correctly and was calibrated prior to testing. A possible explanation for the poor data results that can be concluded at this time is that perhaps the strain gauges used in the rosettes were too large and therefore subject to bi-axial strain which cause erroneous readings.

Table 5-3: Shear testing results.

Girder	Maximum Load (kN)	Nominal Shear Capacity (kN)	Max Displacement @ a Load (mm)
4	805	692	202
5	706	614	213
6	817	701	268

The loads recorded for each experiment were converted to a nominal shear capacity using Equation 15. The shear force due to the girders' self-weight of the girder had already been calculated and was equal to 61.05 kN.

$$V_n = P \left(\frac{l-x}{x} \right) + 61.05 \text{ kN} \quad (\text{Eq. 15})$$

For example, the nominal shear capacity for girder one would be:

$$V_n = 805.34 \text{ kN} \left(\frac{18.90 \text{ m} - 4.15 \text{ m}}{18.90 \text{ m}} \right) + 61.05 \text{ kN} = 691.98 \text{ kN} \quad (\text{Eq. 16})$$

Table 5-4: Comparison of experimental versus theoretical nominal shear capacity.

Girder	Experimental Shear Capacity (kN)	Theoretical Shear Capacity (kN)	Increase Over Theoretical Shear Capacity (%)
4	692	478	45
5	614	439	40
6	701	451	55

It is clear that the theoretical shear capacity calculations were not all that accurate in predicting the experimental results. By comparison there was a 45, 40, and 55 percent difference between the experimentally observed shear capacity and the theoretical shear capacity for girders four, five, and six, respectively. The major reason for this discrepancy is that the equations used to calculate the nominal shear capacity within the AASHTO LRFD design manual are overly conservative in that the procedure has been simplified to reduce the number of steps required to calculate shear capacity.

Girder Four

The mode of failure for girder four was a flexure-shear failure. This was expected due to the distance of the load from the end support. The mechanism of failure was an explosion of the compression zone at the point of load. Interestingly, the girder had sheared asymmetrically; the west facing side failed within the region between the loading mechanism and the closest support whereas the east facing support failed between the loading mechanism and the far support. Loading eccentricities were at a minimum and therefore it was concluded that stress concentrations at the post-tensioning duct were the probable cause.

During this test, the pump used for extending the jacking device had stopped functioning and it was necessary to release the load and change the pump. In doing so the load cell was displaced giving an erroneous reading. This reading was corrected in the final plot. Once the pump was changed the girder was retested and monotonically loaded to failure. The first visible flexural cracks occurred under the point of loading at a resistance of about 400 kN. Diagonal shear cracks began to appear around 600 kN. As more force was applied, loss of concrete on the bottom of the webs occurred yet no strands ruptured. The cracks increased in number and size up to the ultimate load of 805 kN. This value of 805 kN converts to a nominal section shear resistance of 692 kN, 45 percent greater than the theoretically calculated nominal section shear capacity. Figures 5-13 and 5-14 display the loading versus displacement plot of the test. Figures 5-15 and 5-16 are photographs of the girder after failure was reached.

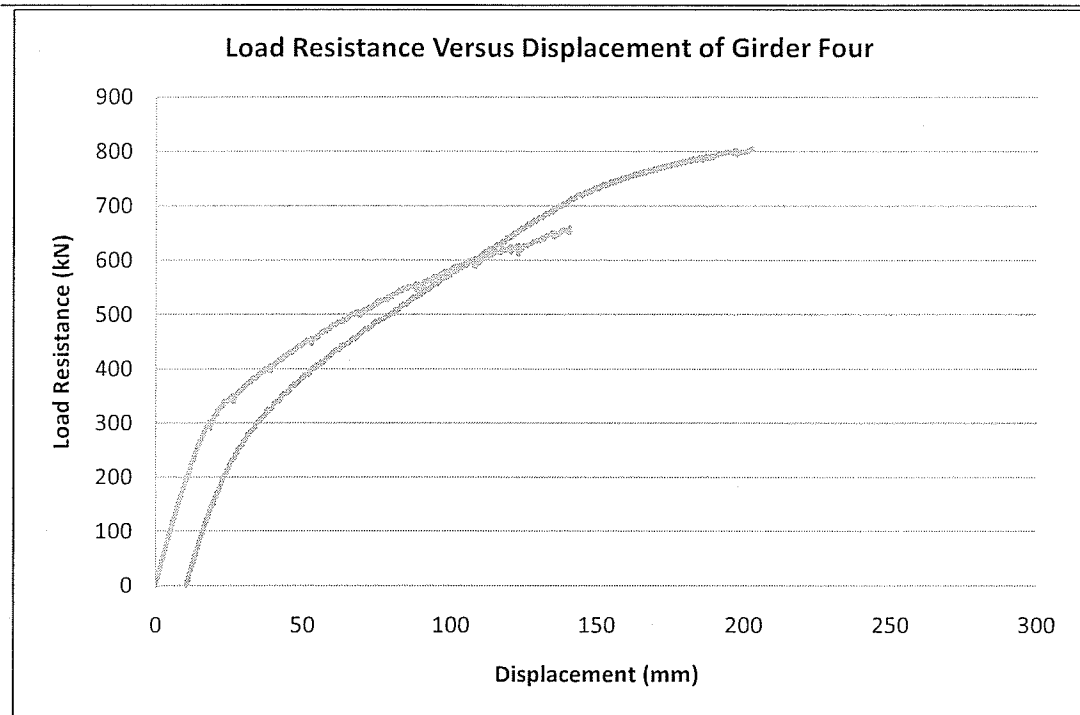


Figure 5-13: Load resistance versus displacement for shear testing of girder four.

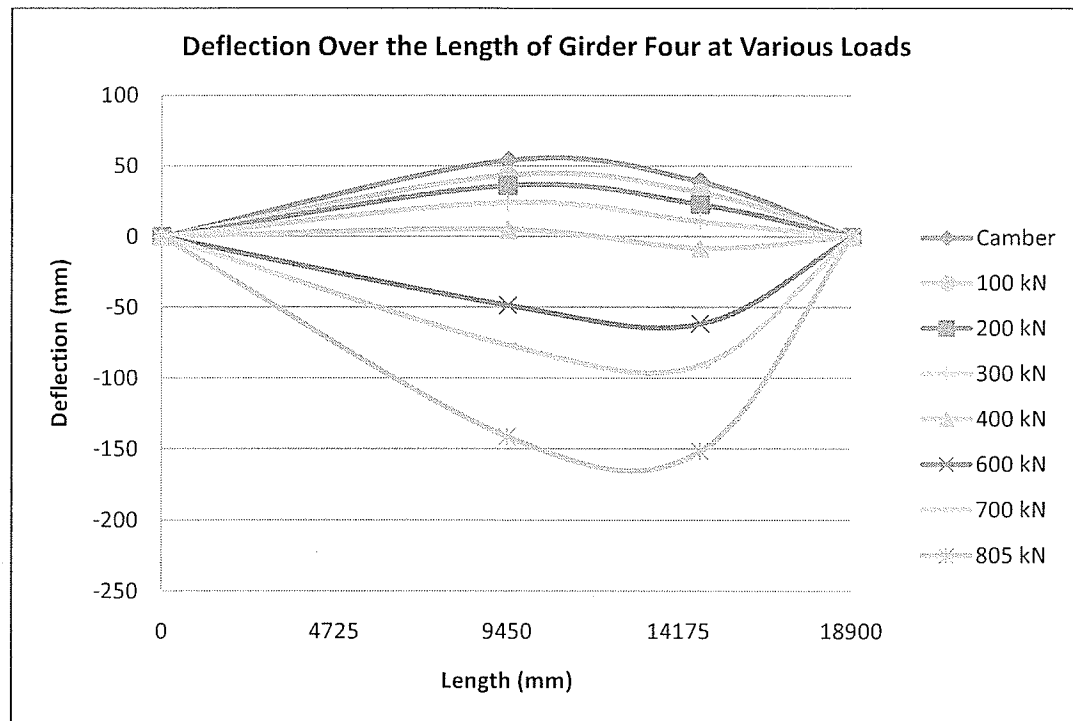


Figure 5-14: Deflection over the length of the girder for various loads during shear test one.

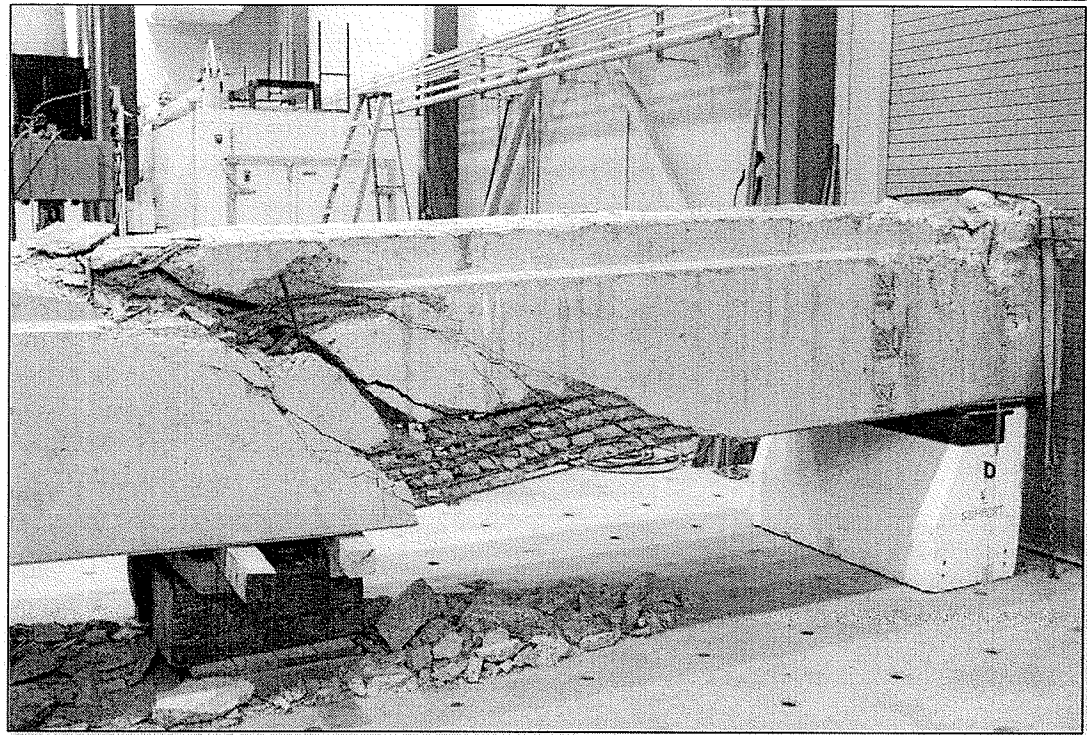


Figure 5-15: Failure near the quarter span on the west side of girder four.

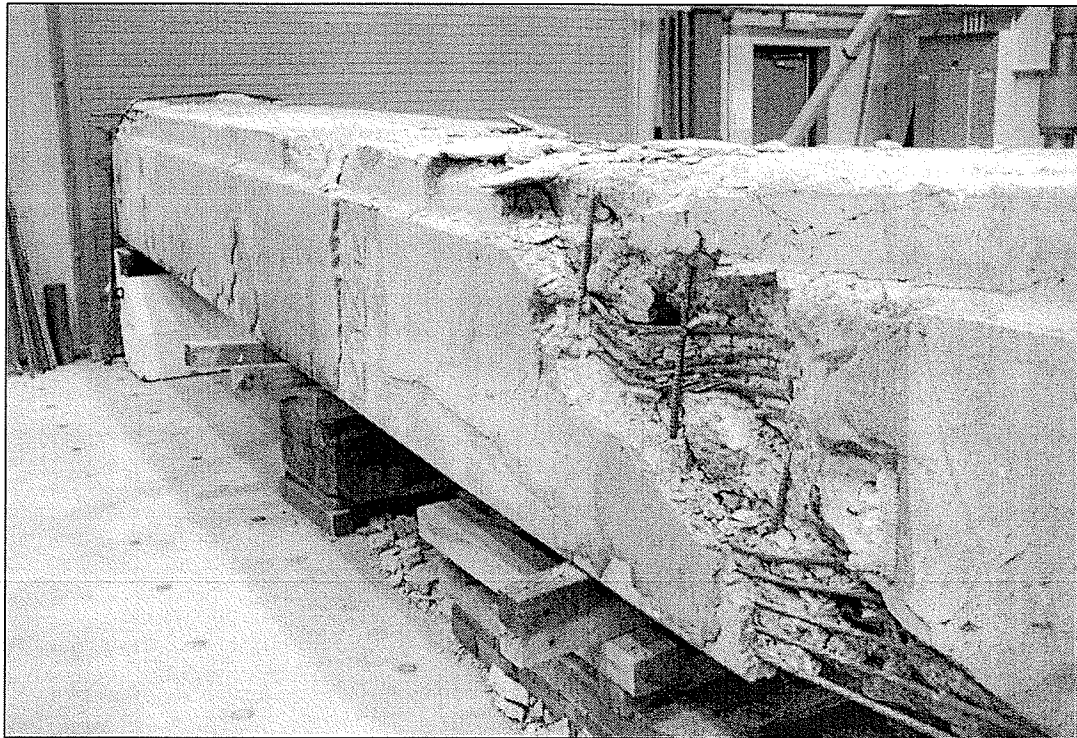


Figure 5-16: Failure near the quarter span on the east side of girder four.

Girder Five

Girder five failed in a flexure-shear failure fashion. The mechanism of failure was an explosion of the compression zone at the point of load. Although this girder was classified as being in poor condition in relation to the other girders it failed prematurely due to damage caused during demolition to the west facing web near the end block. This zone was inadequate to resist shear forces and succumb to an early failure. Girder five sheared asymmetrically within the region between the loading mechanism and the far support on the west web and between the near support and the loading mechanism on the east web. Loading eccentricity was also ruled out and it was determined that the absence of concrete cover on the bottom of the west facing web opposed to the near support shear region decreased the shear resistance of that zone.

The first visible flexural cracks occurred under the point of loading at a capacity of about 350 kN. Diagonal shear cracks began to appear around 500 kN. Beyond 500 kN there was a substantial amount of concrete delaminations and cover loss on the bottom of the webs as well as a ruptured strand on the east facing web. The cracks increased in number and size up to the ultimate load of 706 kN. This value converts to a nominal section shear resistance of 615 kN which was 40 percent greater than the theoretically calculated nominal section shear resistance of a girder with a cover loss of 75 mm and two ineffective strands. It is important to keep in mind that this girder was not able to resist to its potential due to the demolition damage. This damage can be clearly seen in Figure 5-20. Figures 5-17 and 5-18 display the loading versus displacement plot of the test. Figures 5-19 through 5-22 are photographs of the girder after failure was reached.

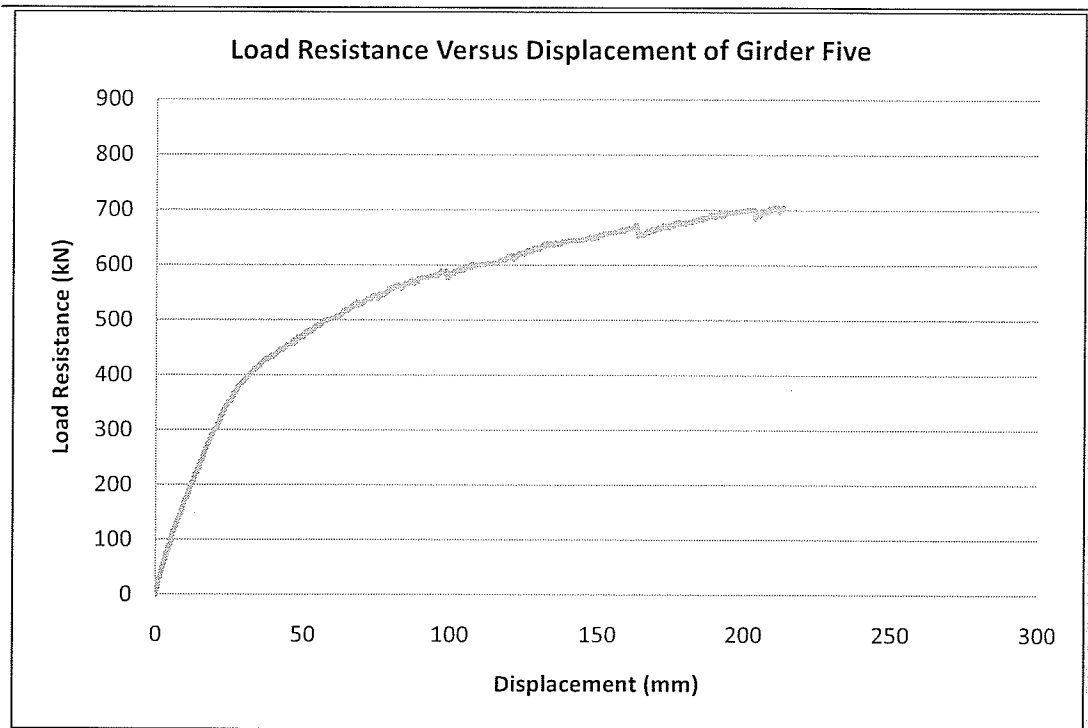


Figure 5-17: Load resistance versus displacement for the shear testing of girder five.

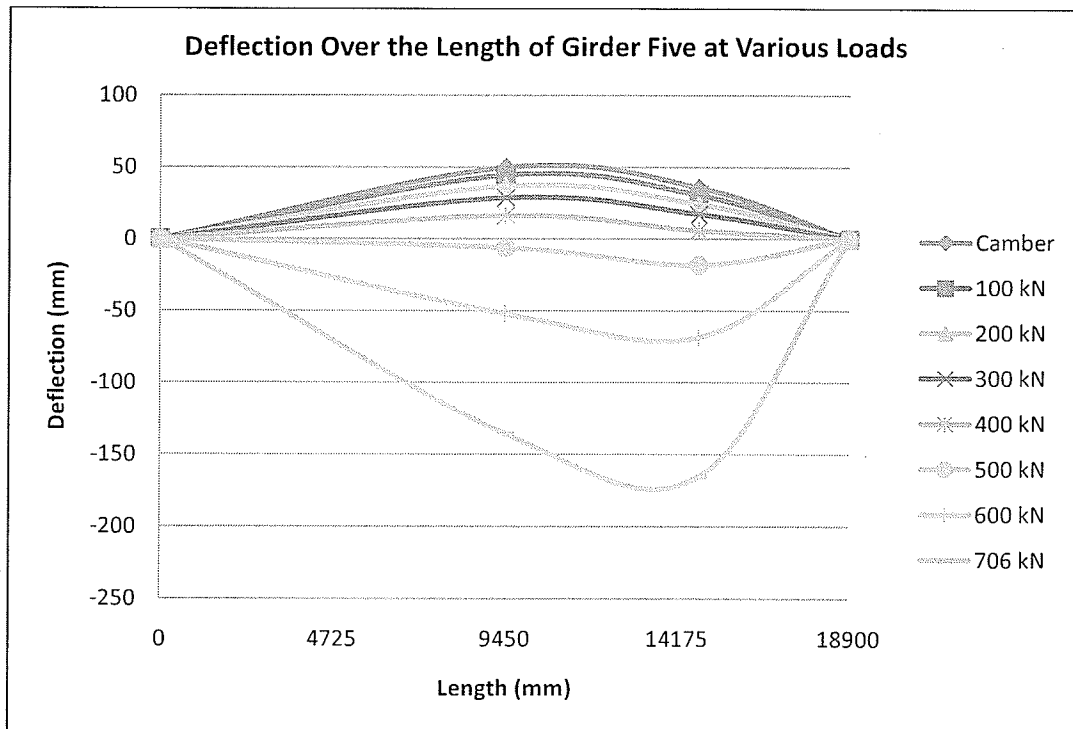


Figure 5-18: Deflection over the length of the girder for various loads during shear test two.

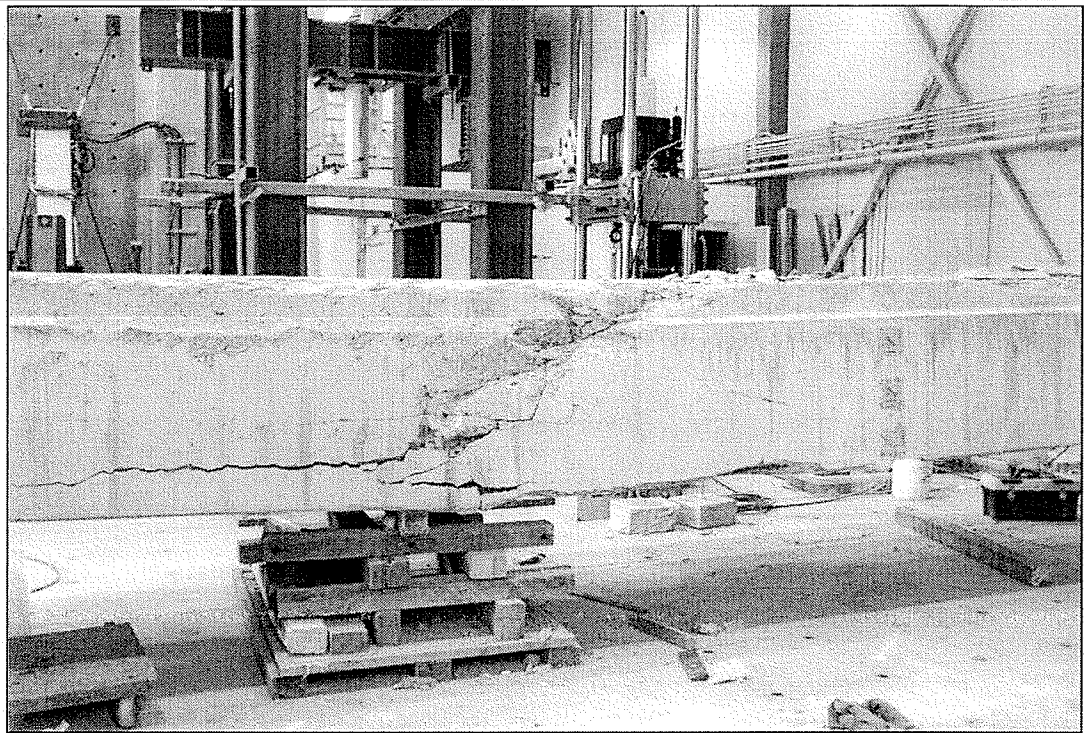


Figure 5-19: Failure near the quarter span on the west side of girder five.

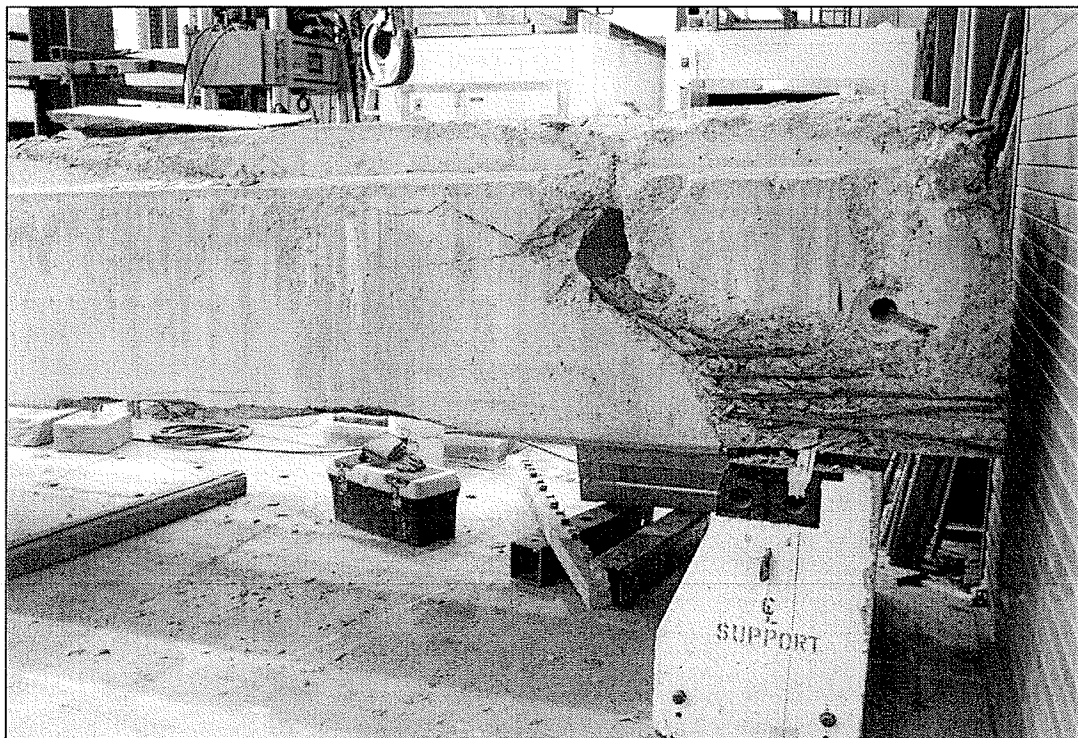


Figure 5-20: Failure at the support on the west side of girder five.

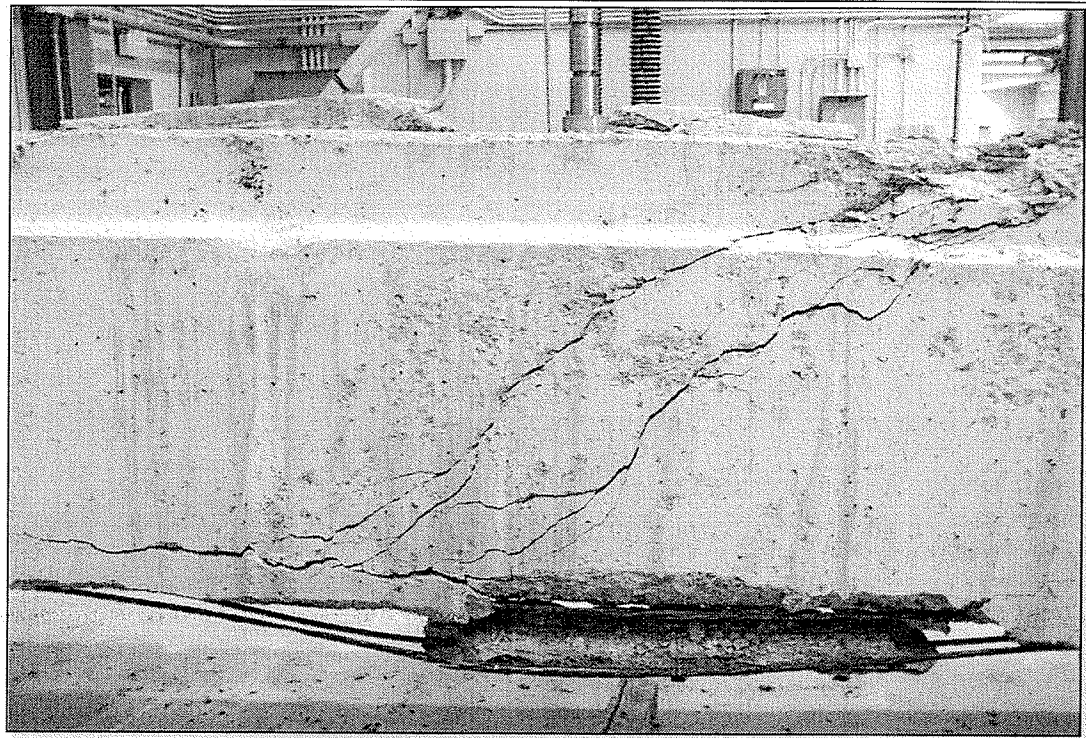


Figure 5-21: Failure between the support and quarter span on the east side of girder five.

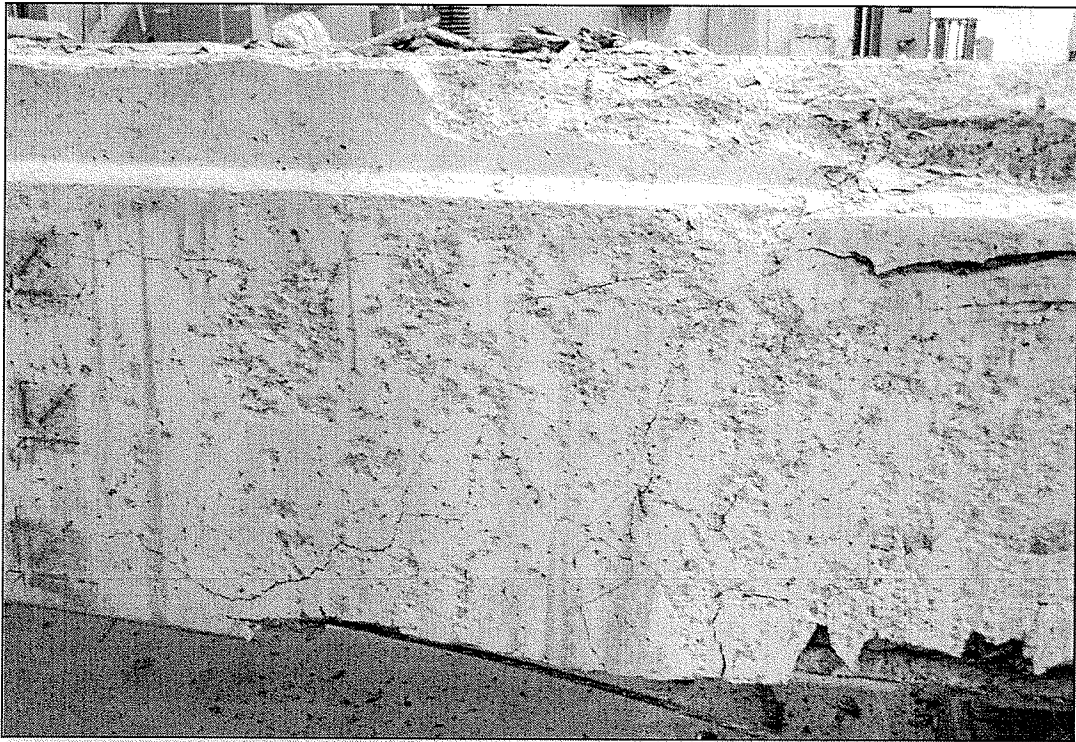


Figure 5-22: Diagonal cracking at the quarter span on the east side of girder five.

Girder Six

Girder six failed in a flexural shear failure fashion. The mechanism of failure was an explosion of the compression zone at the point of load. Although being classified as being in poor condition, girder six resisted a greater ultimate load than girder four. As with the previous girders tested in shear, girder six also sheared asymmetrically within the region between the loading mechanism and the far support on the west web and between the near support and the loading mechanism on the east web. The reduction of concrete cover on the west web allowed the propagation of cracking and subsequent failure on that side.

At a load of 350 kN, concrete from the already delaminated cover zones began to spall off the webs to the floor. The first visible flexural cracks occurred under the point of loading at a resistance of about 415 kN. Diagonal shear cracks began to appear around 625 kN. As more force was applied there was a substantial amount of concrete delaminations and spalling on the bottom of the webs as well as a ruptured strand on the east facing web. The cracks increased in number and size up to the ultimate load of 817 kN. This value converts to a nominal shear capacity of 701 kN which was 55 percent greater than the theoretically calculated nominal shear capacity of a girder with 50 mm of cover loss and one ineffective strand. Figures 5-23 and 5-24 display the loading versus displacement plots of the test. Figures 5-25 and 5-26 are photographs of the girder after failure was reached.

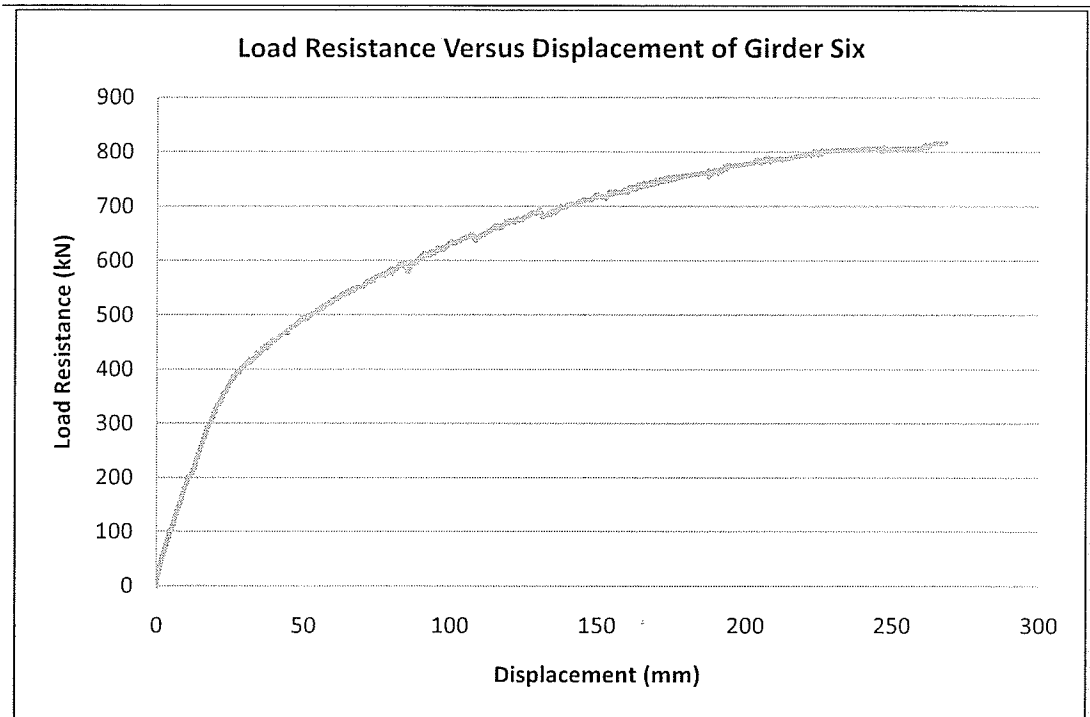


Figure 5-23: Load resistance versus displacement for shear test three.

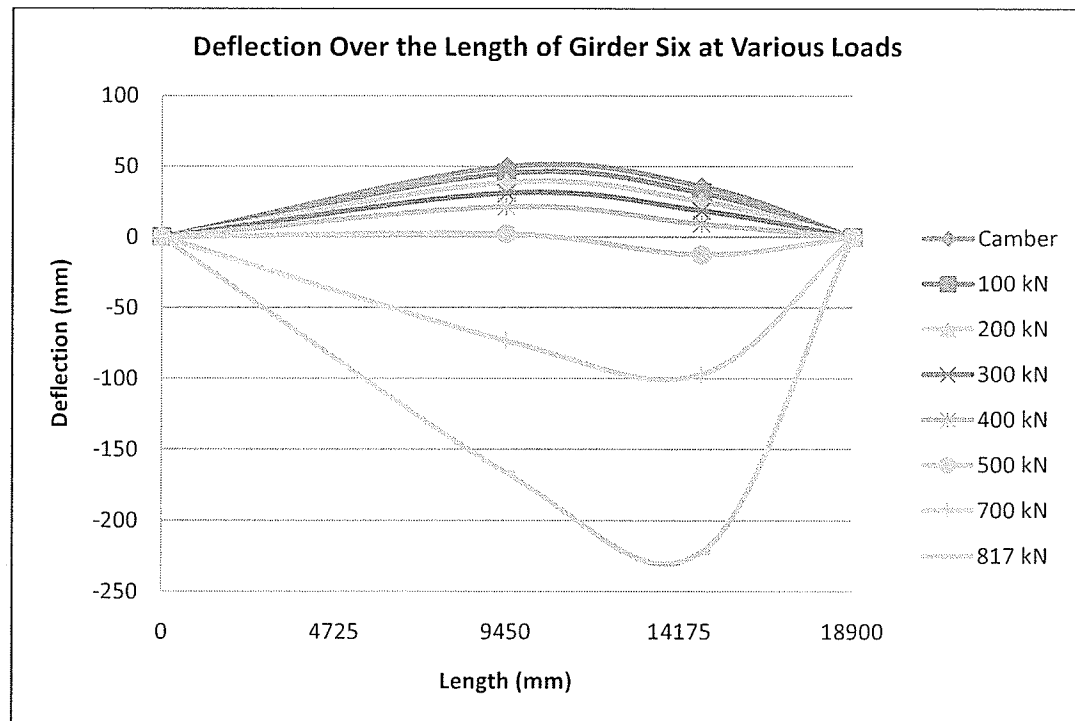


Figure 5-24: Deflection over the length of the girder for various loads during shear test three.

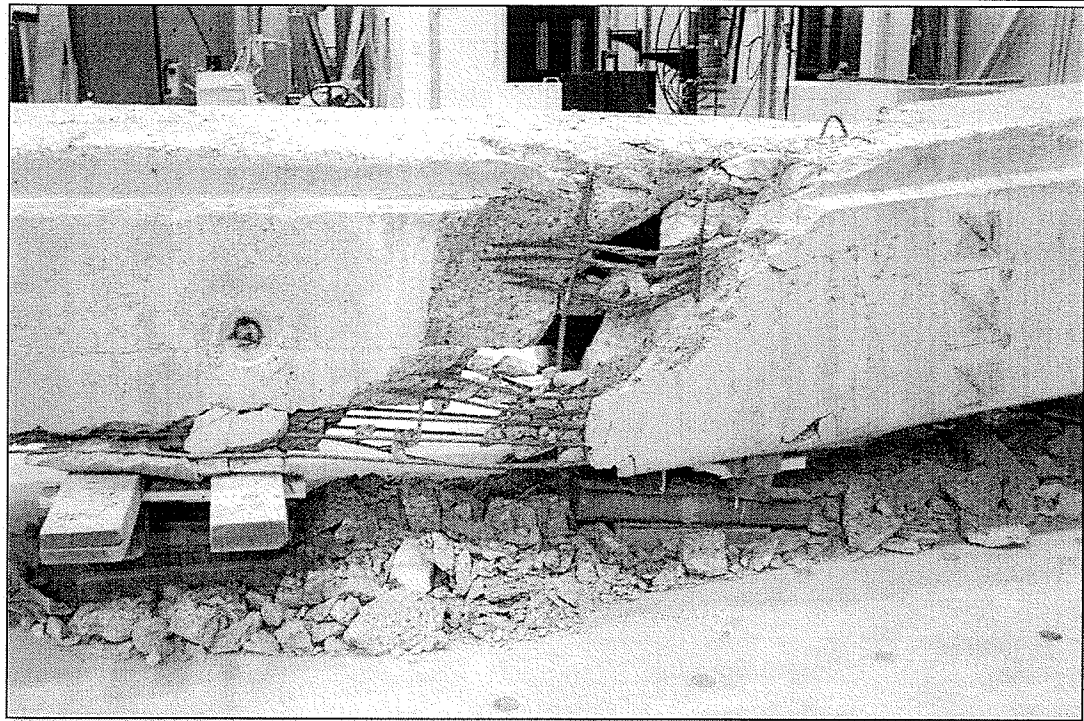


Figure 5-25: Failure near the quarter span on the west side of girder six.

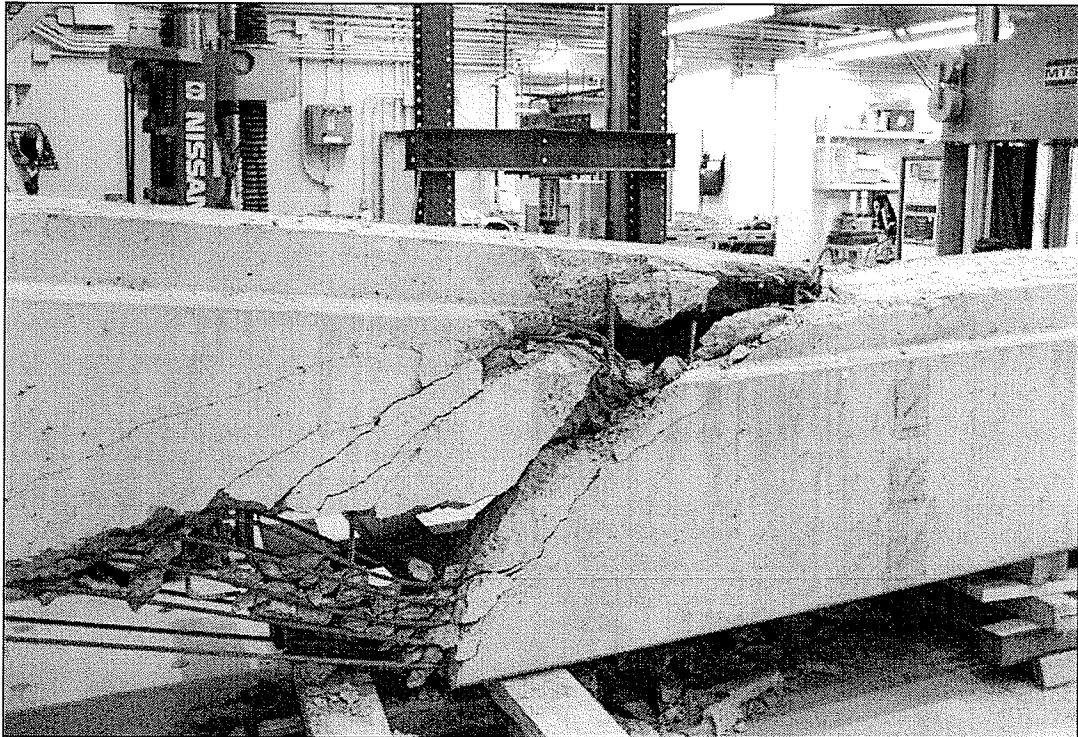


Figure 5-26: Failure zone on the east side of girder six.

5.4 Concrete Strength Testing Results

The results of the compressive cylinder test yielded a profound average increase in concrete strength. The original design 28-day concrete strength was to be no less than 37.92 MPa. The mean experimentally obtained value of the concrete some 40 years later was found to be 62.94 MPa. Each test result was multiplied by 0.95 to correct for an air dried moisture condition. This mean value was corrected for sample size in the following paragraph. The common failure type among the cylinders was a cone failure. A cone failure is a good indication of actual concrete strength as it demonstrates that there were no stress concentrations like that which causes the core surface to shear off leading to a columnal type failure. Cylinder test one yielded a result less than the 28-day design strength. It is possible that its lower density and failure type contributed to an early failure. In Table 5-5, the full results of the concrete strength testing are shown.

Table 5-5: Experimental results from the compression strength tests.

Girder	Location	Height (mm)	Height Factor	Density (kg/m ³)	Failure Load (kN)	Concrete Strength (MPa)	Failure Type
1	Flange	112.5	0.97	2218.90	152.93	37.20	Cone/Split
	Web	123.0	0.98	2308.08	248.80	61.18	Cone
2	Flange	134.0	0.99	2362.54	250.68	62.44	Cone/Split
	Web	92.0	0.94	2303.61	195.85	46.16	Columnal
3	Flange	139.5	1.00	2286.40	276.34	69.39	Cone
	Web	125.5	0.98	2295.71	264.63	65.25	Cone
4	Flange	139.0	1.00	2237.73	261.31	65.57	Cone
	Web	130.5	0.99	2203.71	210.63	52.23	Cone
5	Flange	139.5	1.00	2318.52	335.03	84.13	Cone
	Web	125.5	0.98	2306.21	266.71	65.76	Cone
6	Flange	137.0	1.00	2272.32	291.87	73.01	Cone
	Web	130.0	0.99	2291.27	294.67	73.03	Cone
Average	-	-		2283.75	254.12	62.94	-

Once the mean concrete strength was found it was necessary to calibrate this value to account for the number of samples tested as required by Annex A14.1 (*equivalent material strengths from tests of samples*) of the CHBDC. The sample size correction equation yields a strength value of 51.47 MPa. Table 5-6 outlines the statistical parameters and other values used for this calculation.

Table 5-6: Concrete strength correction parameters.

Mean Strength (MPa)	Standard Deviation (MPa)	Coefficient of Variation (%)	n (# of samples)	k_c (modification factor due to # of samples)
62.94	12.71	20.19	12	1.06

To correct for the sample size the following equation specified by the CHBDC was used:

$$f'_c = 0.9\bar{f}_c \left[1 - 1.28 \left[\frac{(k_c V)^2}{n} + 0.0015 \right]^{0.5} \right] \quad (\text{Eq. 7})$$

$$f'_c = 0.9 \times 62.94 \text{ MPa} \left[1 - 1.28 \left[\frac{(1.06 \times 0.20)^2}{12} + 0.0015 \right]^{0.5} \right] = 51.47 \text{ MPa} \quad (\text{Eq. 18})$$

Concrete increases in strength over time and therefore the subsequent 28-day strength of the fully corrected concrete strength can be calculated. This can then be compared to the design 28-day concrete strength. Equation 19 can be used to find the 28-day strength of the fully corrected experimentally observed concrete strength. It should be noted that although the girders were in service for 40 years, the testing was completed three years afterward and therefore time (t) was taken as 43 years.

$$f'_{c(28)} = f'_{c(t)} \left(\frac{4 + 0.85t}{t} \right) \quad (Eq. 6)$$

$$f'_{c(28)} = 51.47 \text{ MPa} \left(\frac{4 + 0.85(43 \text{ yrs} \times 365 \text{ days})}{(43 \text{ yrs} \times 365 \text{ days})} \right) = 43.77 \text{ MPa} \quad (Eq. 20)$$

The difference between the design 28-day strength and the corrected experimental 28-day expected strength was 5.85 MPa. There are a few possibilities to explain this discrepancy. It may have been possible that the design 28-day strength was not an absolute value but rather a minimum expected value. It may have also been possible that the friction between the loading plates and the core sample was great enough to reduce strain perpendicular to the direction of applied loading. The reduction in strain may have allowed for a greater force to be applied before failure was reached. Additionally, the sampling size may have been too small. A relatively large coefficient of variation was observed from the data which can be indicative of a small sampling size. Given a larger sample size it is plausible that the mean concrete strength would have been less and therefore the fully corrected concrete strength would also have been less. However, the take away point is that the concrete strength was not below the desired design 28-day strength.

The corrected concrete strength of 51.47 MPa increased the theoretically calculated flexural and shear capacities increased by an average of about four and nine percent, respectively, for the three girders tested in flexure and three girders tested in shear. The theoretically calculated capacities based on the experimentally found concrete strength are tabulated in Tables 5-7 and 5-8.

Table 5-7: Increases in nominal flexural capacities due to the increase of concrete strength.

Girder	Condition	Theoretical Nominal Flexural Capacity (kNm)	Increased Theoretical Flexural Capacity (kNm)	Increase Above Design Capacity (%)
1	Strands and cover intact	2771	2877	3.8
2	Strands and cover intact	2771	2877	3.8
3	50 mm of cover loss, 2 ineffective strands	2565	2675	4.3

Table 5-8: Increases in nominal shear capacities due to the increase of concrete strength.

Girder	Condition	Theoretical Shear Strength (kN)	Increased Theoretical Shear Capacity (kN)	Increase Above Design Capacity (%)
4	Ideal	521	478	8.9
5	75 mm of cover loss, 2 ineffective strands	467	429	8.9
6	50 mm of cover loss, 1 ineffective strand	492	451	9.1

The four and nine percent increases in flexural moment and shear do not represent a significant increase in capacity. In instances where a rating factor is a few points below the minimum target rating of one, this increase may allow for a passing rating where previously the rating was below one. However, the increase in concrete strength does little to increase the accuracy of the ultimate theoretical capacity compared to the experimental observation.

5.5 Chloride Ion Content Testing Results

The results of the chloride ion content test did not reveal a significant amount of chloride present in the flange or the web of the six girders tested. In fact, the greater percentages of present chloride are only marginally greater than those values expected present at the time of curing. Only girders three and five which were classified as being in poor condition exhibited greater than 20 percent probability of chloride-caused corrosion. The full results are presented in Table 5-9.

Table 5-9: Chloride ion content testing results.

Girder	Location	Depth (inches)	Cl (%)	lb/cu. Yd.	Probability of Failure (%)
1	Flange	1	0.060	0.155	Insignificant
		2	0.019	0.046	Insignificant
	Web	1	0.188	0.480	Insignificant
		2	0.041	0.103	Insignificant
2	Flange	1	0.013	0.034	Insignificant
		2	0.009	0.021	Insignificant
	Web	1	0.033	0.086	Insignificant
		2	0.022	0.055	Insignificant
3	Flange	1	0.250	0.620	20 to 25
		2	0.157	0.390	Insignificant
	Web	1	0.270	0.650	20 to 25
		2	0.135	0.320	Insignificant
4	Flange	1	0.077	0.194	Insignificant
		2	0.047	0.108	Insignificant
	Web	1	0.128	0.310	Insignificant
		2	0.121	0.300	Insignificant
5	Flange	1	0.174	0.440	Insignificant
		2	0.107	0.250	Insignificant
	Web	1	0.176	0.440	Insignificant
		2	0.181	0.490	Insignificant
6	Flange	1	0.134	0.310	Insignificant
		2	0.047	0.121	Insignificant
	Web	1	0.210	0.600	20 to 25
		2	0.175	0.430	Insignificant

a greater chloride ion contented may have been expected given the strand deterioration observed on some of the girders. It should be made clear that chlorides are not required for exposed steel to corrode. In addition, given the fact that the girders were not subject to water leaching through the shear keys throughout their entire service life and that Manitoba Highways and Transportation uses as little de-icing salt as possible the results of this testing are appropriate. Furthermore, examination of the upper layer steel strands after shear and flexural testing demonstrated only minor surface rust. Therefore it can be said that chloride ions were not a significant contributor to the deterioration observed on the girders.

5.6 Air Void Ratio and Spacing Factor Testing Results

The air void tests yielded interesting results and shed light on the possible cause of the loss of cover from the bottom of the girder webs. The average air void content of 2.8 percent was below the minimum required air void content of 3.0 percent. Many individual tests yielded results well below this minimum. More worrisome was the spacing factor of the air voids determined by the tests. To ensure the concrete is not susceptible to frost damage the spacing between air voids should not exceed a maximum value of 260 μm . The test results yield an average spacing factor of 790 μm , well above the acceptable limit. Table 5-10, the results of the air void tests are shown.

Table 5-10: Hardened concrete air void property testing results.

Girder	Sample Identification	Air Content (%)	Specific Surface (μm^{-1})	Spacing Factor (μm)
1	Flange	2.0	11.04	675
	Web	1.7	15.07	534
2	Flange	3.5	5.49	1011
	Web	3.0	8.44	744
3	Flange	1.4	11.48	731
	Web	1.8	9.93	768
4	Flange	2.6	6.58	996
	Web	1.7	8.46	916
5	Flange	5.3	5.81	792
	Web	2.6	10.46	651
6	Flange	3.5	7.84	730
	Web	4.3	5.66	926
Average	-	2.8	8.9	790
CSA A23.1-04 frost resistant concrete limits:		3.0 minimum	no limit	260 maximum

The results of the testing demonstrated that the samples did not meet the criteria of frost resistant concrete and therefore the girders were susceptible to frost damage. This correlates with the observed surface scaling seen on the webs of the girders. In addition, this can explain the loss of cover seen on the bottom of the webs. Since this was a zone of water accumulation, moisture would have infiltrated the concrete during thawing and potentiated damage during freezing. Therefore, the air void properties of the concrete were a major contributor to the deterioration observed on the girders.

6. LOAD RATING RESULTS

This section examines the results of the load rating analysis compiled for each girder using theoretical calculations and experimentally observed values for both the CHBDC bridge evaluation method and the AASHTO LRFR method.

Due to the deterioration seen on the girders (especially girders three, five and six) only the ultimate limit state was analyzed as it was assumed that the service limit had already been surpassed. The theoretical ultimate limit state analysis was carried out at a distance equal to the shear depth (d_v) from the bearing edge, a distance of 4.45 meters from the center of the bearing support, and at each fifth length from the bearing center to the mid-span. The mid-span and 4.45 meter distance from the bearing center theoretical rating factors were compared against the experimentally observed moment and shear capacities at those locations.

For this analysis a conservative approach was taken and it was assumed that the girders were acting completely independent of one another. A single girder would not be subjected to more than half of an evaluation load as dimensionally it was not possible for a truck to load a girder with more than half its weight. The girders had a width of 1219 mm where as the distance between the inner tires of a heavy truck are 1350 mm. As such, within the CHBDC and the AASHTO load rating analysis in this section, the lateral distribution of loading was taken as 0.5. Additionally, given the ten foot lane width and a four foot girder width, the lateral distribution of the distributed lane load was taken as 0.4.

For each of the load rating systems only the interior girders were analyzed. Vehicle loading on the exterior girders would be a rare loading case as the exterior girders are not encompassed within the actual defined lanes. Furthermore, the various cases of deterioration for shear and flexural loading covered in the specimen condition section of this report were analyzed. The bending load rating analysis included an ideal condition case and a case where two of the four bottom strands were ineffective and 50 mm of concrete cover had been lost from the bottom of the webs. The flexure-shear load rating analysis included an ideal condition, a case where 50 mm of concrete had been lost from the bottom of the webs with one ineffective strand, and a case where 75 mm of concrete had been lost from the webs with two ineffective strands.

6.1 CHBDC Bridge Evaluation

6.1.1 Influence Analysis of Evaluation Loading Levels

An influence moment and shear analysis was carried out to determine the maximum loading for each evaluation vehicle. In most cases the combination of a lane and 80 percent truck load was the dominant loading scenario. Although, the CHBDC does not require a dynamic loading factor to be applied to the combined truck and lane loading, the difference in maximums between truck load alone and truck and lane load combined was on the order of less than ten percent and therefore the dynamic load factor was applied. In Figures 6-1 and 6-2, the maximum shear and flexural moments are given for each evaluation level along the length of the girder. It can be seen from the figures that the E2 level evaluation loading is largely the governing load.

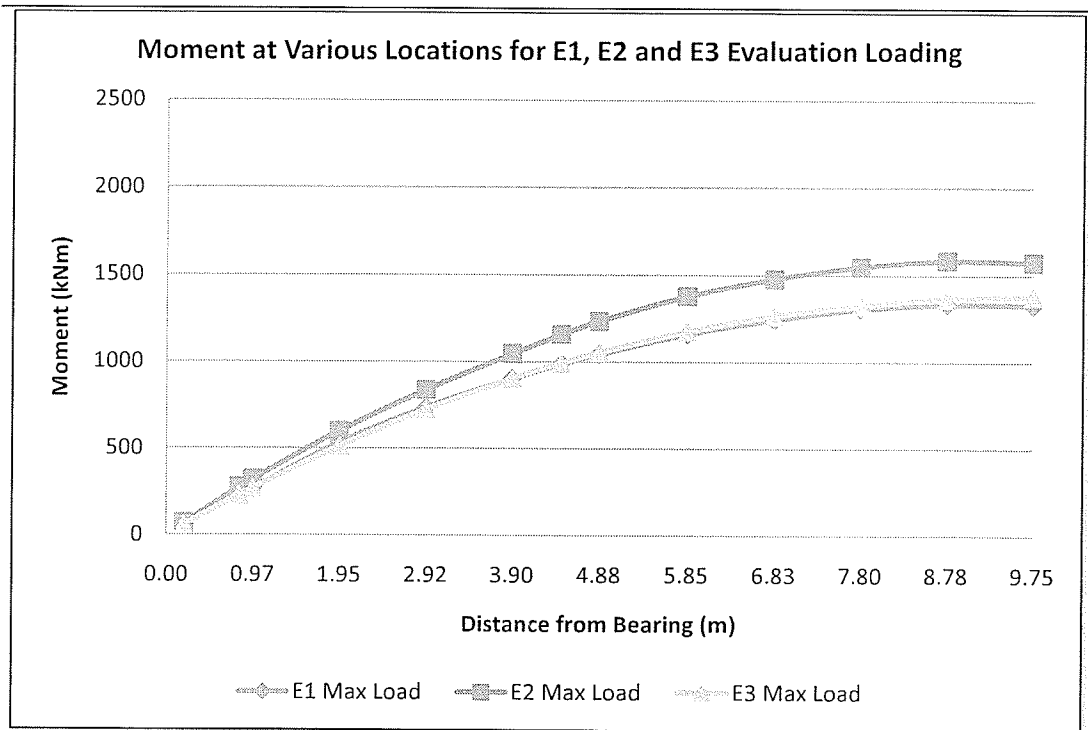


Figure 6-1: Moment at various location for E1, E2, and E3 evaluation loading.

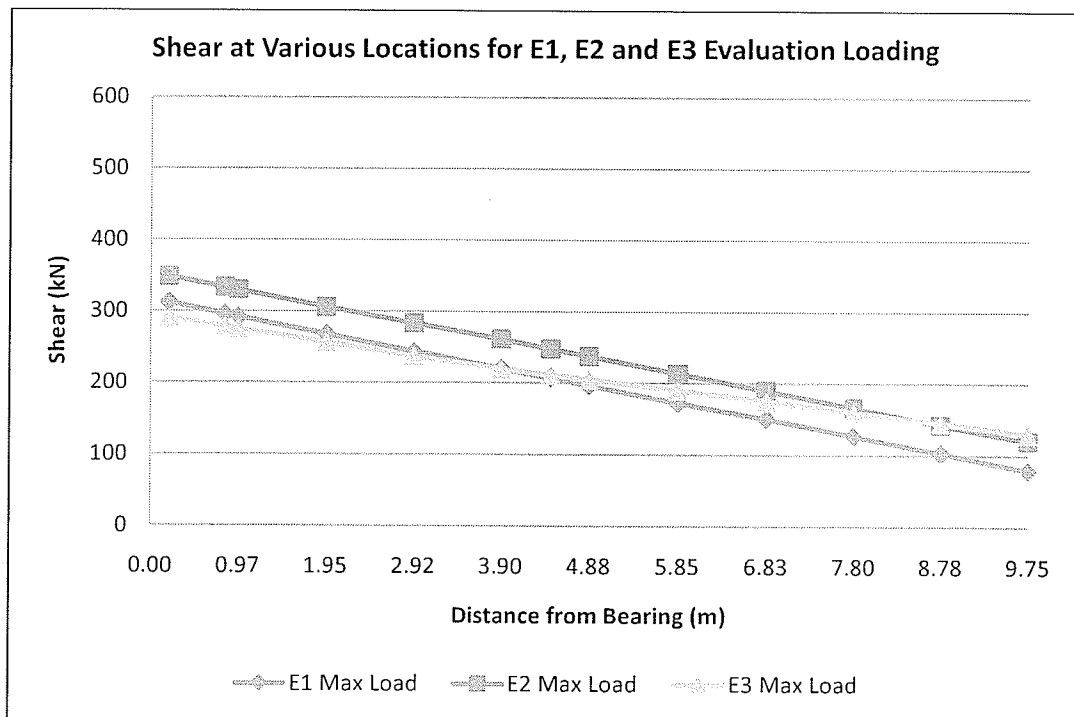


Figure 6-2: Shear at various locations for E1, E2, and E3 evaluation loading.

6.1.2 Assumptions and Load Factors

The loading factors of the CHBDC bridge evaluation are determined through the target reliability index. To arrive at a target reliability index the system behavior, element behavior and inspection level are required to be taken into account. The system behavior was classified as a category “S2”, where element failure probably will not lead to a total collapse. The element behavior was classified as a category “E1”, where the element being considered is subject to sudden failure with little or no warning but will retain post-failure capacity. The inspection level was classified as a category “INSP2”, where inspection is to the satisfaction of the evaluator, with the results of each inspection recorded and is available to the evaluator. These categorizations yielded a target reliability index (β) for normal heavy truck traffic of 3.50.

The target reliability index of 3.50 generated a maximum dead load for factory-produced, cast in place and surfacing components of 1.09, 1.18, and 1.45, respectively. This reliability index also yielded a live load factor for normal truck traffic (E1, E2, and E3) of 1.61.

Additional factors including the dynamic load allowance for normal vehicle traffic was taken as 1.33 as given by the CHBDC. Although, no dynamic load allowance was required to be applied to the truck and uniformly distributed loading together, for this analysis this factor was applied as it was felt that it reflected the actual loading dynamics more accurately. Given the properties of the girders, the selected resistance adjustment factor was 0.94.

6.1.3 Theoretical Bridge Evaluation Results

This analysis was carried out using the moment and shear capacities calculated under the CSA S6-06. These calculations employed the appropriate material factors for steel reinforcing, pre-stressing, and concrete and were on the order of 10 to 15 percent less than those capacities calculated by the AASHTO LRFD method.

The results of the theoretical CHBDC evaluation analysis demonstrated that no girders met the required rating factor of one. The governing failure case did not receive a rating factor greater than one at all points examined along the length of the girder and therefore it can be said that the girders within this program did not pass the evaluation. The full results of the theoretical evaluation analysis are shown in Figures 6-3 to 6-6.

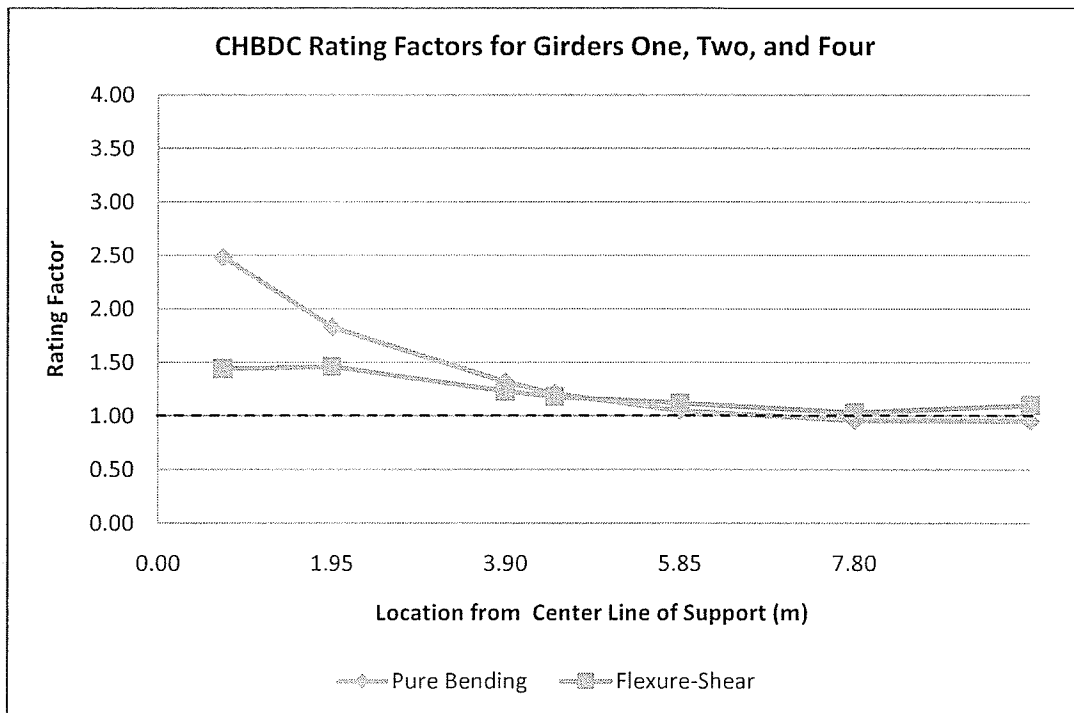


Figure 6-3: CHBDC rating factors at various locations along the length of girders one, two, and four.

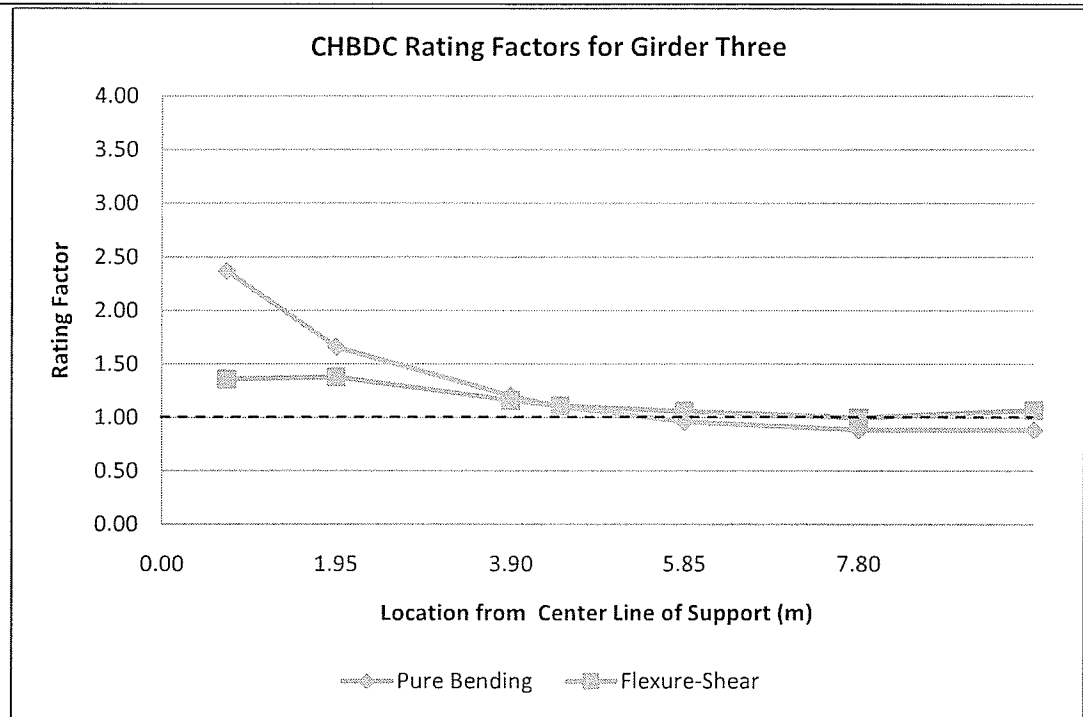


Figure 6-4: CHBDC rating factors at various locations along the length of girder three.

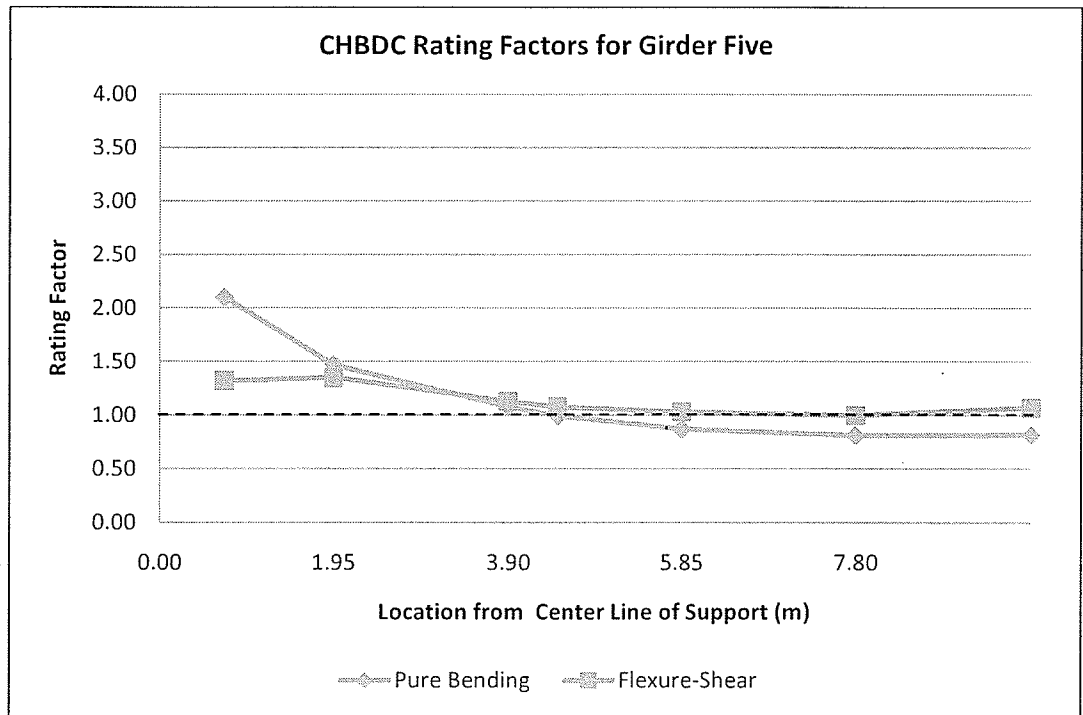


Figure 6-5: CHBDC rating factors at various locations along the length of girder five.

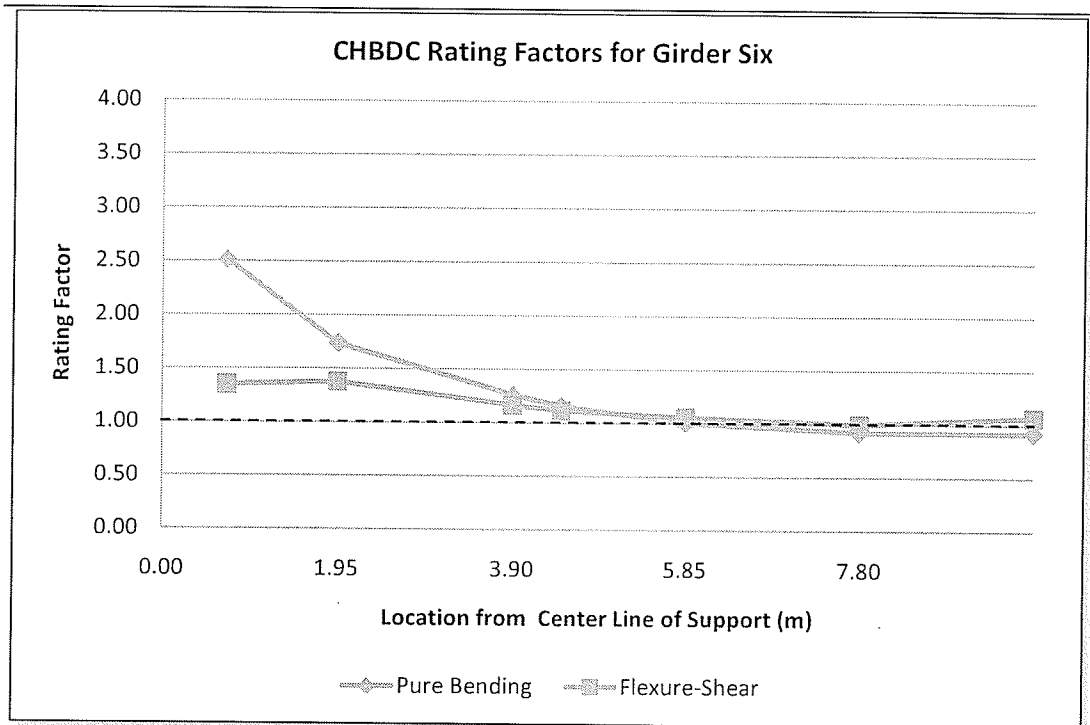


Figure 6-6: CHBDC rating factors at various locations along the length of girder six.

6.1.4 Experimental Bridge Evaluation Results

Comparison of the theoretical girder capacities to the experimental capacities of each girder of this analysis, it was found that the experimental analysis yields a significantly greater rating factor than the theoretical analysis. The increase in rating factor was on average 50 points greater than the theoretical analysis for pure bending and at least 90 points greater than the theoretical analysis for flexure-shear. The pure bending scenario was the dominating failure case at both the quarter and mid-span. The results of this comparison can be found in Tables 6-1 to 6-6.

Table 6-1: Comparison of theoretical and experimental rating factors for girder one at the mid-span.

Values Analyzed	Limit State		Governing Evaluation Load
Experimental	Ultimate	Pure Bending	1.56
		Flexure-shear	2.17
Theoretical	Ultimate	Pure Bending	0.95
		Flexure-shear	1.10

Table 6-2: Comparison of theoretical and experimental rating factors for girder two at the mid-span.

Values Analyzed	Limit State		Governing Evaluation Load
Experimental	Ultimate	Pure Bending	1.49
		Flexure-shear	2.09
Theoretical	Ultimate	Pure Bending	0.95
		Flexure-shear	1.10

Table 6-3: Comparison of theoretical and experimental rating factors for girder three at the mid-span.

Values Analyzed	Limit State		Governing Evaluation Load
Experimental	Ultimate	Pure Bending	1.36
		Flexure-shear	1.92
Theoretical	Ultimate	Pure Bending	0.89
		Flexure-shear	1.07

Table 6-4: Comparison of theoretical and experimental rating factors for girder four near the quarter span.

Values Analyzed	Limit State		Governing Evaluation Load
Experimental	Ultimate	Pure Bending	1.68
		Flexure-shear	2.13
Theoretical	Ultimate	Pure Bending	1.21
		Flexure-shear	1.18

Table 6-5: Comparison of theoretical and experimental rating factors for girder five near the quarter span.

Values Analyzed	Limit State		Governing Evaluation Load
Experimental	Ultimate	Pure Bending	1.44
		Flexure-shear	1.86
Theoretical	Ultimate	Pure Bending	0.99
		Flexure-shear	1.08

Table 6-6: Comparison of theoretical and experimental rating factors for girder six near the quarter span.

Values Analyzed	Limit State		Governing Evaluation Load
Experimental	Ultimate	Pure Bending	1.70
		Flexure-shear	2.16
Theoretical	Ultimate	Pure Bending	1.16
		Flexure-shear	1.12

In total, it was found that the experimental analysis yielded a rating factor greater than one for all girders. In most cases the rating factor was on the order of at least 35 to 115 points greater than the target value of one. Overall, this load rating method is less conservative than the AASHTO load rating method in terms of the live and dead load factors as well as the design loading used. Also, this method does not employ a condition factor to be applied to the capacity. However, the CHBDC method is as, or more conservative with regards to resistance factors. This system requires the use of material factors to be applied to the theoretical bending and shear capacities in addition to a resistance factor whereas the AASHTO method does not. In addition, a dynamic live loading factor was applied although not required by code. Therefore, it was concluded that although the theoretical and experimental analyses could only be compared at the quarter and mid-span, the girders examined within this program passed the CHBDC bridge evaluation.

6.2 AASHTO Load and Resistance Factor Rating

6.2.1 Influence Analysis of Loading Levels

The LRFR analysis was carried out with the HS-20 and the HSS-30 design loads. Comparing the evaluation levels of the CHBDC bridge evaluation to the HS-20 and HSS-30 design loads of the AASHTO LRFR method it was found that the maximum CHBDC evaluation loading falls somewhere between the HS-20 and the HSS-30 design loads. Comparing the HSS-30 design truck to the HS-20 design truck demonstrates approximately a two to one difference especially at locations closer to the mid-span for bending and closer to the bearing support for shear. Figures 6-3 and 6-4 show the moment and shear effects of the HS-20 and HSS-30 design truck loading.

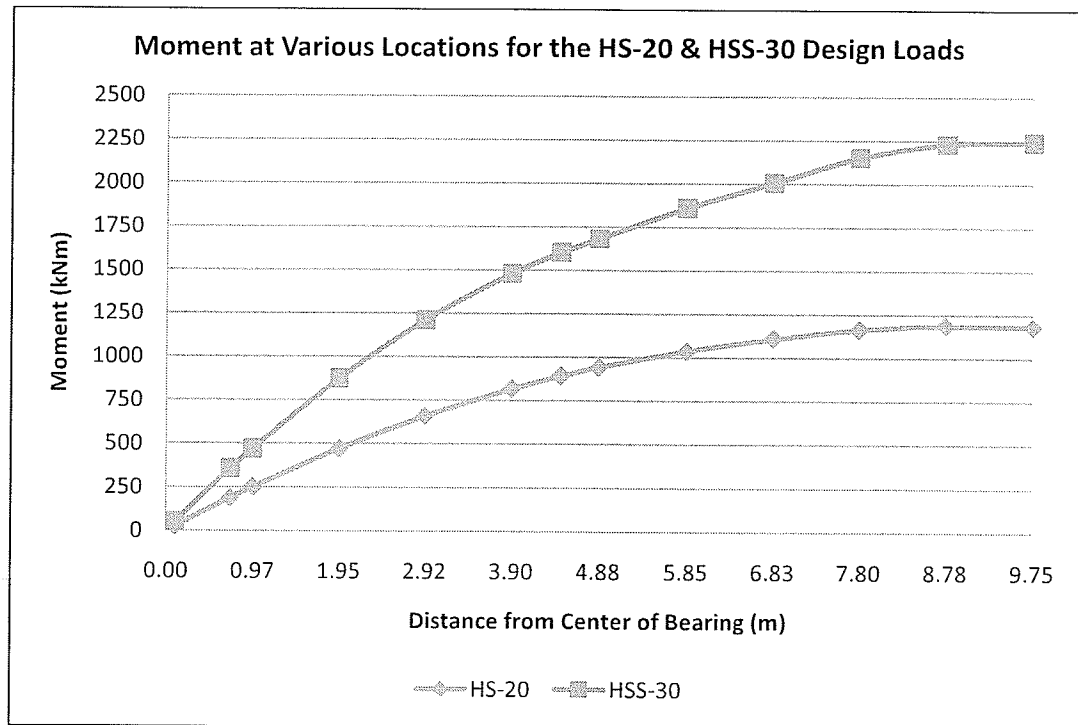


Figure 6-7: Moment at various locations for the HS-20 and HSS-30 truck loading.

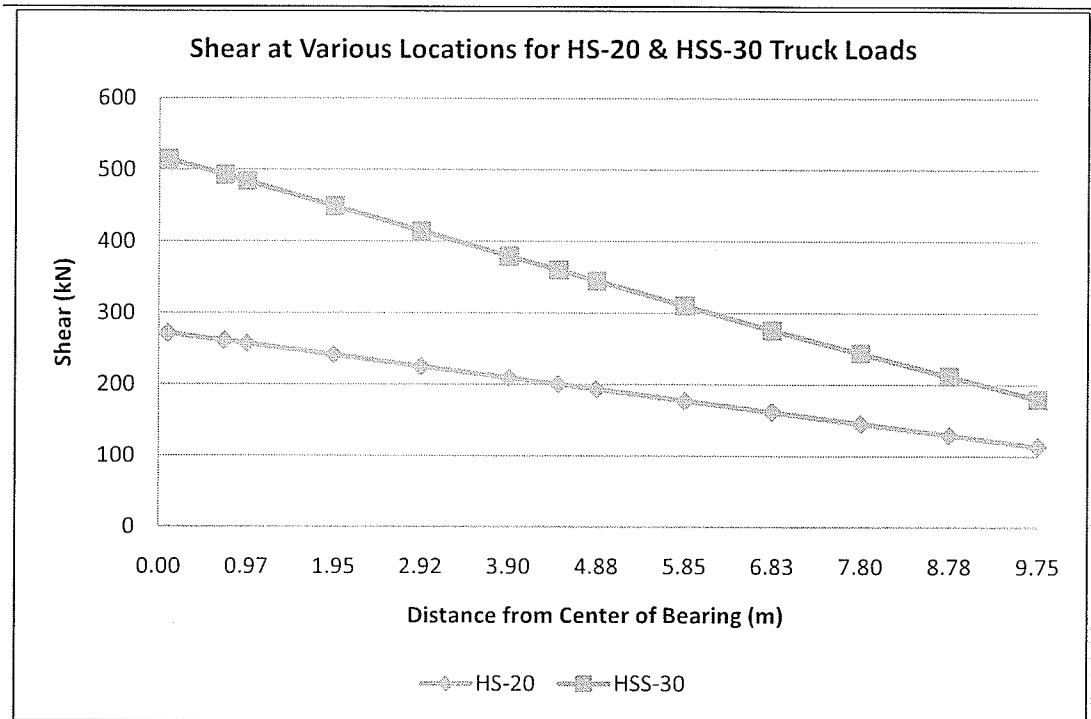


Figure 6-8: Shear at various location for the HS-20 and HSS-30 truck loading.

6.2.2 Assumptions and Load Factors

The dead load factors for the self-weight (and other factory components), and the wearing surface was taken as 1.25 and 1.50 respectively. Inventory and operating live load factors were taken as 1.75 and 1.35. The dynamic live loading factor was taken as 1.33 corresponding to a roadway with cracks and surface deviations. These are all commonly used values for these factors. Much like the resistance adjustment factor within the CHBDC evaluation, the LRFR incorporates resistance, condition, and system factors. The values used were 1.0 for flexure resistance, 0.9 for shear resistance, and 1.0 for the system factor. Although the condition of each girder was taken into account when calculating the theoretical moment and shear capacities, the appropriate condition factor was applied to each girder. A value of 1.00, 0.95, or 0.85 was applied to girders

categorized as being in good, fair, or poor condition. Although conservative, these values were used within the load rating analysis of the experimentally observed values as well.

6.2.3 Theoretical Load Rating Results

The results of the theoretical loading rating analysis demonstrated that girders one, two, and four were capable of sustaining the HS-20 design loading as each girder received a rating factor of no less than one. This is not surprising as these particular girders were in relatively good condition. With respect to the HS-20 loading, at all locations except the mid-span the governing mode of failure was a flexure-shear failure.

The results of the HSS-30 design load rating analysis did not yield a rating factor greater than one at any location for the flexure-shear failure case. Additionally, at all locations the flexure-shear failure was the governing rating factor. For those locations where the dominating rating factor was the flexure-shear case the failures were largely tension reinforcement controlled. The only exception being with girders one and four at the $0.2 \times l$ (3.90 meter) point where failures were stirrup controlled. A summary of the theoretical load rating factors for both the HS-20 and HSS-30 under the inventory state are found in Figures 6-9 to 6-13.

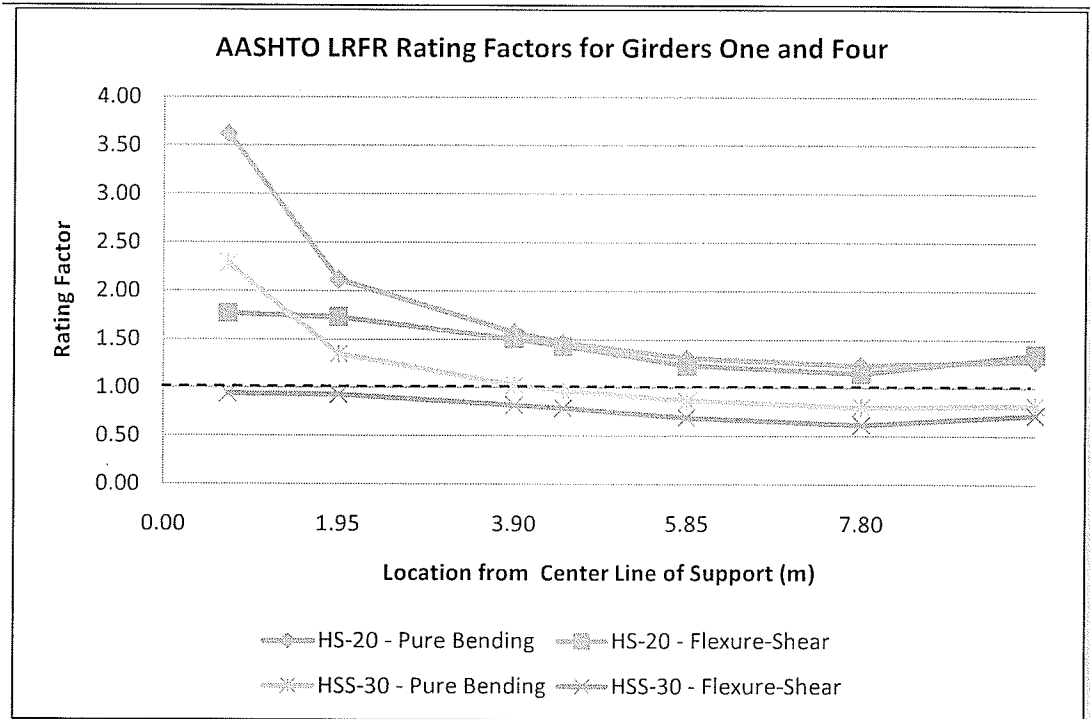


Figure 6-9: AASHTO rating factors at various locations along the length of girders one and four.

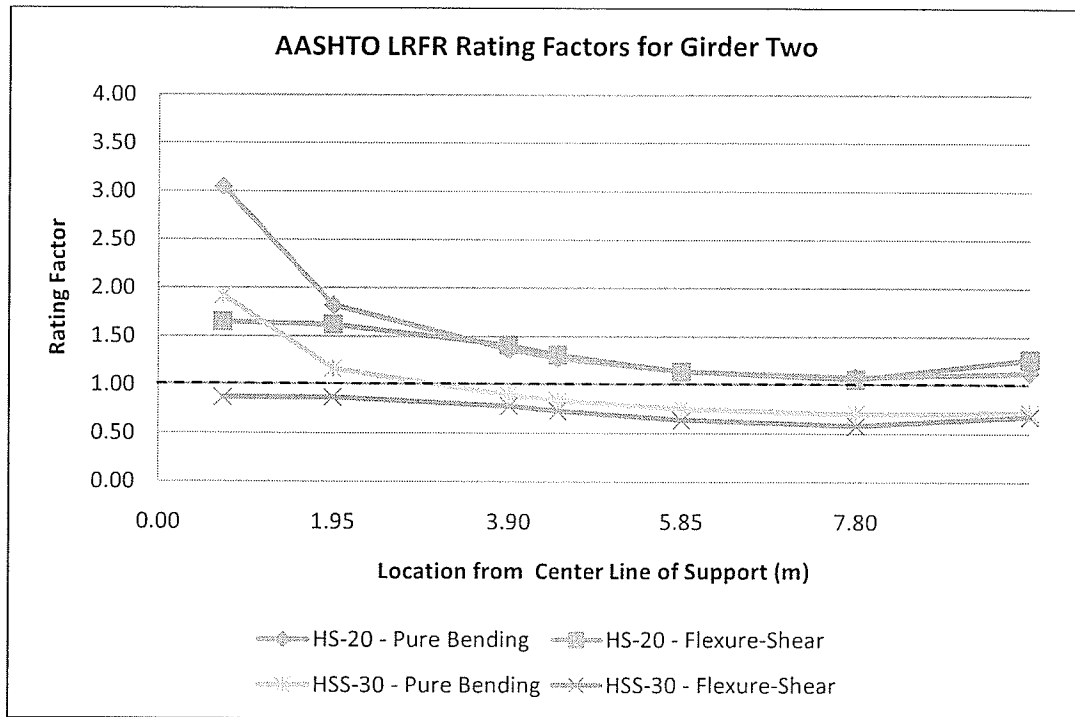


Figure 6-10: AASHTO rating factors at various locations along the length of girder two.

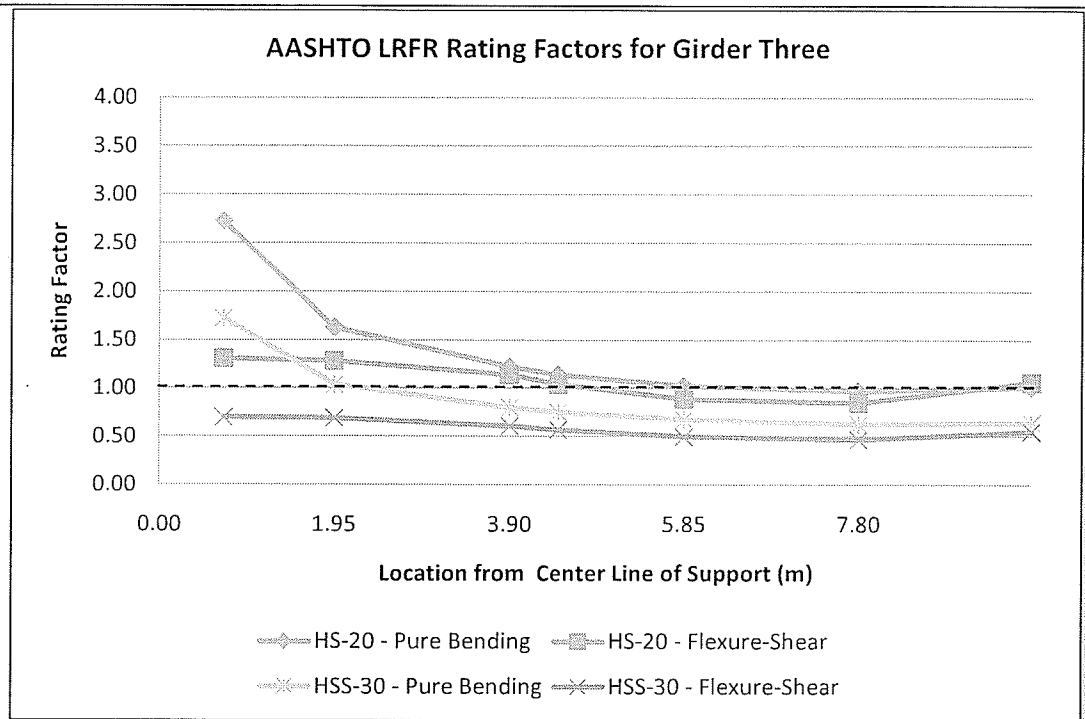


Figure 6-11: AASHTO rating factors at various locations along the length of girder three.

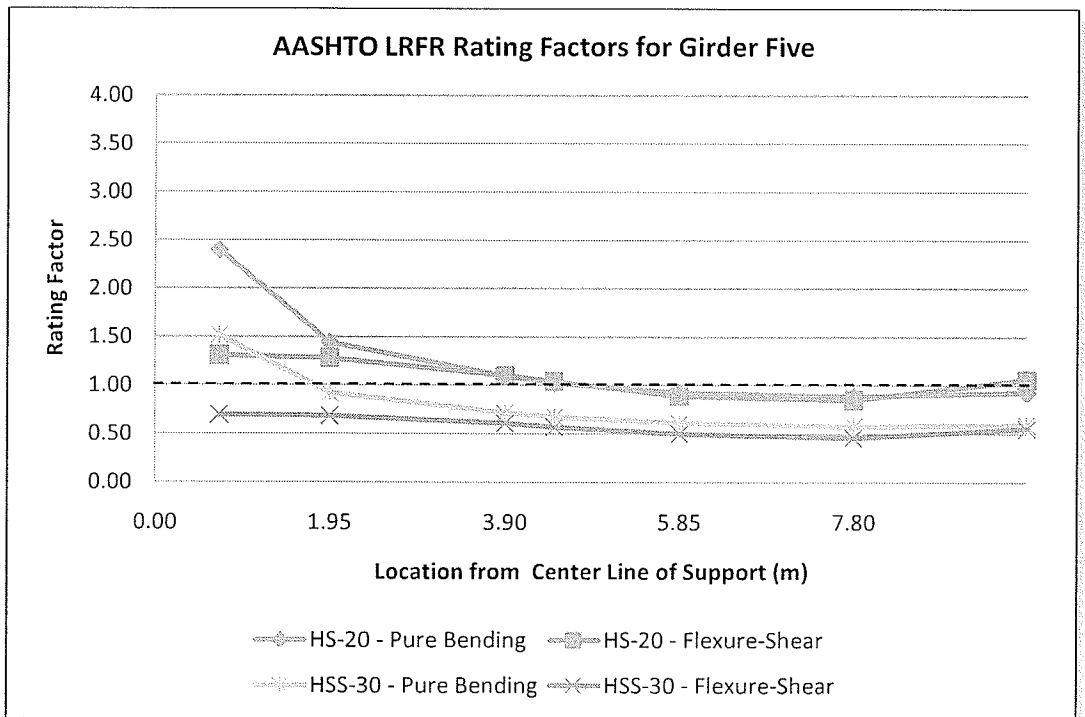


Figure 6-12: AASHTO rating factors at various locations along the length of girder five.

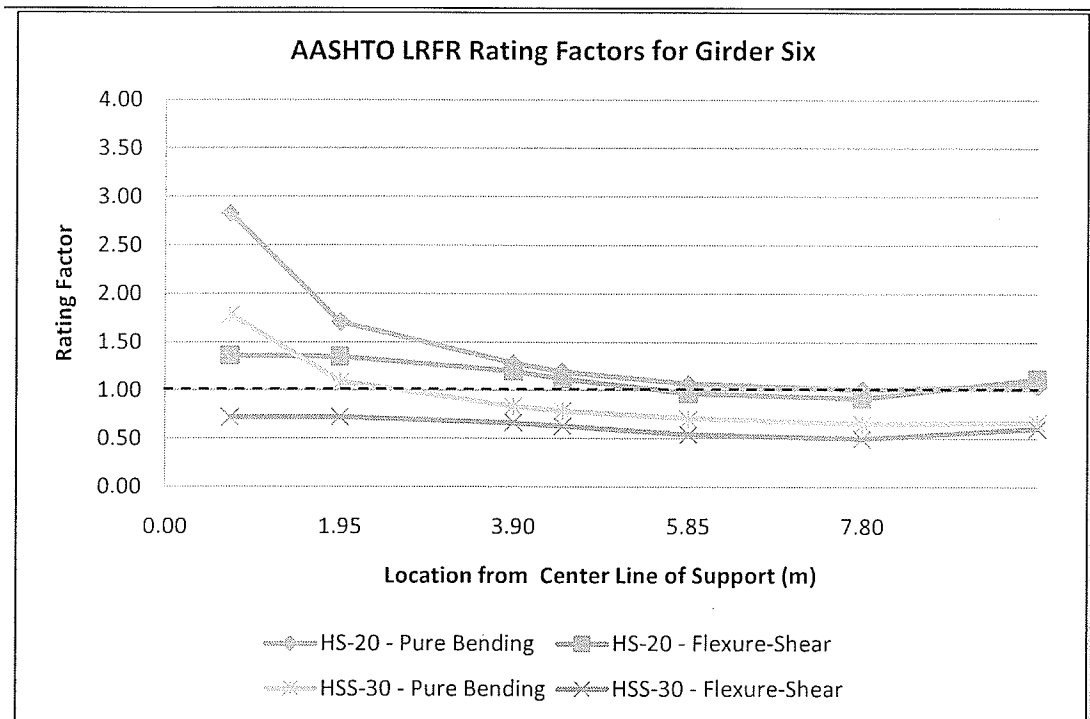


Figure 6-13: AASHTO rating factors at various locations along the length of girder six.

6.2.4 Experimental Load Rating Results

Comparing the theoretical and experimental load rating results of each girder, it was found that again the experimental analysis yielded a significantly greater rating factor than the theoretical analysis. The increase in rating factor was generally 30 points greater over the theoretical analysis for bending and 50 points greater over the theoretical analysis for flexure-shear. The results of this comparison can be found in Tables 6-7 to 6-12. Note that the comparison for girders one, two, and three were analyzed at the mid-span and the comparison for girders four, five, and six were analyzed near the quarter span.

Table 6-7: Comparison of theoretical and experimental rating factors for girder one at the mid-span.

Values Analyzed	Limit State		HS 20		HSS 30	
			<i>Inventory</i>	<i>Operating</i>	<i>Inventory</i>	<i>Operating</i>
Experimental	Strength I:	Pure Bending	2.03	2.63	1.07	1.38
		Flexure-Shear	2.22	2.87	1.40	1.81
Theoretical	Strength I:	Pure Bending	1.28	1.66	0.81	1.06
		Flexure-Shear	1.35	1.75	0.72	0.93

Table 6-8: Comparison of theoretical and experimental rating factors for girder two at the mid-span.

Values Analyzed	Limit State		HS 20		HSS 30	
			<i>Inventory</i>	<i>Operating</i>	<i>Inventory</i>	<i>Operating</i>
Experimental	Strength I:	Pure Bending	1.82	2.35	0.96	1.24
		Flexure-Shear	2.03	2.63	1.28	1.66
Theoretical	Strength I:	Pure Bending	1.13	1.46	0.72	0.93
		Flexure-Shear	1.27	1.65	0.68	0.88

Table 6-9: Comparison of theoretical and experimental rating factors for girder three at the mid-span.

Values Analyzed	Limit State		HS 20		HSS 30	
			<i>Inventory</i>	<i>Operating</i>	<i>Inventory</i>	<i>Operating</i>
Experimental	Strength I:	Pure Bending	1.42	1.84	0.75	0.97
		Flexure-Shear	1.67	2.16	1.05	1.36
Theoretical	Strength I:	Pure Bending	1.01	1.31	0.64	0.83
		Flexure-Shear	1.06	1.37	0.55	0.71

Table 6-10: Comparison of theoretical and experimental rating factors for girder four at the quarter span.

Values Analyzed	Limit State		HS 20		HSS 30	
			<i>Inventory</i>	<i>Operating</i>	<i>Inventory</i>	<i>Operating</i>
Experimental	Strength I:	Pure Bending	2.31	2.99	1.28	1.67
		Flexure-Shear	2.29	2.97	1.27	1.65
Theoretical	Strength I:	Pure Bending	1.47	1.90	0.97	1.25
		Flexure-Shear	1.43	1.85	0.79	1.02

Table 6-11: Comparison of theoretical and experimental rating factors for girder four at the quarter span.

Values Analyzed	Limit State		HS 20		HSS 30	
			<i>Inventory</i>	<i>Operating</i>	<i>Inventory</i>	<i>Operating</i>
Experimental	Strength I:	Pure Bending	1.62	2.10	0.90	1.17
		Flexure-Shear	1.64	2.12	0.91	1.18
Theoretical	Strength I:	Pure Bending	1.02	1.90	0.67	0.87
		Flexure-Shear	1.04	1.85	0.57	0.74

Table 6-12: Comparison of theoretical and experimental rating factors for girder six at the quarter span.

Values Analyzed	Limit State		HS 20		HSS 30	
			<i>Inventory</i>	<i>Operating</i>	<i>Inventory</i>	<i>Operating</i>
Experimental	Strength I:	Pure Bending	1.91	2.48	1.06	1.38
		Flexure-Shear	1.92	2.49	1.07	1.39
Theoretical	Strength I:	Pure Bending	1.19	1.90	0.79	1.02
		Flexure-Shear	1.12	1.85	0.63	0.82

For girders one, two, and three where the concentrated load was located at the mid-span the governing failure case was pure bending. The quarter span analysis shows that pure bending was the governing failure condition. However, the moment capacity derived from the experimental loading at this location is not representative of a pure bending moment and it is well known that a flexure-shear failure case is most likely to occur. Therefore, the flexure-shear should be taken as the governing values.

The results of this analysis demonstrated that the girders within this research program were capable of safely carrying the HS-20 load. While the experimental analysis was only conducted at the mid and quarter spans, the rating factors for both pure bending and flexure-shear under the inventory and operating conditions were well above the minimum passing rating factor of one.

Under the inventory check, the HSS-30 design loading does not receive a rating factor greater than one for all girders when the experimentally observed girder capacities are employed. Under the operating check, the HSS-30 design loading receives a passing rating factor for all but girder three. The AASHTO load rating manual permits the condition factor to be increased by 0.05 if section properties are well known. Since the capacities were known in this case the condition factor for girder three could be raised to 0.90 increasing the rating factor to 1.05. However, uncertainties still exist as only two locations were analyzed and it is well known that the $0.4 \times l$ location is critical for prestressed girders with singly draped strands. Therefore it is uncertain if this would raise the rating factor above one at this location.

The HSS-30 design loading is conservative compared to current legal truck configurations within Manitoba therefore it is probable that the girders within this program have the capacity to resist heavy truck traffic. However this statement cannot be made with absolute confidence and as such it was concluded that the girders within this testing program were not adequate to resist current heavy vehicle traffic loads with a reasonable level of safety under the AASHTO load and resistance factor rating method.

7. CONCLUSIONS & RECOMMENDATIONS

Within this research program, six pre-stressed concrete bridge girders were comprehensively examined. The testing program included three flexural tests, three shear tests, and three material tests. The material testing of the concrete was comprised of a strength test, a chloride ion content test, and an air void properties test. In addition, the condition of each girder was catalogued prior to and after testing. The girders were load rated using the CHBDC and the AASHTO LRFR methods.

The flexural and shear testing was able to conclusively demonstrate that while some of the girders were observed to be in poor condition, all the girders performed better than was expected by theoretical calculations. It was concluded that this increase in flexural and shear resistance over expected values was due largely to the conservatism within the Canadian and American design codes.

In regards to the environmental deterioration observed on the girders, the material testing was able to reveal the likely cause. Chloride salts used to melt ice from roadway surfaces is often a major contributing factor in road and bridge deterioration. However, the results of the chloride ion tests did not show that this was the cause of the damage seen on the girders. This was confirmed by observations of the pre-stressing reinforcement after flexural and shear testing which exhibited only minor surface rust. The experimental results of the air void content testing demonstrated that the concrete was susceptible to freeze-thaw damage. Cyclic freeze-thawing of absorbed moisture which drained from the road surface caused cracking at the bottom of the webs exposing the steel to the

environment instigating further deterioration. This inability to resist frost damage was also observed from concrete scaling on the web surfaces. Despite the fact that the concrete was not resistant to frost damage the concrete strength had not been diminished. Compressive concrete tests yielded an average compressive strength over design of 36 percent.

Although there was some level of deterioration observed on the majority of tested girders, their capacity to resist flexural and shear loading was greater than expected. This was further reinforced by the results of the load rating evaluations performed on the girders. Using the experimentally observed moment and shear capacities, the girders examined had the ability to safely resist normal heavy truck traffic loading under the CHBDC method of bridge evaluation

Using the AASHTO load and resistance factor rating system it was found that both the HS-20 and HSS-30 design loads did not yield a passing rating factor for all girders under the theoretical capacity analysis. When using the experimentally observed bending and flexure-shear capacity of each girder, the HS-20 design load yielded a passing rating factor for each girder under the inventory check. However, the HSS-30 design load narrowly failed to yield a passing rating factor for all girders. Therefore, under the AASHTO LRFR these six girders were not able to provide a reasonable level of safety when carrying heavy truck traffic.

The moment and shear testing within this program demonstrated a considerable difference between the theoretical and experimentally observed girder capacities. It is recommended that within Manitoba, bridges of this nature should be load tested to increase the accuracy of load rating analysis. This difference between theory and reality also demonstrates the need for research to be conducted to reduce the level of conservatism of flexure and shear design capacities calculated within the Canadian and American design codes.

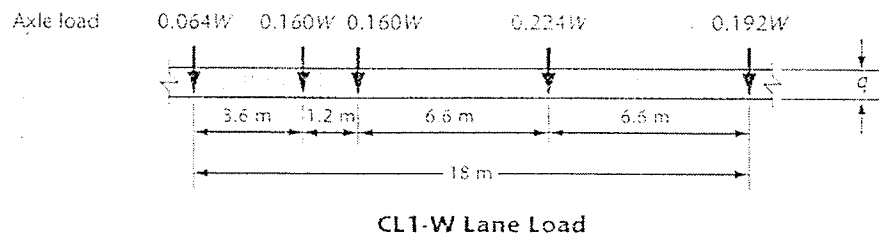
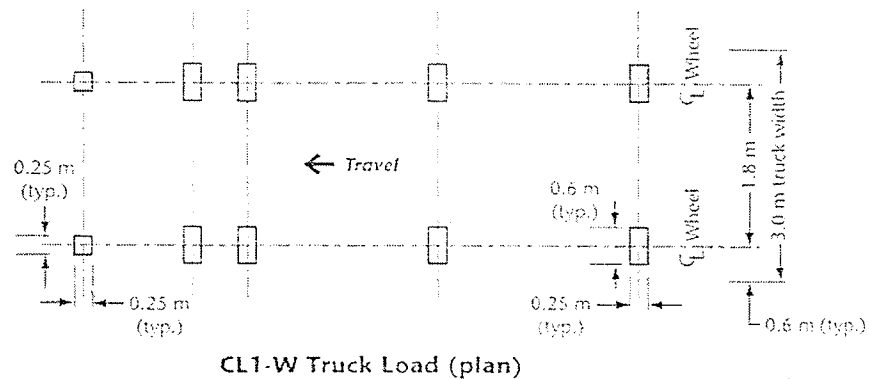
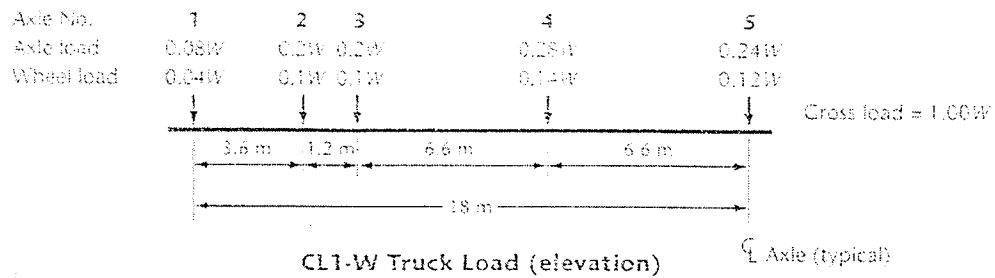
Bridge infrastructure is becoming more of a concern in Canada primarily because the majority of the current infrastructure is reaching its expected life span. The study of concrete components under simulated laboratory aging can provide important insight into the reaction of said components to loading and environmental effects. However, the examination of real world effects on formerly in-service bridge components greatly narrows the gap between theory and qualitative analysis, and quantitative performance characteristics increasing the level of understanding and knowledge of component reactions to expected service inputs. It is recommended that whenever possible, decommissioned bridge components should be comprehensively examined to further this endeavor.

REFERENCES

- [1] B. Gerwick, *Construction of Prestressed Concrete Structures*, 2nd Ed., Wiley-IEEE, 1997
- [2] T. Anlbom, C. Shield and C. French, "Full-scale Testing of Prestressed Concrete Bridge Girders," *Experimental Techniques*, vol. 21, no. 1, pp. 33-35, Jan-Feb, 1997.
- [3] Canadian Prestressed Concrete Institute, "*Precast and Prestressed Concrete*," third edition, 1996.
- [4] R. Feldman, "Volume Change and Creep of Concrete," *Canadian Building Digest*, [Online], vol. 119. Available: irc.nrc-cnrc.gc.ca/pubs/cbd/cbd119_e.html [Feb. 2009]
- [5] A. Nowak, H. Nassif and L DeFrain, "Effect of Truck Loads on Bridges," *Journal of Transportation Engineering*, vol. 119, no. 6, pp. 853-867, December 1993.
- [6] *Truck Size and Weight Study*. U.S. Department of Transport/Federal Highway Administration. [Online]. Available: fhwa.dot.gov/reports/tswstudy/TSWfinal.htm [Feb 10, 2009]
- [7] R. Al-Zaid and A Nowak, "Fatigue Strength of Prestressed Concrete Girder Bridges," *Canadian Journal of Civil Engineering*, vol. 15, no. 2, pp. 199-205, 1988.
- [8] Precast/Prestressed Concrete Institute, *Bridge Design Manual*, 2nd Ed., 2003.
- [9] M. Saeed Mirza, O. Ferdjani, A. Hadj-Arab, K. Joucdar, and A. Khaled, "An Experimental Study of Static and Dynamic Responses of Prestressed Concrete Box Girder Bridges," *Canadian Journal of Civil Engineering*, vol. 17, no. 3, pp. 481-493, January, 1990.
- [10] M. Saito, M. Ohta and H. Ishimori, "Chloride Permeability of Concrete Subject to Freeze-Thaw Damage," *Cement and Concrete Composites*, vol. 16, pp. 233-239, 1994.
- [11] G. Litvan, "Deterioration of Parking Garages," 2001, *National Research Council Canada* [Online], irc.nrc-cnrc.gc.ca/pubs/bsi/84-4-print_e.html, accessed 2008.
- [12] C. Crumpton and J. Bukovatz, "Corrosion and Kansas Bridge," Transportation Research Record N500, *Transportation Research Board*, pp. 25-31, 1974.
- [13] *Advanced Concrete Technology: Constituent Materials*, 1st edition, J. Newman and B.S. Choo, Butterworth-Heinemann, 2003.

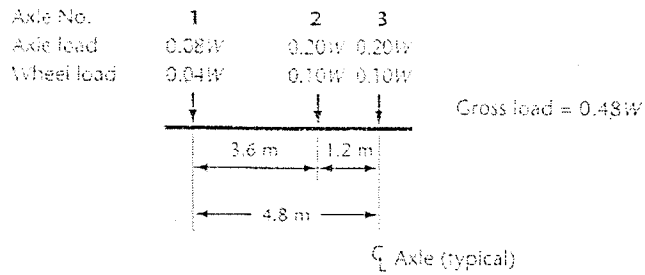
-
- [14] *Freeze-Thaw Resistance of Concrete with Marginal Air Content*. Dec. 2006, U.S. Department of Transport/Federal Highway Administration, [Online], Available: fhwa.dot.gov/pavement/pccp/pubs/06117/06117.pdf [Jan. 2009]
- [15] T. Cho, "Prediction of Cyclic Freeze-Thaw Damage in Concrete Structures Based on Response Surface Method," *Construction and Building Material*, vol. 21, pp. 2031-2040, 2007.
- [16] J. MacGregor, *Reinforced Concrete: Mechanics and Design*, 3rd Ed., Prentice Hall, 1997
- [17] Canadian Standards Association CAN/CSA A23.2-04, A23.2-4B: Obtaining and Testing Drilled Cores for Compressive Strength Testing, 2004.
- [18] Canadian Standards Association CAN/CSA Annex14.1: Equivalent Material Strengths from Test of Samples, 2006.
- [19] Canadian Standards Association CAN/CSA A23.2-04, A23.2-4B: Sampling and Determination of Water-soluble Chloride Ion Content in Hardened Grout or Concrete, 2004.
- [20] Canadian Standards Association CAN/CSA A23.1-04: Concrete Materials and Methods of Concrete Construction, 2004.
- [21] Annual Book of ASTM Standards, Standard Test Method for Microscopical Determination of Parameters of the Air-Void System in Hardened Concrete Designation: C 457-98, 1998.
- [22] Canadian Highway Bridge Design Code, CAN/CSA-S6-06, Canadian Standards Association, 2006.
- [23] A. Au, C. Lam, A. Agarwal, B. Tharmabala "Bridge Evaluation by Mean Load Method per the Canadian Highway Bridge Design Code," *Canadian Journal of Civil Engineering*, vol. 31, no. 4, pp. 678-686, August, 2005.
- [24] Guide Manual for Condition Evaluation and Load and Resistance Factor Rating (LRFR) of Highway Bridges, AASHTO, 2005.

APPENDIX

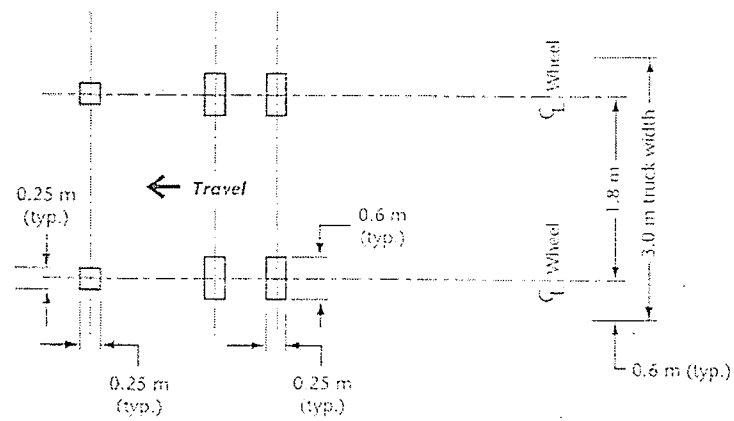


Note: The values of the uniformly distributed load, q , for each highway class (see Section 1) are as follows:
 (a) Class A: 9 kN/m;
 (b) Class B: 8 kN/m; and
 (c) Class C or D: 7 kN/m.

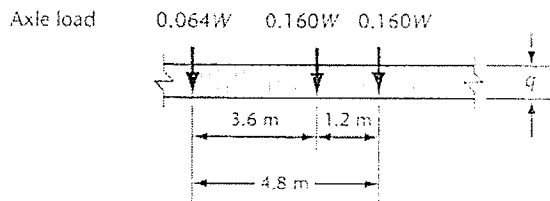
Figure A-1: CHBDC evaluation level one, CL1-W truck and lane load [22].



CL3-W Truck Load (elevation)



CL3-W Truck Load (plan)



CL3-W Lane Load

Note: The values of the uniformly distributed load, q , for each highway class (see Section 1) are as follows:
 (a) Class A: 9 kN/m;
 (b) Class B: 8 kN/m; and
 (c) Class C or D: 7 kN/m.

Figure A-3: CHBDC evaluation level three, CL3-W truck and lane load [22].

LRFD DESIGN LIVE LOAD (HL-93)

(LRFD 3.6.1)

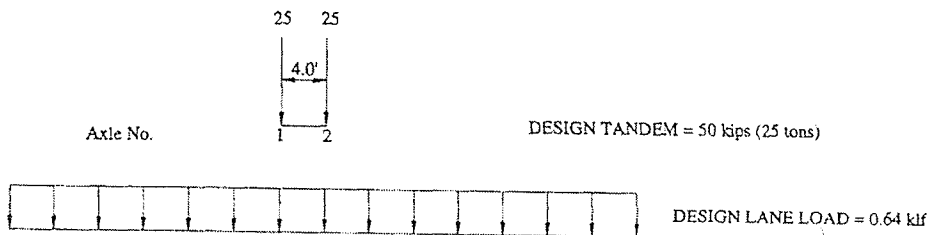
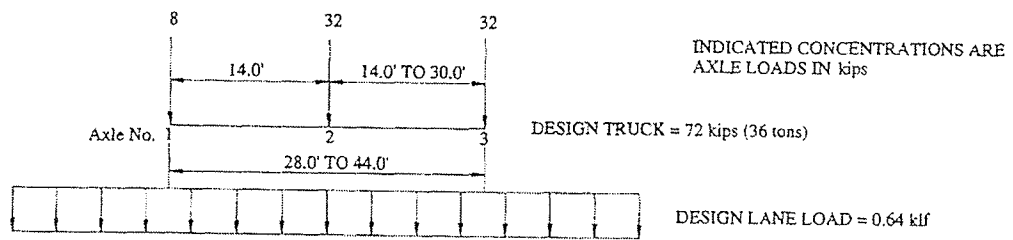
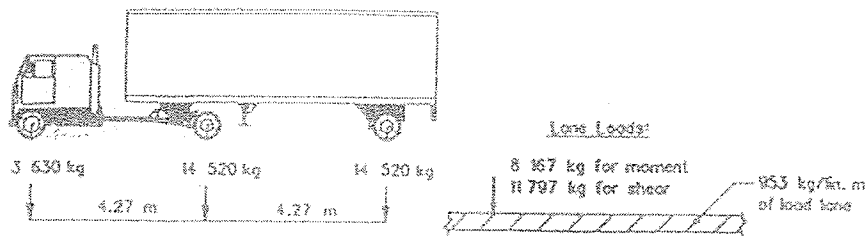


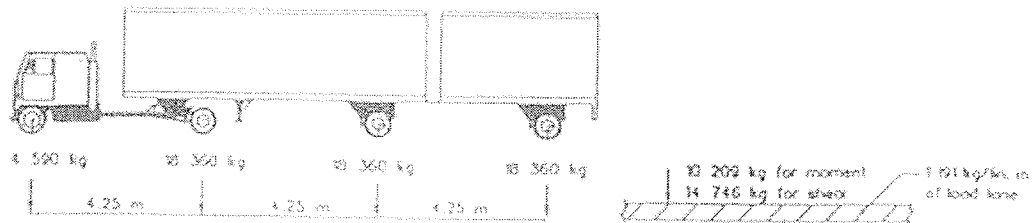
Figure A-4: AASHTO LRFD design live load [24].

A.A.S.H.T.O.

HS 20 (MS 18.15)
 C.V.M.+32 670 kg



Modified AASHTO
 HSS 25 (MS 27.95)
 C.V.M.+59 670 kg



Modified AASHTO
 HSS 30 (MS 27.23)
 C.V.M.+70 785 kg

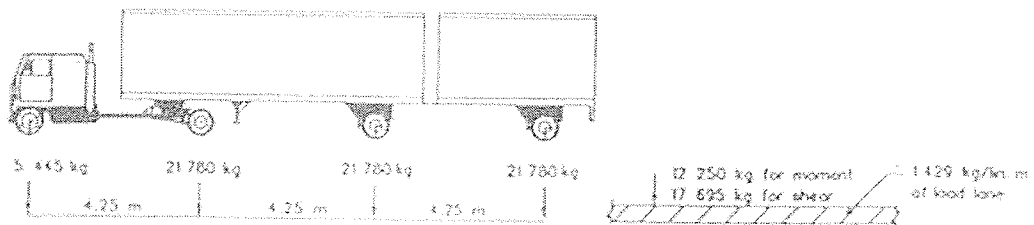


Figure A-5: AASHTO HS-20, HSS-25 and HSS-30 design truck and lane loading.

AASHTO LEGAL LOADS

a) AASHTO Trucks—Apply for all span lengths and load effects

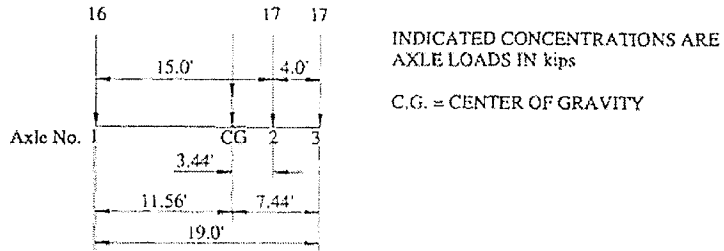


Figure B.6-2 Type 3 Unit WEIGHT = 50 kips (25 tons).

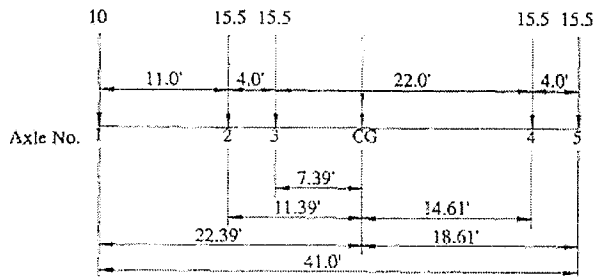


Figure B.6-3 Type 3S2 Unit WEIGHT = 72 kips (36 tons).

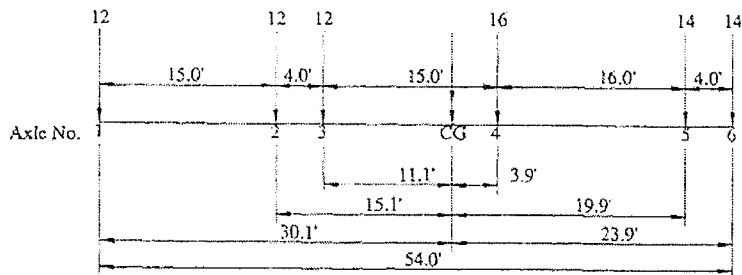
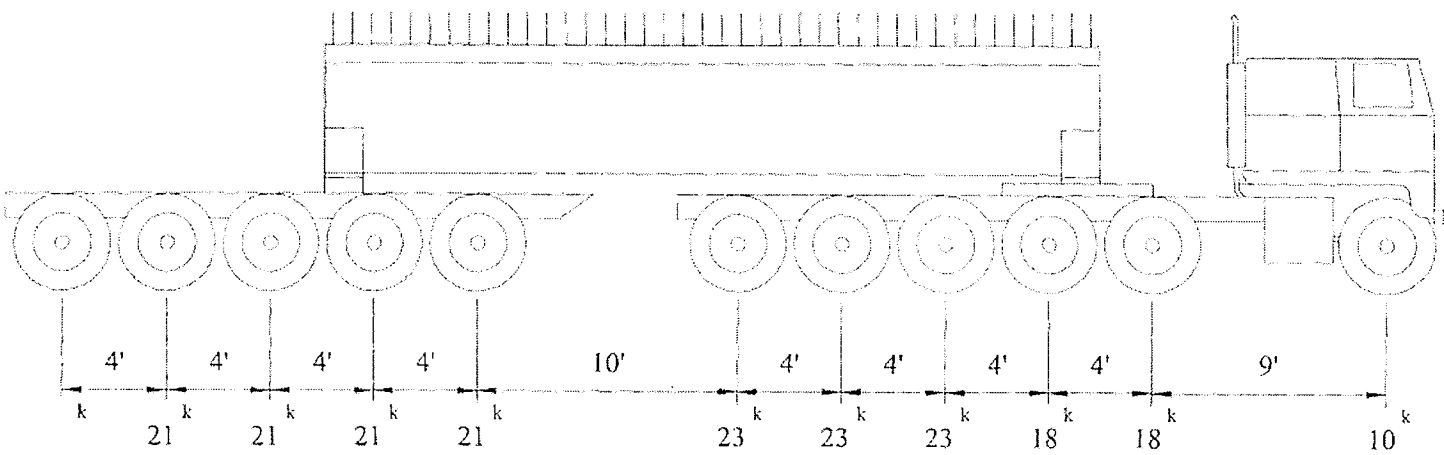


Figure B.6-4 Type 3-3 Unit WEIGHT = 80 kips (40 tons).

Figure A-6: AASHTO legal loads [24].



PERMIT TRUCK
LOADING CONFIGURATION

Figure A-7: AASHTO permit truck example [24].